UNIVERSITÉ DE NICE-SOPHIA ANTIPOLIS

ECOLE DOCTORALE STIC

SCIENCES ET TECHNOLOGIES DE LINFORMATION ET DE LA COMMUNICATION

T H E S E

pour l'obtention du grade de

Docteur en Sciences

de l'Université de Nice - Sophia Antipolis

Mention: Automatique, traitement du signal et des images

presentée et soutenue par

Leandro Ronchini Ximenes

Tensor-based MIMO relaying communication systems

Thése dirigée par Gérard FAVIER et André L. F. de ALMEIDA

soutenue le 25 Mars 2015

Jury :

M. Luc DENEIRE	Université de Nice-Sophia Antipolis	*Président*
M. Rémy BOYER	Université Paris-Sud	*Rapporteur*
M. João M. T. ROMANO	Universidade de Campinas (UNICAMP)	*Rapporteur*
Mme. Elisabeth de CARVALHO	Aalborg University	*Examinateur*
M. João C. M. MOTA	Universidade Federal do Ceará (UFC)	*Examinateur*
M. Gérard FAVIER	Université de Nice-Sophia Antipolis	*Directeur de thèse*
M. André L. F. de ALMEIDA	Universidade Federal do Ceará (UFC)	*Directeur de thèse*

Dados Internacionais de Catalogação na Publicação
Universidade Federal do Ceará
Biblioteca de Pós-Graduação em Engenharia - BPGE

X34m Ximenes, Leandro Ronchini.
Tensor-based MIMO relaying communication systems / Leandro Ronchini Ximenes. – 2015.
154 f. : il. color. , enc. ; 30 cm.

Tese (doutorado) – Université de Nice-Sophia Antipolis, Ecole Doctorale STIC, Sciences et Technologies de Linformation et de la Communication, Nice, 2015.
Área de concentração: Processamento Automatizado dos Sinais e das Imagens.
Orientação: Prof. Dr. André Lima Férrer de Almeida.
Orientação: Prof. Dr. Gérard Favier.

1. Teleinformática. 2. Tensores. 3. Sistemas cooperativos. 4. Estimação de canais. I. Título.

CDD 621.38

Abstract

In cooperative communication systems, two or more transmitting terminals are combined to increase the diversity and/or the power of the signals arriving at a particular receiver. Therefore, even if the devices do not have more than one antenna, or if a significant propagation loss is present between the two communicating nodes, the various transmitting elements can act as a virtual antenna array, thus obtaining the benefits of the multiple antenna (MIMO) systems, especially the increase in the capacity. Recently, tensor decompositions have been introduced as an efficient approach for channel estimation in cooperative communication systems. However, among the few works devoted to this task, the utilization of the PARAFAC tensor decomposition for modeling the received signals did not allow the development of techniques for joint symbol and channel estimation. Aiming to avoid the use of pilot sequences, which limits the overall spectral efficiency by dedicating a portion of the bandwidth only for the channel estimation task, the objective of this thesis is to provide new tensor-based strategies, including transmission systems and semi-blind receivers, for one-way two-hop MIMO relaying systems. Based on a Khatri-Rao space-time coding at the source and two different Amplify-and-Forward (AF) relaying strategies, two transmission schemes are proposed. For these systems, named PT2-AF and NP-AF, the received signals at the destination node follow respectively a PARATUCK2 and a nested PARAFAC tensor model. Exploiting uniqueness properties of these tensor models which are established in the thesis, several semi-blind receivers are derived. Some of these receivers are of iterative form using an ALS algorithm, whereas some other ones have closed-form solutions associated with Khatri-Rao factorizations. Some simulation results are finally presented to illustrate the performance of the proposed receivers which are compared to some state-of-the-art supervised techniques.

Keywords: Cooperative systems, MIMO, relaying, amplify-and-forward, tensors, semi-blind receivers, PARAFAC, PARATUCK2, nested PARAFAC.

Résumé

Dans les communications coopératives, deux ou plusieurs terminaux de transmission sont combinés pour accroître la diversité et/ou la puissance des signaux arrivant à un récepteur. Par conséquent, même si les dispositifs n'ont pas plus d'une antenne, ou s'il y a une perte de propagation significative entre les deux noeuds de communication, ces différents éléments de transmission peuvent agir comme un réseau d'antennes virtuelles, obtenant ainsi les bénéfices d'un système multi-antennes (MIMO), en particulier l'augmentation de la capacité de transmission. Récemment, l'analyse tensorielle s'est avérée une approche efficace pour l'estimation de canaux dans les systèmes coopératifs. Cependant, parmi les quelques travaux consacrés à cette tâche, l'utilisation de la décomposition tensorielle PARAFAC pour modéliser les signaux reçus ne permet pas l'estimation conjointe des symboles et des canaux de communication. Afin d'éviter l'utilisation de symboles pilotes qui limite l'efficacité spectrale du fait de l'utilisation d'une partie de la largeur de bande pour l'estimation de canal, l'objectif de cette thèse est de fournir de nouvelles approches tensorielles, en termes de systèmes de transmission et de récepteurs semi-aveugles, pour des systèmes de communication MIMO avec relai mono-directionnels, à deux sauts. Deux systèmes de transmission sont proposés en utilisant un codage spatio-temporel du type Khatri-Rao et deux stratégies de traitement Amplify-and-Forward (AF) au relai. Pour ces systèmes, appelés PT2-AF et NP-AF, les signaux reçus au niveau de la destination satisfont respectivement des modèles tensoriels du type PARATUCK2 et nested PARAFAC. En exploitant les propriétés d'unicité de ces modèles tensoriels établies dans la thèse, plusieurs récepteurs semi-aveugles sont dérivés. Certains de ces récepteurs sont du type ALS, tandis que d'autres sont des solutions non itératives basées sur des factorisations de produits de Khatri-Rao. Des résultats de simulation sont présentés pour illustrer les performances des récepteurs proposés qui sont comparés à des estimateurs supervisés.

Mots-clés: systèmes coopératifs, MIMO, *relaying*, *amplifly-and-forward*, tenseurs, récepteurs semi-aveugles, PARAFAC, PARATUCK2, nested PARAFAC.

Resumo

Em comunicações cooperativas, dois ou mais terminais de transmissão são combinados para aumentar a diversidade e/ou a potência dos sinais que chegam a um determinado receptor. Portanto, mesmo que os dispositivos não disponham de mais de uma antena, ou que então haja uma grande perda por propagação entre dois pontos comunicantes, os diversos elementos transmissores podem atuar como um arranjo virtual de antenas, obtendo-se assim vantagens dos sistemas de múltiplas antenas (MIMO), sobretudo o aumento da capacidade de transmissão. Recentemente, a chamada análise tensorial tem se mostrado uma abordagem eficiente para a estimação de canais em sistemas com diversidade cooperativa. Contudo, nos poucos trabalhos dedicados a essa tarefa, a utilização da decomposição tensorial *PARAFAC* para a modelagem dos sinais recebidos não possibilitou o desenvolvimento de técnicas de estimação conjunta de canais e símbolos. Com a idéia de se evitar o uso de seqüências de treinamento, que limita a eficiência espectral da transmissão por dedicar uma parte da largura de banda apenas para a tarefa de estimação dos canais, o objetivo desta tese é prover novas estratégias de comunicação, em termos de sistemas de transmissão e receptores semi-cegos, baseados em tensores adaptados a sistemas cooperativos MIMO unidirecionais de dois saltos. Dois sistemas de transmissão são propostos utilizando uma codificação espaço-temporal do tipo Khatri-Rao na fonte e duas estratégias de processamento Amplify-and-Forward (AF) no relay. Para estes sistemas, nomeados *PT2-AF* e *NP-AF*, os sinais recebidos no chamado nó de destino satisfazem os modelos tensoriais do tipo *PARATUCK2* e *nested PARAFAC*. Explorando as propriedades de unicidade destes modelos tensoriais estabelecidas nesta tese, vários receptores semi-cegos são derivados. Alguns destes receptores são do tipo ALS, enquanto outros são de soluções baseadas na factorização de produtos de Khatri-Rao. Resultados de simulação são apresentados para ilustrar os desempenhos dos receptores propostos em comparação a alguns estimadores supervisionados.

Palavras-chave: Sistemas cooperativos, *relaying*, MIMO, amplify-and-forward, tensores, receptor semi-cego, estimação de canais, PARAFAC, PARATUCK2, nested PARAFAC.

Acknowledgments

Gathering the work developed during the last 3 and half years, and organizing it into a concise and clear form in this manuscript, was an intense, laborious work. In similar way, fitting into a single page all my gratitude for all wonderful people that helped me achieve this milestone is not an easy task.

Comme d'habitude, et dans ce sens tout à fait juste, mes plus grands remerciements vont à mes deux co-directeurs de thse, M. Gérard Favier et M. André Lima Ferrer de Almeida. Au Prof. Favier, je remercie chaleureusement pour me aider des différentes façons. Merci de m'aider de fixer sur Nice et dans l'I3S, et puis m'aider a devenir un meilleur chercheur. Au prof. André, qui avait une participation active sur mon doctorat, soit au cours de mon séjour à Fortaleza ou à travers nos réunions hebdomadaires par vidéoconférence, je t'adresse aussi mes remerciements pour l'aide dans ces plus de cinq années d'amitié et d'enseignement.

I also dedicate my most sincere thanks to the people who participated in my daily life. Firstly my dedication goes to those who shared with me the ups and downs of a student life in a doctoral school, as they were as closest to family as I could get in Nice. Neetya Shrestha, José Henrique de Morais Goulart, Fernando Ireta Muñoz, Michele Nazareth da Costa, Dino Lopez Pacheco and Leonardo Hidd Fonteles. I thank you all for sharing so many lunches, coffees, buses and stories with me during these last years. And finally, I thank all my friends from Nice (and region) that were not part of my academic life, but helped me feel home at France.

Se o curso do doutorado foi uma via de certos sacrifícios, dedico então os ultimos agradecimentos à minha família. Embora meios de comunicao pareçam encurtar a distância, ela não pode substituir o contato físico entre as pessoas ou perfeitament transmitir emoções, e assim inevitavelmente perdi momentos preciosos com as pessoas que eu mais amo.

List of Figures

List of Tables

List of Acronyms

AF Amplify-and-Forward

ALS Alternating Least Squares

BALS Bilinear ALS

BER Bit Error Rate

CF Compress-and-Forward

CPP-ALS Combined PARAFAC/PARATUCK2

CSI Channel State Information

DALS Double ALS

DF Decode-and-Forward

DFT Discrete Fourier transform

DKRF Double Khatri-Rao Factorization

DMT Diversity-multiplexing trade-off

FSK Frequency-Shift Keying

HOSVD Higher-Order Singular Value Decomposition

KRST Khatri-Rao Space-Time

LS Least Squares

LSKRF Least Squares Khatri-Rao Factorization

MIMO Multiple-Input and multiple-Output

MMSE Minimum Mean Square Error

NMSE Normalized Mean Square Error

NP-AF Nested PARAFAC-based Amplify-and-Forward relaying

NPALS Nested PARAFAC-ALS

NRE Normalized Reconstruction Error

PARAFAC PARallel FACtor

PSK Phase-Shift Keying

PT2-AF PARATUCK2-Based Amplify-and-Forward relaying

PT2-ALS PARATUCK2-ALS

QAM Quadrature Amplitude Modulation

RD Relay-Destination

SD Source-Destination

SDF Selective Decode-and-Forward

SNR Signal-to-Noise Ratio

SPP-ALS Sequential PARAFAC/PARATUCK2

SR Source-Relay

SRD Source-Relay-Destination

ST Space-Time

STB Space-Time Block

STF Space-Time-Frequency

STT Space-Time Trellis

SVD Singular Value Decomposition

TST Tensor Space-Time

VD Vandermonde

ZF Zero-Forcing

Notation

In this thesis the following conventions are used. Scalar variables are denoted by upper-case letters $(A, B, \ldots)$, vectors are written as boldface lower-case letters $(\mathbf{a}, \mathbf{c}, \ldots)$, matrices correspond to boldface capitals $(\mathbf{A}, \mathbf{B}, \ldots)$, and tensors are written as calligraphic letters $(\mathcal{A}, \mathcal{B}, \ldots)$. The meaning of the following symbols are, if nothing else is explicitly stated:

$\mathbb{C}$	set of complex-valued numbers
$\mathbb{C}^I$	set of complex-valued I-dimensional vectors
$\mathbb{C}^{I\times J}$	set of complex-valued $(I \times J)$-matrices
$\mathbb{C}^{I_1\times\cdots\times I_N}$	set of complex-valued $(I_1 \times \cdots \times I_N)$-tensors
a^*	complex conjugate of $a \in \mathbb{C}$
$\lvert\mathbf{a}\rvert$	modulus of $\mathbf{a}$
$\lVert\mathbf{a}\rVert_2$	l-2 norm of $\mathbf{a}$
$\mathbf{A}^T$	transpose of $\mathbf{A}$
$\mathbf{A}^H$	Hermitian transpose of $\mathbf{A}$
$\mathbf{A}^{-1}$	inverse of $\mathbf{A}$
$\mathbf{A}^{\dagger}$	Moore-Penrose pseudo-inverse of $\mathbf{A}$
$\lVert\mathbf{A}\rVert_F$ $(\lVert\mathcal{A}\rVert_F)$	Frobenius norm of $\mathbf{A}(\mathcal{A})$
$\mathbf{I}_N$	Identity matrix of dimension $N \times N$
$\mathbf{1}_{N_1\times N_2}$	All-ones matrix of dimension $N_1 \times N_2$
$\mathbf{0}_{N_1\times N_2}$	All-zeros matrix of dimension $N_1 \times N_2$
$\mathbf{A}_{i_1,i_2} = a_{i_1,i_2}$	(i_1, i_2)-th element of matrix $\mathbf{A}$
$\mathbf{A}_{i_1\cdot}$ $(\mathbf{A}_{\cdot i_2})$	i_1-th row (i_2-th column) of $\mathbf{A}$
$\mathcal{A}_{i_1,i_2,i_3} = a_{i_1,i_2,i_3}$	(i_1, i_2, i_3)-th element of tensor $\mathcal{A}$
$\mathbf{A} \otimes \mathbf{B}$	The Kronecker product of $\mathbf{A}$ with $\mathbf{B}$,
$\mathbf{A} \diamond \mathbf{B}$	The Khatri-Rao (column-wise Kronecker) product.
$\mathbf{A} \circ \mathbf{B}$	The Hadamard product of $\mathbf{A}$ with $\mathbf{B}$,
$\mathrm{vec}(\mathbf{A})$	The vectorization operator.
$D_i(\mathbf{A})$	Diagonal matrix with diagonal entries given by i^{th} row of $\mathbf{A}$
$E\{.\}$	Expected value of its argument
$tr[\mathbf{A}]$	Trace of $\mathbf{A}$

Contents

Chapter 1

Introduction

1.1 Un bref aperçu des communications sans fil

Dans la perspective sur communications sans fil, les utilisateurs mobiles sont sont constamment échangent des données à tès haut débit, comme par les services de multimédia et les applications interactives. Pour répondre à la demande continue pour les taux de transmission plus élevés avec une grande fiabilité du signal, Claude E. Shannon avait indiqué la nécessité d'augmenter les capacités des canaux de communication. En raison de l'attenuation du signaux envoyé à l'air libre, l'augmentation de la capacité de canal en utilisant une puissance d'émission élevée ou encore une bande passante plus large ne sont pas souhaitable, une fois que ces deux ressources sont peu abondants et limitées par des contraintes opérationnelles, comme la consommation d'énergie et l'attribution du spectre réglementé. Au cours des deux dernières décennies, une alternative à augmenter les performances d'un lien sans fil a été d'utiliser des techniques de diversité. Ces techniques permettent le récepteur d'avoir des répliques de la message originale. Dans ce sens, si une réplique du signal a t profondment attnue, les autres peuvent avoir des atténuations plus légeres. Dans les systèmes de communication sans fil, les diversités de signaux sont généralement de *temps*, *fréquence* et de *espace* [1, 2].

En particulier pour la diversité spatiale, les répliques de signaux sont causées en général par la propagation par multi-trajets. Des nombreuses réflexions et réfractions rencontrées par les signaux créent de nombreuses versions non corrélées de la message d'origine, de sorte que plusieurs antennes au niveau du récepteur peuvent les exploiter pour améliorer l'estimation de symbole - ce qui est notée de *gain de diversité*. D'autre part, l'augmentation du nombre d'antennes à l'émission permet également un plus grand nombre de symboles être envoyer simultanément, ce qui augmente le taux de transmission - en donnant un *gain de multiplexage*. De nombreux travaux ont été consacrés à maximiser l'un de ces gains, car il est un compromis naturel entre la fiabilité (gain de diversité) et le taux de transmission (gain de multiplexage), c'est-à-dire l'utilisation de plusieurs antennes à l'émetteur pour envoyer plusieurs versions d'un même symbole ou multiplexer plusieurs symboles différents en même temps. Dans tous les cas, la technique d'employer plusieurs antennes à la fois émetteur et le récepteur est appelée MIMO, et elle a révolutionné les communications sans fil dans les deux dernières décennies.

Malgré les avantages de la diversité spatiale par multiples antennes, dans de nombreuses cas il est difficile d'avoir plus d'une antenne dans un dispositif mobile en raison de l'interaction électromagnétique entre les éléments étroitement espacés. Dans ce cas, les répliques de signaux associés à différents trajets de propagation deviennent corrélées par le couplage par induction mutuelle entre les antennes, ce qui réduit les avantages de l'emploi de la technique MIMO. Pour surmonter cela et d'autres questions, les systèmes coopératifs ont été proposé.

1.2 Réseau coopératif avec relais

Dans les communications coopratives, deux ou plusieurs noeuds de transmission sont combinés pour augmenter la diversité et/ou le puissance du signal sur un noeud de réception. Parmi les différentes formes de coopération, cela qui a reçu une attention particulière de la communauté de recherche est la coopération par relais [3, 4, 5, 6, 7]. Pour les systèmes mobiles assistée par relais, multiples terminaux mobiles sont utilisés pour créer un système virtuel MIMO [8, 9, 10]. Par conséquent, plusieurs noeuds d'une seule antenne peuvent travailler de manière coordonnée pour propager un message commun à un noeud de destination, et alors un réseau multi-antenne peut être émulé, et les avantages de la diversité d'émission peuvent être atteints. En outre, lorsque les liens directs entre les sources et la destination sont profondément atténués, des relais intermédiaires peuvent être utilisés pour atténuer ce problème en fournissant également un gain de puissance.

En général, les stratégies de coopération avec relais sont classés de plusieurs façons, par exemple:

- la topologie du réseau: la communication *half-duplex* ou *full-duplex*, *one-way* ou *two-way*, nombre de relais, nombre de sauts de transmission, entre autres;
- le protocole de transfert: *amplify-and-forward (AF)* [11], *decode-and-forward (DF)*[12, 3, 4], *selective-decode-and-forward (SDF)* [13] et *compress-and-forward (CF)* [12].

Certains de ces classifications sont brièvement expliquées dans ce qui suit.

Par définition, un relais *full-duplex* peut simultanément émettre et recevoir des signaux dans la même bande de fréquences (par exemple, le temps ou la fréquence), alors que le relais *half-duplex* effectue ces deux procédés dans des bandes non chevauchantes. En raison de la difficulté d'annuler des interférences propres au relais - le signal à transmettre est typiquement 150 dB plus fort que le signal reçu, comme souligné dans [13] - le relais *full-duplex* est habituellement peu pratique avec le technologies radio actuelles.

En général, les relais *half-duplex* ne fonctionnent pas réception et la transmission en même temps. Dans un scénario avec un seul relais multi-antenne entre deux noeuds, ces deux phases non chevauchantes sont intrinsèquement liées à la notion de deux-sauts. Dans la théorie des réseaux, un saut correspond à la transmission d'un bloc de données d'un noeud à un autre, et donc dans un système de deux-sauts le premier saut correspond à la pleine réception des signaux par le relais à partir d'un noeud source, et le seconde saut correspond à leur retransmission vers un noeud destination. Dans un scénario avec plusieurs relais, le nombre de sauts est fonction du nombre de relais, de la façon dont elles communiquent entre eux et également de l'orientation de la transmission – i.e. une transmission unidirectionnelle (*one-way*) ou bidirectionnelle (*two-way*) .

En raison de la présence d'interférence propre, étant donné que les signaux reçus par chaque noeud contient une partie de sa propre information transmise, une partie de l'efficacité de la communication bidirectionnelle est compromise. En théorie, l'interférence propre pourrait être annulée, mais que le nombre de noeuds dans le réseau augmente, l'impact de l'interférence propre devenue désastreuse, favorisant ainsi le déploiement de la transmission unidirectionnelle.

Le protocole de transmission est lié au traitement de signal effectué par les relais, et ils sont en général divisés en régénératifs et non-régénératifs, ce qui signifie que le signal d'origine est récupéré ("régénérée) au relais avant son renvoi au noeud suivant. Les représentants les plus importants de ces protocoles sont respectivement le *decodage-and-forward (DF)* et le *amplify-and-forward (AF).*

L'exigence deu protocole DF est que le relais décode avec succès les informations de la source, et donc le relais doit être adaptée àvecune structure capable de calcul pour une telle tâche. Pour réduire les coûts de mise en oeuvre et l'exploitation complexes de relais, une alternative est de déployer le protocole AF.

Amplifier-and-forward a été introduit en [11] et est le protocole le plus simple à mettre en oeuvre, ce qui explique pourquoi il a reçu autant d'attention au cours des dernières années. Il simplement amplifie le signal reçu au niveau du relais afin de lutter contre les pertes de trajet entre la source et la destination . En raison de sa transformation linéaire simple, les performances de ce protocole souffre du fait qu'il amplifie également les bruits et interférences aux antennes de l'équipement.

1.3 La modélisation tensorielle pour les communications coopératives avec relais

Pour l'amélioration de la qualité du signal, une autre forme pour améliorer les performances est par l'utilisation de techniques d'estimation aveugles. En général, la détection de symboles à un récepteur nécessite la connaissance de la CSI. Classiquement, les matrices de canal sont estimées en utilisant des séquences de formation (pilotes) symboles, donc CSI estimation ne est faite en résolvant un système d'équations bilinéaires, où les coefficients de canal sont les seules inconnues. Dans ce cas, l'estimation de canal est dit être supervisé ou non-aveugle. Depuis une période de transmission est dédiée uniquement à l'estimation canal ne correspondent pas aux informations de transmission, l'efficacité spectrale est réduit. En outre, si les coefficients d'évanouissement de canal varient rapidement, son temps cohérente peut être trop court pour l'estimateur basé sur la formation d'estimer avec précision le CSI. Estimation aveugle arrive souvent alors quand les symboles transmis peuvent être détectés au niveau du récepteur, sans la nécessité de la CSI. Dans cette thèse, estimation aveugle est traité comme un synonyme pour l'estimation conjointe des symboles et des canaux. Bien que le CSI ne est pas nécessaire pour détecter les symboles avec un estimateur aveugle, sa connaissance est importante pour une optimisation de transmission éventuelle.

Dans un scénario de relais, lorsqu'il est décidé d'employer le protocole AF, qui vise à simplifier la charge de calcul dans les stations de relais, un algorithme de décodage est utilisée à la destination seulement. Dans le contexte de systèmes à deux bonds à sens unique, l'utilisation de techniques de précodage à la source et / ou le relais nécessite généralement l'instantané CSI connatre le *source-relais* et *relay-destination* canaux - estimation de canal commune - pour mener à bien l'optimisation de transmission [14, 15, 16, 17]. Avec noeuds antennes multiples, des stratégies fondées pilotes point-à-point conventionnelles ne fournissent pas d'estimation de canal à la fois de houblon séparément à la destination , depuis le AF protocole ne échelles les signaux, et donc la récepteur ne peut estimer le produit des deux matrices de canal. Au cours des dernières années analyse tensorielle a été proposé de remédier à ce problème.

Cependant, en dépit de l'intérêt croissant de l'utilisation de tenseurs pour le codage espace-temps, encore très peu de travaux proposent des systèmes à base-tenseur pour les communications coopératives. Seulement récemment une analyse de tenseur est révélé être une approche efficace pour l'estimation de canal et / ou la détection de symbole dans les systèmes de relayage de coopération [18, 19, 20, 21, 22, 23].

Dans [24] (et plus tard dans [25, 26]) Lioliou et al. proposé un, forme fermée méthode supervisée pour estimer les deux canaux d'un aller simple AF système relayer avec des gains variant dans le temps d'amplification. Bien que techniquement ces oeuvres ne exploitent pas les propriétés multidimensionnelles de tenseurs, des travaux basés tenseur-ont abordé le même concept de gains de relais variant dans le temps de proposer des alternatives pour résoudre le problème d'estimation de canal dans les systèmes coopératifs.

Ainsi, les quelques études concernant la modélisation de tenseur de coopération MIMO systèmes se concentrent sur le problème de l'estimation de canal en utilisant des séquences de formation, en laissant de cté les avantages intrinsèques de l'estimation aveugle, déjà exploité par des méthodes basées tenseur pour les systèmes non coopératifs. Les exceptions sont les oeuvres [21, 22], où PARAFAC à base de récepteurs aveugles pour une multi-utilisateur de liaison montante système coopératif sont proposées. Ces travaux intègrent explicitement “ la coopération ” comme la troisième dimension des données reçues en plus de l’espace (antennes de réception) et de temps (périodes de symbole) dimensions, qui se fait en regroupant les noeuds mono-antennes (utilisateurs et relais) en grappes. Cette approche inhabituelle a limité l’efficacité spectrale, puisque seulement une grappe transmet à la fois, tandis que les autres doivent rester silencieux.

Cette thèse vise à combler l’écart dans la littérature des aveugles-estimation utilisant tenseurs pour les communications de relayage de coopération. Estimation conjointe des symboles et des canaux dans un système de communication AF à deux bonds est possible en adoptant le même variant dans le temps processus de relayer [24, 18, 20], mais le recours à un KRST codant pour moduler les symboles à la source au lieu de l’utilisation de séquences d’apprentissage orthogonales connues. Plus loin, nous vous proposons deux stratégies de traitement différentes au relais, afin que nous puissions exploiter le tenseur de données de réception soit comme un modèle de PARATUCK2 ou un modèle de PARAFAC imbriquée, deux présentant les propriétés d’unicité essentiels nécessaires pour estimer aveuglément les paramètres désirés. Ces deux schémas de transmission conduisent au développement d’une variante de récepteurs semi-aveugles, qui sont étudiés en fonction de leurs conditions d’identifiabilité, la complexité et les performances de calcul.

Chapter 2

Introduction

Contents

2.1 A brief overview of wireless communications

In the long-standing perspective on the future of the wireless communications, mobile users are constantly sharing data that need high-bandwidth transfers, as services of real-time multimedia and interactive applications. To meet the continuous demand for higher transmission rates and signal reliability, Shannon in [27] had stated the necessity of increasing the capacities of the communication channels. Due to signal fading through propagation in open air, increasing channel capacity by employing a higher transmission power or a broader bandwidth is in general undesirable, once that both resources are scarce and limited by operational constraints, such as energy consumption and regulated spectrum allocation. In the last two decades, an alternative to increase the performance of a wireless link was to use the diversity techniques. These techniques provide the receiver with replicas of the original message experiencing uncorrelated propagation channels. In this sense, if a component of the signal is over a deep fading, caused for example by shadowing or path loss, other components have a high probability of suffering a lighter attenuation. In wireless communication systems, signal diversities are commonly of: *time*, e.g. by transmitting sequences of redundant bits; *frequency*, e.g. using spread spectrum techniques like direct-sequence (DS) and frequency-hopping (FH); and *space* [**?**, 2].

Particularly for spatial diversity, the replicas of the signals are caused in general by the multi-path propagation. In a rich-scattering scenario, such as a densely urban area, countless reflexions and refractions experienced by the traveling signals create numerous uncorrelated versions of the original message, so employing multiple antennas at the receiver let such redundancy to be exploited, improving for example symbol estimation – providing what is denoted *diversity gain*. On the other hand, increasing the number of antennas at transmission also lets a greater number of symbols to be sent simultaneously, increasing the transmission rate – providing *multiplexing gain*. Many works have been dedicated to maximizing one of these gains, since there is a natural trade-off between reliability (diversity gain) and transmission rate (multiplexing gain) [28], i.e. using multiple antennas at the transmitter to send multiple versions of a same symbol or multiplexing several distinct symbols at the same time. In all cases, the technique of employing multiple antennas at both transmitter and receiver is called Multiple-Input and multiple-Output (MIMO), and it has revolutionized the modern wireless communications in the past two decades.

Indeed, since the fundamental works of Foschini [29] and Telatar [30] on the benefits of multiple antennas on the channel capacity, uncountable works have decided to exploit one or more diversities in conjunction with the spatial diversity. A prominent field arose in the development of the space-time coding techniques. As the name suggests, time and space (antenna) diversities are combined, providing a welcoming flexibility to deal with the Diversity-multiplexing trade-off (DMT).

Early works on multiple antennas at the transmitter were done by Guey et al. [31] and by Foschini [32], and Tarokh et al. [33, 34] proposed a class of Space-Time Trellis (STT) codes, which could performed excellently in terms of symbol detection, but at a high complexity cost at the receiver due to the need of a Viterbi decoder. To address this issue, Alamouti in [35] introduced what is called nowadays as Space-Time Block (STB) coding [36, 37], by presenting a simple scheme using two transmit antennas and a single receive antenna to achieve full transmit diversity and full rate, yet having a linear decoding.

In spite of all benefits from exploiting the spatial diversity with arrays of multiple antennas, in many occurrences it is difficult to have more than one of them in a small mobile terminal, mainly due to the electromagnetic interaction between the closely-spaced radiating elements. In this case, the signal replicas associated with different propagation paths become correlated by the mutual coupling between the antennas, reducing the benefits of employing the MIMO technique. To overcome this and other issues, the use of the *cooperative diversity* was proposed [38, 13, 39, 9].

2.2 Cooperative relay networks

In cooperative communications, two or more transmitting nodes are combined to increase signal diversity and/or power at a receiving node. Among the different forms of cooperation, one that has received special attention from the research community is the cooperative relaying [**?**, 4, 5, 6, 7]. For relay-assisted mobile systems, multiple links including mobile terminals to a base station, mobile terminals to relay stations and relay stations to a base station are used to create a virtual MIMO system [8, 9, 10]. Therefore, several single antenna nodes can work coordinately to propagate a common message to a destination node, so a multiple antennas array can be emulated, and the benefits of the transmit diversity can be achieved. In addition, when the direct links between the sources (co-channel users) and the destination (base station) are deeply attenuated, intermediate relay stations can be used to mitigate this issue by providing also a power gain. Besides, many works have also pointed out the benefits of relaying networks on reducing energy waste in broadcasting transmissions ([40] and references therein). In an era where the number of wireless devices increases tirelessly, in which concepts as Internet of Things propose a revolution on how people and machines interact, exploiting a large ensemble of collaborative nodes – referred as *user-cooperation* in [41] – to enhance the connectivity sounds a sure step into the envisioned decentralized networks of the future [42, 43, 44, 45].

Although relaying systems were extensively used in analog radio and television broadcast in the past, its interest in wireless communications suffered an abrupt reduction after the early 80's. Van der Meulen in [46, 47] was the first one to study the capacity of the three-terminal relay channel, further investigated by Cover and El Gamal in 1979 [12]. Until the end of 90's, there were sparse contributions on relaying networks, but remarkable advances in wireless communications, such as the previously mentioned derivation of the capacity of multi-antenna systems by [29, 30] and the development of space-time codes in [33, 34, 36, 37, 35, 32]. These advances have given a new lease of life to relaying in digital communications, and now a much larger body of research is available in the literature, for example in the areas of relay selection [48, 49], relay beamforming [50] and cooperative secrecy [51].

In general, relaying strategies are classified in many ways, e.g.:

- the network topology: full- or half-duplex communication, one- or two-way orientation, number of relays, number of transmission hops, among others;
- the forwarding protocol: e.g. Amplify-and-Forward (AF) [11], Decode-and-Forward (DF) [12, **?**, 4], Selective Decode-and-Forward (SDF) [13] and Compress-and-Forward (CF) [12].

Some of these classifications are briefly explained in the following.

2.2.1 Network topology

By definition, a full-duplex relay can simultaneously transmit and receive signals in the same band (e.g. time or frequency), while the half-duplex relay performs these two processes in non-overlapping bands. Due to the difficulty of canceling (self-)interference at the relay – the signal to be transmitted is typically 150 dB stronger than the received signal, as highlighted in [13] – full-duplex relaying is usually impractical with the current radio technologies.

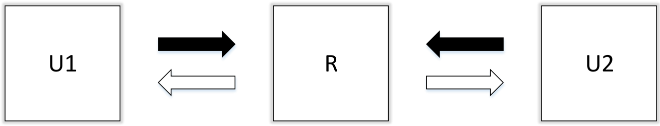

Figure 2.1: Two-way half-duplex relaying

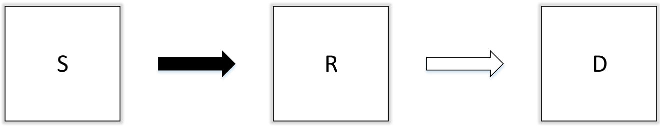

Figure 2.2: One-way half-duplex relaying

In general, half-duplex relays do not operate reception and transmission at the same time. In a scenario with only one relaying process between two nodes, these two non-overlapping phases are inherently linked to the concept of dual-hoping (or two-hop). In network theory, a hop corresponds to the transmission of a block of data from one node to another, and thus in a two-hop relaying the first hop corresponds to the full reception of the signals by the relay from a source node, and the second hop corresponds to their subsequent retransmission to a destination node. In a scenario with multiple relays, the number of hops depends on the number of relays, on how they communicate among each other and also on the orientation of the transmitted message– i.e. one-way or two-way.

The two-way communication channel was first introduced by Shannon in [52] to enable simultaneous bidirectional communication, but it was mostly in the past decade that two-way systems in relay networks started receiving the deserved attention from the research community ([53] and references therein). A conventional two-way half-duplex system is shown in Fig 2.1. Two nodes (U1 and U2) send their signals to the relay R in the first hop (black arrow), which forwards a (mixed) version of such signals back to the origin nodes in the second hop (white arrow).

Due to the presence of self-interference, given that the signals received by each node contains a portion of its own transmitted information, part of the efficiency of the two-way communication is compromised. In theory, self-interference could be canceled out, but as the number of nodes in the network increases – as in the case of large ad hoc networks – the impact of the self-interference become disastrous, thus favoring the deployment of one-way relaying. The one-way system is shown in Fig. 2.2, where S denotes a source of information, and D denotes a destination node.

It is well known, and not hard to figure out, that the one-way strategy leads to an unavoidable loss in spectral efficiency with respect to the two-way counterpart. In a perfect

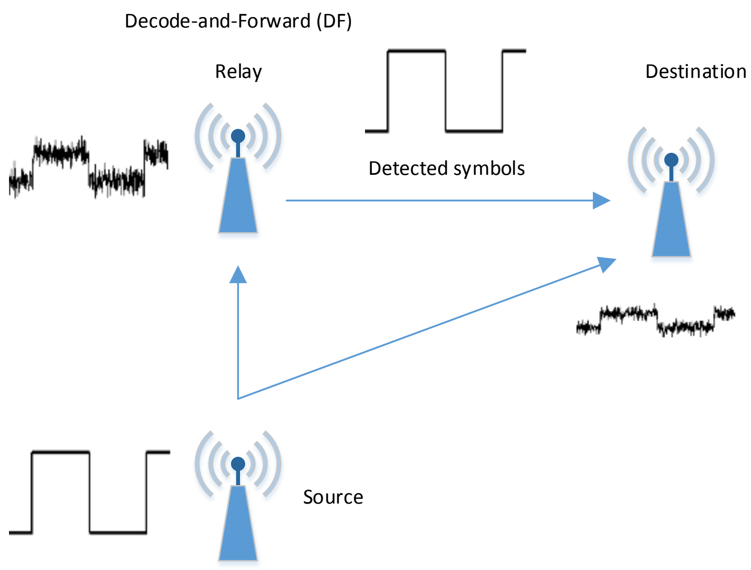

Figure 2.3: Decode-and-forward (DF) protocol

scenario (with full elimination of self-interference by the nodes), the two-way protocol corresponds to the superimposition of two one-way transmissions (U1 $\rightarrow$ R $\rightarrow$ U2 and U1 $\leftarrow$ R $\leftarrow$ U2). Thus, the two-way system can convey information in two hops what the one-way system does in four.

2.2.2 Forwarding protocol

The forwarding protocol is related to the signal processing performed by the relays, and they are in general divided into the regenerative and non-regenerative classes, which means whether the original signal is recovered ("regenerated") at the relay prior to its forwarding to the following node. The most important representatives of regenerative and non-regenerative protocols are respectively the decode-and-forward (DF) and the Amplify-and-forward (AF).

Decode-and-forward (DF) is a protocol where the relay performs decoding and re-coding of the signals before forwarding the data to the receiver. The general concept of the DF protocol was firstly introduced by Cover and Gamal [12] and later redefined in [?, 4]. An illustrative scheme of the DF protocol with a single relay and a direct link is shown in Fig. 2.3, expressing the signal sent to the destination by the relay as a recovered version of the signal sent by the source.

The requirement for an efficient cooperation in this protocol is that the relay successfully decodes the information from the source, and therefore the relay must be adapted with a computationally capable structure for such task. To reduce the costs of implementing and

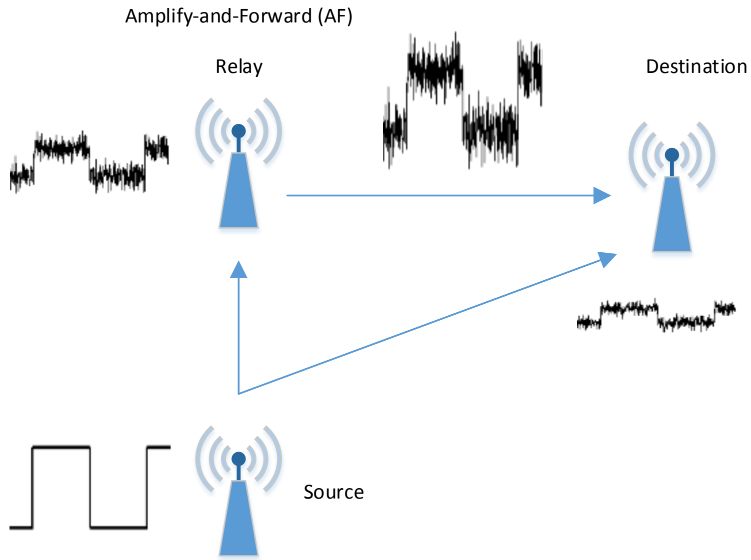

Figure 2.4: Amplify-and-forward (AF) protocol

operating complex relaying stations, an alternative is to deploy the AF protocol.

Amplify-and-forward was introduced in [11] and is the simplest protocol to implement, which explains why it has received so much attention from the academia and the industry in the past few years. It simply amplifies the received signal at relay in order to combat the path losses between the source and the destination. Due to its simple linear processing, the performance of this protocol suffers from the fact that it also amplifies noises and eventual interferences at the antennas of the relay, as shown in Fig. 2.4.

2.3 Tensor modeling for relay-based cooperative wireless communications

It was mentioned in this chapter that increasing signal strength, bandwidth and employing diversity techniques are common means to improve a wireless link. Another form to enhance performance is through the use of blind estimation techniques. In general, symbol detection at a receiver requires the knowledge of the Channel State Information (CSI). Conventionally, the channel matrices are estimated by using sequences of training (pilot) symbols, so CSI estimation is done by solving a system of bilinear equations, where the channel coefficients are the only unknowns. In this case, the channel estimation is said to be supervised or non-blind. Since a period of transmission is dedicated only to channel estimation, not actual information transmission, the spectral efficiency is reduced. Furthermore, if the fading coefficients of channel vary rapidly, its coherent time may be too short for the training-based estimator to accurately estimate the CSI. Blind estimation usually happens then when the transmitted symbols can be detected at the receiver without the need of the CSI. In this thesis, blind estimation is treated as a synonymous for joint estimation of symbols and channels. Although the CSI is not necessary to detect the symbols with a blind estimator, its knowledge is important for an eventual transmit optimization.

In a relaying scenario, when it is decided to employ the AF protocol, which aims to simplify the computational burden at the relay stations, a decoding algorithm is used at the destination only. In the context of two-hop one-way systems, the use of precoding techniques at the source and/or the relay generally requires the instantaneous CSI knowledge of both *source-relay* and *relay-destination* channels – joint channel estimation – to carry out transmit optimization [14, 15, 16, 17]. With multiple-antenna nodes, conventional point-to-point pilot-based strategies do not provide channel estimation of both hops separately at the destination, since the AF protocol only scales the signals, and thus the receiver can only estimate the product of the two channel matrices. In recent years tensor analysis has been proposed to overcome this issue.

For point-to-point (non-cooperative) multiple-antenna communication systems, tensor-based methods have been proposed in a number of works [54, 55, 56, 57] to solve the problem of blind estimation. In those cases, the dimensionality of a tensor is usually linked to a number of diversities to be exploited (e.g. space, time, frequency and code).

Sidiropoulos et al. in [54] for the first time applied tensor decompositions in telecommunications. By modeling a multiuser point-to-point DS-CDMA system using the PARallel FACtor (PARAFAC) tensor model [58, 59],both symbol and channel matrices could be ointly estimated at the receiver.

This innovative approach in signal processing casted a light on the possibilities of using tensor analysis on several other applications. Until then tensor decompositions were mostly restricted to evaluate empirical data in psychometrics and chemometrics (e.g. [58, 60]). Following [54], Sidiropoulos also developed the flexible class of Khatri-Rao Space-Time (KRST) codes based on the PARAFAC tensor model [61].

De Almeida et al. [56] modeled a transmission scheme based on two allocation matrices for selection of antennas and data streams. There, the set of received signals could be organized in a third-order tensor data following a PARATUCK2 decomposition [62, 60]. Other tensor-based transmission schemes also approached the use of allocation matrices, as the Tensor Space-Time (TST) coding [63], which introduced a more complex scheme than [56] by resorting to a more general tensor model, i.e. PARATUCK-$(2, 4)$; and the Space-Time-Frequency (STF) coding in [57], which extended the tensor-based Space-Time (ST) coding of [56] to exploit the frequency diversity.

More recently, [64] proposed the Double Khatri-Rao space-time-frequency (D-KRSTF) coding scheme, based on the nested PARAFAC tensor decomposition introduced therein, where a fourth-order tensor could be written by the combination of two third-order PARAFAC models.

The different ways of designing the transmission schemes led to different tensor models for the received signals (e.g. PARAFAC, PARATUCK2, PARATUCK-(2,4) and nested PARAFAC), each system having its own interesting properties. For all these non-cooperative transmission schemes, new blind receivers were proposed to allow a joint symbol and channel estimation without requiring pilot sequences for CSI acquisition. For more comprehensive and detailed presentation of the use of tensors in wireless communications, please see [65, 66].

However, despite of the growing interest of using tensors for space-time coding, still very few works propose tensor-based systems for cooperative communications. Only recently tensor analysis has shown to be an efficient approach for channel estimation and/or symbol detection in cooperative relaying systems [18, 19, 20, 21, 22, 23].

In [24] (and later in [25, 26]) Lioliou et al. proposed a supervised, closed-form method to estimate both channels of a one-way AF relaying system with time-variant amplifying gains. Although technically these works do not exploit the multidimensional properties of tensors, tensor-based works have approached the same concept of time-variant relay gains to propose alternatives to address the channel estimation issue in cooperative systems.

In the works [18, 19, 20] the signals collected at the destination node through a number of time-blocks are stored in third-order tensors that follow the PARAFAC model. In [18, 19], a tensor formulation is applied to two-way MIMO relaying systems, and the channels are estimated by firstly canceling self-interference in each node, and then by solving the estimation itself in an algebraic manner similar to [24].

The approach proposed in [20] also allows a simultaneous estimation of the both partial channels in a one-way scenario, but uses an Alternating Least Squares (ALS) algorithm instead. Relying on a mild condition to ensure the essential uniqueness of the PARAFAC decomposition [67], the use of this iterative algorithm provided less constrained identifiability conditions than its competitor [24], leading to an eventual gain in spectral efficiency in some scenarios.

Another iterative method for channel estimation was recently proposed in [23]. Although innovative in the proposal of a supervised channel estimation in a three-hop system, the Tucker2 tensor model adopted therein has no inherent properties of uniqueness of its solution, so a very restrictive relaying strategy is employed, where the receiver needs to combine the signals from two (intersecting) paths (one of them following a PARAFAC model) to proper estimate the channels.

Thus, the few studies concerning tensor modeling of cooperative MIMO systems focus on the problem of channel estimation using training sequences, leaving aside the intrinsic benefits of the blind estimation, already exploited by tensor-based methods for non-cooperative systems. The exceptions are the works [21, 22], where PARAFAC-based blind receivers for an uplink multiuser cooperative system are proposed. These works explicitly incorporate "cooperation" as the third dimension of the received data in addition to space (receive antennas) and time (symbol periods) dimensions, which is done by grouping single-antenna nodes (users and relays) in clusters. This unusual approach has limited spectral efficiency, since only one cluster transmits at a time, while the others must stay silent.

By looking at these different cooperative schemes, we can see that the trilinear PARAFAC decomposition is not suitable to model a system with joint symbol and channel estimation in MIMO AF relaying networks. Therefore, to employ more complex ST coding at source and to enable blind-estimation in these scenarios, it is needed to resort to more complex tensor models.

This thesis intends to fill the gap in the literature of blind-estimation using tensors for cooperative relaying communications. Joint estimation of symbols and channels in a two-hop AF communication system is possible by adopting the same time-variant relaying process of [24, 18, 20], but resorting to a KRST coding to modulate the symbols at the source instead of using known orthogonal training sequences. Further on, we propose two different processing strategies at the relay, so we can exploit the receiving data tensor either as a PARATUCK2 model or a nested PARAFAC model, both presenting the essential uniqueness properties necessary to blindly estimate the desired parameters. These two transmission schemes lead to the development of a variant of semi-blind receivers, which are studied in terms of their identifiability conditions, computational complexities and performances.

A summary of the state of the art tensor-based methods for Amplify-and-Forward (AF) cooperative systems is presented in Table 5.1.

2.4 Thesis organization and contributions

Besides the introduction and conclusion chapters, the thesis manuscript is organized into 4 main chapters, whose content and contributions are briefly described below:

Chapter 2. Important fundamentals of tensors are treated in this chapter, followed by the presentation of three tensor decompositions (i.e. PARAFAC, PARATUCK2 and nested PARAFAC) and their essential uniqueness properties.

The contribution presented in this chapter is the derivation of two new essential uniqueness theorems for the nested PARAFAC tensor model, concerning the sufficient condition to ensure the unique recovering of the factors of this decomposition and their

	Blind	Tensor model	Iterative	Main feature
Roemer et al. [18, 19]	No	PARAFAC	No	Two-way relay model
Rong et al. [20]	No	PARAFAC	Yes	Relay model similar to [24]
Fernandes et al. [21]	Yes	PARAFAC	Yes	Single-antenna, clustered nodes
Almeida et al. [22]	Yes	PARAFAC	Yes	Variation of [21] with DS-CDMA
Cavalcante et al. [23]	No	Tucker2	Yes	Three-hop model
PT2-AF [68]	Yes	PARATUCK2	Yes	KRST coding at source
NP-AF [69]	Yes	Nested PARAFAC	Yes/No	KRST coding at at source and relay

Table 2.1: State of the art tensor-based works for AF relaying systems

ambiguity issues.

Chapter 3. This chapter contains the largest body of contributions of this thesis, which concerns the development of new tensor-based transmission schemes for a one-way relaying system and of semi-blind receivers adapted to them.

Employing a simplified KRST coding at source, two different AF relaying strategies lead to the following transmission protocols:

- PARATUCK2-Based Amplify-and-Forward relaying (PT2-AF): the time-varying nature of the relay AF processing is defined by the existence of time frames, where each frame corresponds to the amplifying gains associated with a specific data-stream transmitted by the source. The receiving signal tensor at destination follows a PARATUCK2 model .

- Nested PARAFAC-based Amplify-and-Forward relaying (NP-AF): Instead of associating each time-frame with a data-stream, the relay performs another KRST coding, spreading the whole block of signals into another time domain (dimension). The data tensor is not longer modeled by a third-order PARATUCK2 model, but following the fourth-order nested PARAFAC model.

A number of semi-blind receivers adapted to these proposed schemes are presented in the rest of the chapter. More specifically, the semi-blind receivers for PT2-AF are

- PARATUCK2-ALS (PT2-ALS): This receiver estimates symbol and channels using an ALS algorithm;

- Sequential PARAFAC/PARATUCK2 (SPP-ALS): Similar to PT2-ALS, but uses as an initialization for the ALS algorithm the symbols estimated from signals received from a direct link. The name of this receiver comes from the fact this symbol initialization is obtained by exploiting a PARAFAC model as in [61];

- Combined PARAFAC/PARATUCK2 (CPP-ALS): In this receiver, the direct link is not used only for symbol initialization, but also provides additional spatial diversity for symbol estimation at each iteration of the algorithm.

For the NP-AF transmission scheme, the semi-blind receivers are:

- Nested PARAFAC-ALS (NPALS): As in PT2-ALS receiver, symbols and channels are estimated with a single ALS process;

- Double ALS (DALS) and Double Khatri-Rao Factorization (DKRF): Each of these is a two-step receiver, formed by either iterative (i.e. DALS) or non-iterative (i.e. DKRF) routines. In both cases, the first step (ALS-X or KRF-X) estimates, from the signals received through the relay link, the symbols and also the compound channel between the source and destination. The second step (ALZ-Z or KRF-Z) corresponds then to extracting from this channel the individual channels that compose the two-hop network.

- CNPALS, CALS-X and CKRF-X: The presence of the direct link can also be used in the NP-AF protocol to improve the semi-blind estimation, in the same way that SPP-ALS and CPP-ALS are variants to PT2-ALS. The routines CNPALS, CALS-X and CKRF-X substitute respectively NPALS, ALS-X and KRF-X for a better symbol estimation.

The hybrid receivers, called in this way due to jointly exploit the direct and relay-assisted links, rather than simply combining both links for a better symbol estimation, lead to a refinement of the channel estimates. This is a remarkable feature not possible with the supervised techniques.

The relationship between the tensor models, the transmission protocol and the semi-blind receivers are depicted in Fig. 2.5.

Chapter 4. This chapter concerns the numerical analysis of transmission schemes and their receivers proposed in the previous chapter. For the PT2-AF and NP-AF protocols the influence of the system parameters, such as number of antennas and source code length,

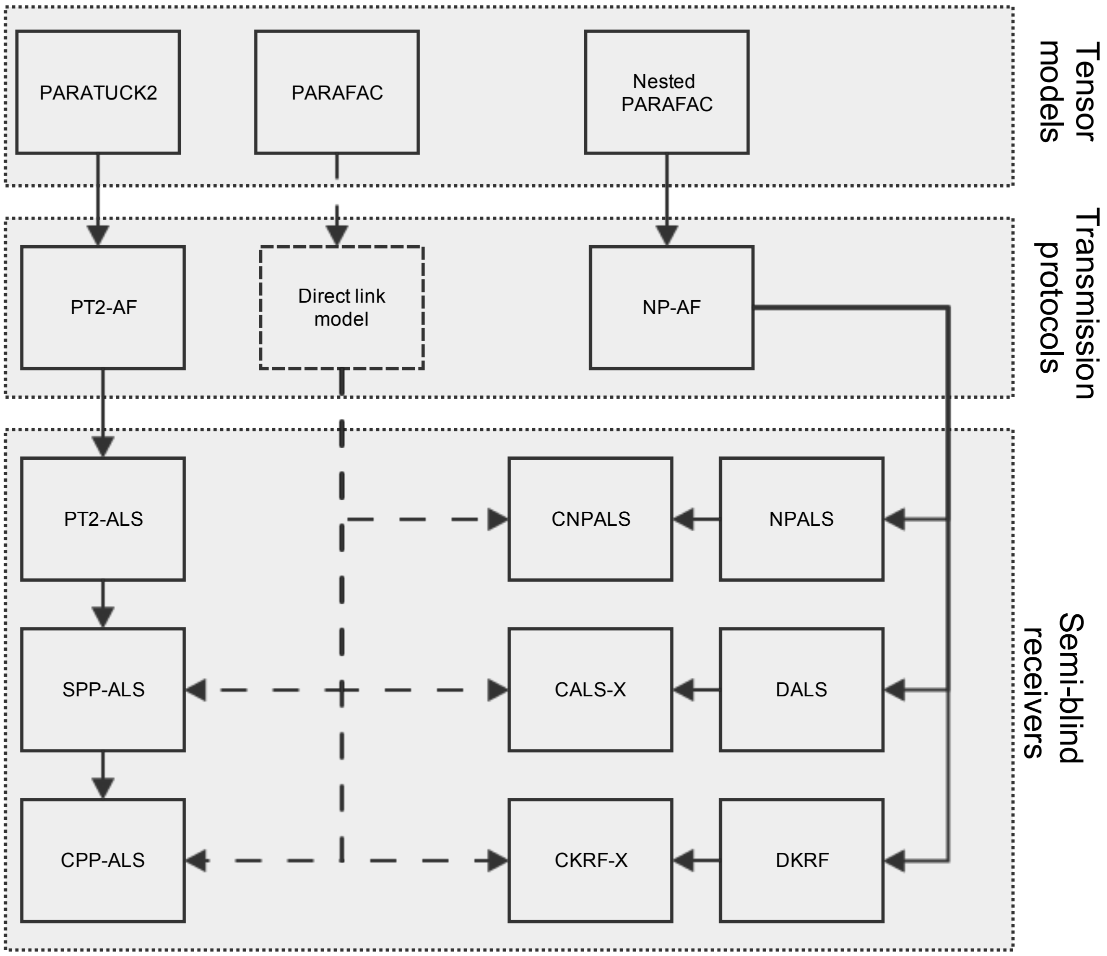

Figure 2.5: Tensor-based transmission protocols and their semi-blind receivers

are evaluated through the utilization of a Zero-Forcing (ZF) receiver with perfect CSI. In addition, all semi-blind receivers for the new one-way relaying schemes are studied in terms of its computational cost and also in terms of Bit Error Rate (BER) and channel Normalized Mean Square Error (NMSE). Comparisons with other state-of-the-art supervised methods are done through extensive use of Monte Carlo computational experiments.

2.4.1 Publications

Part of this work in this thesis was, or soon will be, published in the following publications.

- Journal papers:

1. L. R. Ximenes, G. Favier, A. L. F. de Almeida, and Y. C. B. Silva, "PARAFAC-PARATUCK Semi-Blind Receivers for Two-Hop Cooperative MIMO Relay Systems," IEEE Transactions on Signal Processing, vol. 62, no. 14, pp. 3604–3615, July 2014.

2. L. R. Ximenes, G. Favier, and A. L. F. Almeida, “Semi-blind receivers for non-regenerative cooperative MIMO communications based on nested PARAFAC modeling,” Accepted with major revisions to IEEE Transactions on Signal Processing.

3. L. R. Ximenes, G. Favier, and A. L. F. Almeida, “Closed-form semi-blind receiver for two-hop MIMO relay systems using a double Khatri-Rao space-time coding,” To be submitted to IEEE Signal Processing Letters, 2015.

- Conference paper:

1. L. R. Ximenes, G. Favier, and A. L. F. Almeida, ”MMSE-based blind-receiver for one-way relay-assisted MIMO communications,” in preparation to be submitted to Brazilian Telecommunications Society (SBrT) conference, 2015.

- Participation in journal paper (Subject not belonging to this thesis manuscript):

1. A. L. F. de Almeida, G. Favier, and L. R. Ximenes, “Space-time-frequency (STF) MIMO communication systems with blind receiver based on a generalized PARATUCK2 model,” IEEE Transactions on Signal Processing, vol. 61, no. 8, pp. 1895–1909, April 2013.

Chapter 3

Tensor decompositions

Contents

In this chapter, some fundamentals of tensors that are necessary for the comprehension of this thesis are introduced. The chapter is divided into a first part, containing the concept of tensor itself and the so-called process of matricization of a tensor, while the second part deals with the tensor decompositions to be used in the later chapters, namely PARAFAC [58, 59], PARATUCK2 [62, 70] and nested PARAFAC [64]. When addressing these last two tensor decompositions, the first contributions of this work are presented. For the PARATUCK2 model, a theorem concerning design rules of the matrix factors is proposed to eliminate arbitrary column permutations of their solutions, and for the nested PARAFAC model the new contributions are given in the form of two theorems involving its uniqueness properties.

Other important properties and operators of multilinear algebra, such as the Kronecker and Khatri-Rao products, are confined in Appendix A.

3.1 Fundamentals of tensors

This section is divided into two subsections. The first addresses the definition of tensors, as well as the definitions of the mode-n product and of the tensor rank. The second subsection deals exclusively with the matricization process, which consists in organizing the entries of a higher order tensor into a matrix.

Before introducing the fundamentals of tensors, it is important to present the definition of the Kruskal rank (k-rank). The concept of Kruskal rank was proposed by Kruskal in his work [67] on the essential uniqueness of the PARAFAC decomposition.

Definition 1. *(Kruskal rank (k-rank)) The Kruskal rank $k_{\mathbf{X}}$ is the maximum number such that any subset of $k_{\mathbf{X}}$ columns of $\mathbf{X}$ are linearly independent. Some of its properties are:*

- $0 \leqslant k_{\mathbf{X}} \leqslant \mathit{rank}(\mathbf{X})$;
- *if $\mathbf{X}$ has any two or more linearly dependent non-zero columns, then $k_{\mathbf{X}} = 1$;*
- *if and only if $\mathbf{X}$ has one or more zero columns, then $k_{\mathbf{X}} = 0$;*
- *if $\mathbf{X}$ is a full column rank matrix, then $k_{\mathbf{X}} = \mathit{rank}(\mathbf{X})$;*
- *if the elements of $\mathbf{X}$ are independently drawn from a continuous Gaussian distribution, then $k_{\mathbf{X}} = \mathit{rank}(\mathbf{X})$.*

Indeed, the comprehension of the Kruskal rank is primordial to fully understand the uniqueness properties of the tensor decompositions shown more ahead. Another useful property involving the k-rank is the lemma presented in [71, 72] and restated here.

Lemma 1. *For $\mathbf{A} \in \mathbb{C}^{L \times M}$ and $\mathbf{B} \in \mathbb{C}^{N \times M}$, the Khatri-Rao product $\mathbf{A} \diamond \mathbf{B}$ is full column rank if*

$$k_{\mathbf{A}} + k_{\mathbf{B}} \geqslant M + 1, \tag{3.1}$$

where $k_{\mathbf{X}}$ is k-rank of $\mathbf{X}$.

3.1.1 Tensor definitions

A N-way[1] or N^{th}-order tensor is a multilinear array of dimensionality N. More commonly, tensors are referred only to arrays of order greater than two, also denoted higher-order tensors, since first-order and second-order tensors are better known as vectors and matrices, respectively. Thus, a third-order tensor has three dimensions (or modes), and perhaps its best geometric representation would be as shown in Fig.3.1.

In general, higher-order tensors adopt definitions that are directly generalized from matrices. For example, an entry of a tensor can be referenced in a similar manner to those of a matrix, and the Frobenius norm of a tensor follows the conventional definition of the Frobenius norm of a matrix.

Another important mathematical operation within multilinear algebra is called mode-n product:

[1]The terms N-way or multi-way tensors are not used further in this thesis to avoid confusion with the type of relaying protocol, i.e. one-way and two-way.

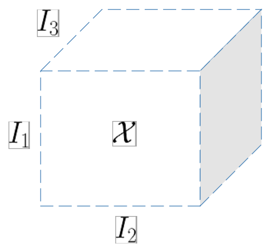

Figure 3.1: Third-order tensor $\mathcal{X} \in \mathbb{C}^{I_1 \times I_2 \times I_3}$

Definition 2. *(Mode-n product) Given a tensor $\mathcal{X} \in \mathbb{C}^{I_1 \times I_2 \times \cdots \times I_n \times \cdots \times I_N}$, the mode-$n$ product of this tensor and matrix $\mathbf{U} \in \mathbb{C}^{J \times I_n}$ is denoted by $\mathcal{X} \times_n \mathbf{U} \in \mathbb{C}^{I_1 \times \cdots I_{n-1} \times J \times I_{n+1} \times \cdots I_N}$, and this operation yields*

$$(\mathcal{X} \times_n \mathbf{U})_{i_1 \cdots i_{n-1}, j, i_{n+1} \cdots i_N} = \sum_{i_n=1}^{I_N} x_{i_1 \cdots i_{n-1}, i_n, i_{n+1} \cdots i_N} u_{j, i_n}. \tag{3.2}$$

In addition, for any indices $1 \leqslant m \leqslant N$ and $1 \leqslant n \leqslant N$, it holds that

$$\mathcal{X} \times_m \mathbf{A} \times_n \mathbf{B} = \mathcal{X} \times_n \mathbf{B} \times_m \mathbf{A}. \tag{3.3}$$

A mode-n product is thus nothing but a linear transformation of the tensor along its n^{th} mode. Further on, expressing the tensor decompositions using the mode-n product will be shown as an useful way to understand them in terms of their factors.

Before moving forward into the process of matricization, it is also important to comprehend the definition of tensor rank:

Definition 3. *(Tensor rank) The rank of $\mathcal{X}$ is defined by the minimum number of rank-one tensors that generate $\mathcal{X}$ as their sum.*

The notion of tensor rank was firstly introduced by Hitchcock in 1927 [73], and then later it was independently proposed by Kruskal in [67]. This definition of tensor rank is consistent with the definition of the matrix rank, where R is the smallest number of rank-one matrices that form a rank-R matrix. In the case of a tensor, a rank-one N-order tensor $\mathcal{X} \in \mathbb{C}^{I_1 \times I_2 \times \cdots \times I_N}$ can be defined by N vector outer products, i.e.

$$x_{i_1, i_2, \cdots, i_N} = a_{i_1}^{(1)} a_{i_2}^{(2)} \cdots a_{i_N}^{(N)}, \tag{3.4}$$

where $a_{i_n}^{(n)}$ is i_n^{th} element of the vector $\mathbf{a}^{(n)} \in \mathbb{C}^{I_N \times 1}$.

Unlike the matrix rank, the tensor rank is not upper-bounded by the smallest dimension of the array.

3.1.2 Matricization

The process of matricization (or unfolding) of a tensor corresponds to organizing its elements in a matrix, usually by concatenating side-by-side the so-called matrix slices.

Given a third-order tensor $\mathcal{X} \in \mathbb{C}^{I_1 \times I_2 \times I_3}$, the horizontal, lateral and frontal slices are denoted by $\mathbf{X}_{i_1\cdot\cdot} \in \mathbb{C}^{I_2 \times I_3}$, $\mathbf{X}_{\cdot i_2 \cdot} \in \mathbb{C}^{I_3 \times I_1}$ and $\mathbf{X}_{\cdot\cdot i_3} \in \mathbb{C}^{I_1 \times I_2}$, respectively. The i_1^{th} horizontal

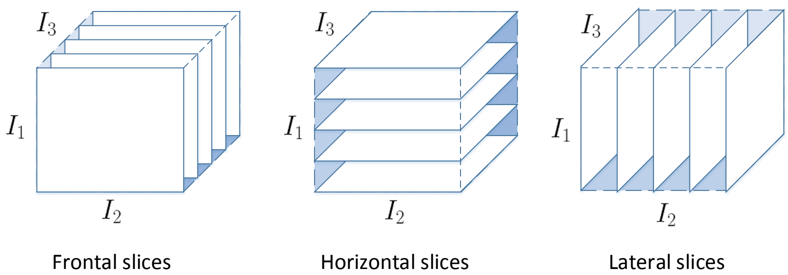

Figure 3.2: Slicing of $\mathcal{X}$

slice is obtained by fixing the (first-mode) index i_1 and varying i_2 and i_3, and equivalent procedures are done to find the lateral and frontal slices. The frontal, horizontal and lateral slices of a third-order tensor are illustrated in Fig. 3.2.

In the literature, there are multiple ways to define an unfolding of a tensor, according, for example, to the indexing order of the elements of the resulting matrix. However, in all definitions the mode-n unfolding of a tensor $\mathcal{X} \in \mathbb{C}^{I_1 \times \cdots I_n \cdots \times I_N}$ is characterized by having one of its dimension equal to I_n. For simplification, we refer to mode-n unfolding as the case where either I_n is the number of rows or columns of the considered matrix, e.g. both $\mathbf{X}_{I_2 I_3 \times I_1}$ and $\mathbf{X}_{I_1 \times I_2 I_3}$ are mode-1 unfoldings of $\mathcal{X}$. Indeed, the former matrix is nothing but a transpose of the latter, i.e. $\mathbf{X}_{I_2 I_3 \times I_1} = (\mathbf{X}_{I_1 \times I_2 I_3})^T$. The graphical representations of the construction of the mode-1, mode-2 and mode-3 unfoldings of a third-order tensor $\mathcal{X} \in \mathbb{C}^{I_1 \times I_2 \times I_3}$ using its frontal, horizontal and lateral slices are given by Figs. 3.3a-3.3c, respectively.

In the case of a third-order tensor, the different unfoldings are linked by

$$\begin{aligned} x_{i_1,i_2,i_3} &= [\mathbf{X}_{I_2 I_3 \times I_1}]_{(i_3-1)I_2+i_2,i_1} = [\mathbf{X}_{I_3 I_1 \times I_2}]_{(i_1-1)I_3+i_3,i_2} \\ &= [\mathbf{X}_{I_1 I_2 \times I_3}]_{(i_2-1)I_1+i_1,i_3} . \end{aligned} \tag{3.5}$$

By convention, the order of dimensions is related to the order of variation of the corresponding indices. For instance, $\mathbf{X}_{I_2 I_3 \times I_1}$ means that index i_2 varies more fast than i_3. By such logic, using the vec(.) operator described in Appendix A gives

$$\mathbf{x}_{I_2 I_3 I_1} = \text{vec}(\mathbf{X}_{I_2 I_3 \times I_1}) = \text{vec}(\mathbf{X}_{I_2 \times I_3 I_1}) \in \mathbb{C}^{I_2 I_3 I_1 \times 1}. \tag{3.6}$$

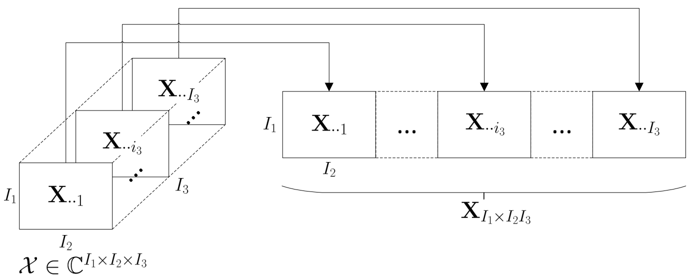

(a) Mode-1 unfolding of $\mathcal{X}$

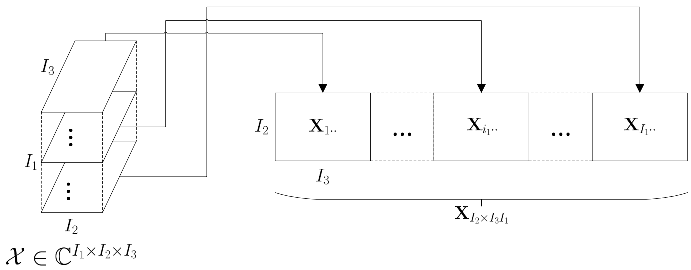

(b) Mode-2 unfolding of $\mathcal{X}$

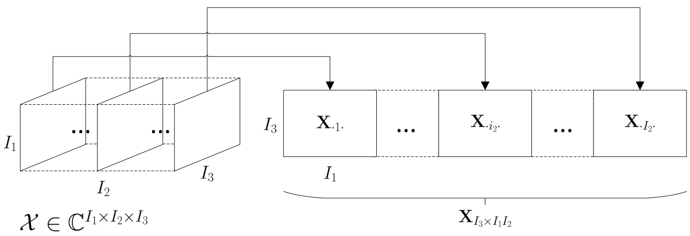

(c) Mode-3 unfolding of $\mathcal{X}$

Figure 3.3: Matrix unfoldings of $\mathcal{X}$

3.2 Tensor decompositions

When one thinks on the benefits of employing tensor analysis for a determined application, usually it is thought on the possibility of exploiting the properties of a specific tensor decomposition. From the variety of existing tensor models, the choice of a proper tensor decomposition usually lies within the trade-off between the degree of representativeness of the model and its uniqueness properties. In general, higher-order tensor decompositions present advantages on both aspects over bilinear decompositions, once more complex models can be represented with more relaxed uniqueness conditions.

Tucker in [74] introduced the *three-mode factor analysis (3MFA)*, nowadays namely Tucker3. This tensor decomposition was further generalized to tensors of higher-orders by Kapteyn [75] and by de Lathauwer [76], receiving respectively the names *N-mode principal component analysis* and Higher-Order Singular Value Decomposition (HOSVD). The Tucker decomposition of a N^{th}-order tensor can be defined by:

Definition 4. *(Tucker decomposition) Given a N^{th}-order tensor $\mathcal{X} \in \mathbb{C}^{I_1 \times I_2 \times \cdots \times I_N}$, its Tucker decomposition is defined in the scalar form as*

$$x_{i_1,i_2,,\cdots,i_N} = \sum_{r_1=1}^{R_1} \sum_{r_2=1}^{R_2} \cdots \sum_{r_N=1}^{R_N} g_{r_1,r_2,\cdots,r_N} a^{(1)}_{i_1,r_1} a^{(2)}_{i_2,r_2} a^{(3)}_{i_3,r_3} \cdots a^{(N)}_{i_N,r_N}, \tag{3.7}$$

where $\mathcal{G} \in \mathbb{C}^{R_1 \times R_2 \times \cdots \times R_N}$ is called core tensor and $\mathbf{A}^{(n)} \in \mathbb{C}^{I_n \times R_n}$ for $n = 1, \cdots, N$ are the loading (factor) matrices. Alternative, concise representations of the Tucker model are

$$\mathcal{X} \triangleq [\![\mathcal{G}; \mathbf{A}^{(1)}, \mathbf{A}^{(2)}, \cdots, \mathbf{A}^{(N)}]\!], \tag{3.8}$$

$$= \mathcal{G} \times_1 \mathbf{A}^{(1)} \times_2 \mathbf{A}^{(2)} \cdots \times_N \mathbf{A}^{(N)}. \tag{3.9}$$

In the literature, the Tucker model is classified as a multilinear decomposition, and the tensor in (3.7) is said of rank-$(R_1, R_2, \cdots, R_N)$. It is important to note that this definition of rank differs from that one in Definition 3. A very limited number of works have proposed to calculate the typical and maximum ranks of a tensor, although the results are restricted to particular tensor dimensions [77, 78, 79].

The mode-n unfolding of the Tucker model is given by

$$\mathbf{X}_{I_{n+1}\cdots I_N I_1 \cdots I_{n-1} \times I_n} = \left[\left(\bigotimes_{i=n-1}^{1} \mathbf{A}^{(i)} \right) \otimes \left(\bigotimes_{i=N}^{n+1} \mathbf{A}^{(i)} \right) \right] \mathbf{G}_{R_{n+1}\cdots R_N R_1 \cdots \times R_n} \left(\mathbf{A}^{(n)} \right)^T, \tag{3.10}$$

and thus the unfoldings of the third-order Tucker decomposition are given by

$$X_{I_j I_k \times I_l} = \left(\mathbf{A}^{(k)} \otimes \mathbf{A}^{(j)} \right) \mathbf{G}_{R_j R_k \times R_l} \left(\mathbf{A}^{(l)} \right)^T, \tag{3.11}$$

where $(j, k, l) \in \{(1, 2, 3); (3, 1, 2); (2, 3, 1)\}$.

Although the Tucker decomposition can be applied to any tensor, it does not present uniqueness of its parameters, i.e. the matrix factors $\mathbf{A}^{(n)} \in \mathbb{C}^{I_n \times R_n}$ for $n = 1, \cdots, N$ cannot be uniquely recovered from the tensor $\mathcal{X}$ without further constraints on the core tensor.

3.3 PARAFAC decomposition

The Paralell Factor Analysis (PARAFAC)[2] decomposition was introduced by Harshman in [58] (and independently by Caroll and Cheng as Canonical Decomposition (CANDECOMP) in [59]), although its origin goes back to Hitchcock in 1927 [73]. Later the CANDECOMP/PARAFAC tensor decomposition was redefined by Kiers [80] as canonical polyadic

[2] Here in this thesis we limit the PARAFAC model to a third-order tensor. In [72] the PARAFAC decomposition is generalized to the N^{th}-order case.

(CP) decomposition, even though historically the term PARAFAC has endured. As a matter of curiosity, the PARAFAC model was initially studied in the areas of psychometrics and phonetics, and more recently this tensor model has been extensively used in signal processing for communications after the pioneering work of Sidiropoulos et al. [54].

Definition 5. *(PARAFAC decomposition) The scalar form of the PARAFAC decomposition of the tensor* $\mathcal{X} \in \mathbb{C}^{I_1 \times I_2 \times I_3}$ *is*

$$x_{i_1,i_2,i_3} = \sum_{r=1}^{R} a^{(1)}_{i_1,r} a^{(2)}_{i_2,r} a^{(3)}_{i_3,r}, \tag{3.12}$$

where $a^{(1)}_{i_1,r}$, $a^{(2)}_{i_2,r}$ *and* $a^{(3)}_{i_3,r}$ *are elements of loading (factor) matrices* $\mathbf{A}^{(1)} \in \mathbb{C}^{I_1 \times R}$, $\mathbf{A}^{(2)} \in \mathbb{C}^{I_2 \times R}$ *and* $\mathbf{A}^{(3)} \in \mathbb{C}^{I_3 \times R}$*, respectively. The tensor* $\mathcal{X}$ *can be alternatively written as*

$$\mathcal{X} \triangleq [\![\mathbf{A}^{(1)}, \mathbf{A}^{(2)}, \mathbf{A}^{(3)}]\!], \tag{3.13}$$

$$= \mathcal{I}_R \times_1 \mathbf{A}^{(1)} \times_2 \mathbf{A}^{(2)} \times_3 \mathbf{A}^{(3)}. \tag{3.14}$$

In (3.12), R is the smallest integer that gives the exact decomposition of $\mathcal{X}$ by the loading matrices. In fact, R, as seen in Definition 3, is then the rank of $\mathcal{X}$. Therefore, the PARAFAC model, alike the Tucker model, can be used to decompose any tensor.

We can also note that the trilinear PARAFAC is a less flexible model than the third-order Tucker, since (3.12)-(3.14) can obtained from (3.7)-(3.9) by restricting $\mathcal{G} = \mathcal{I}_R$. The diagonal identity tensor $\mathcal{I}_R$ forces the interactions between the loading matrices to be among their column vectors of the same index. In return, the more rigid structure of the PARAFAC model allows a unique decomposition of the tensor $\mathcal{X}$. Indeed, the uniqueness properties of a tensor decomposition is intrinsically linked to the interaction of its matrix factors, dictated by the core tensor. The CONFAC [81] decomposition is another good example of the Tucker decomposition with a constrained core tensor. The block representation of the PARAFAC decomposition is shown at Fig. 3.4.

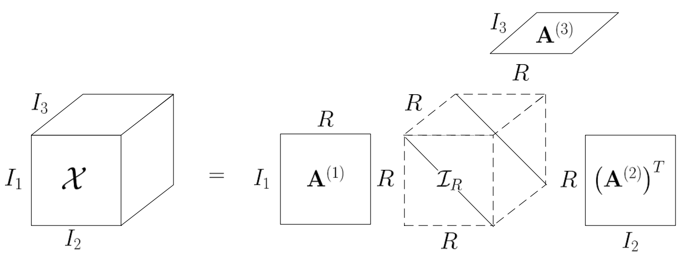

Figure 3.4: PARAFAC block representation

Frontal, horizontal and lateral slices of the PARAFAC model may be found by

$$\mathbf{X}_{\cdot\cdot i_3} = \mathbf{A}^{(1)} D_{i_3}\left(\mathbf{A}^{(3)}\right)\left(\mathbf{A}^{(2)}\right)^T \in \mathbb{C}^{I_1 \times I_2}, \tag{3.15}$$

$$\mathbf{X}_{i_1\cdot\cdot} = \mathbf{A}^{(2)} D_{i_1}\left(\mathbf{A}^{(1)}\right)\left(\mathbf{A}^{(3)}\right)^T \in \mathbb{C}^{I_2 \times I_3}, \tag{3.16}$$

$$\mathbf{X}_{\cdot i_2\cdot} = \mathbf{A}^{(3)} D_{i_2}\left(\mathbf{A}^{(2)}\right)\left(\mathbf{A}^{(1)}\right)^T \in \mathbb{C}^{I_3 \times I_1}, \tag{3.17}$$

and the mode-1, mode-2 and mode-3 unfoldings of $\mathcal{X}$ are given by

$$\mathbf{X}_{I_2 I_3 \times I_1} = (\mathbf{A}^{(3)} \diamond \mathbf{A}^{(2)})(\mathbf{A}^{(1)})^T, \tag{3.18}$$

$$\mathbf{X}_{I_3 I_1 \times I_2} = (\mathbf{A}^{(1)} \diamond \mathbf{A}^{(3)})(\mathbf{A}^{(2)})^T, \tag{3.19}$$

$$\mathbf{X}_{I_1 I_2 \times I_3} = (\mathbf{A}^{(2)} \diamond \mathbf{A}^{(1)})(\mathbf{A}^{(3)})^T. \tag{3.20}$$

A symmetry between the loading matrices in (3.18)-(3.20) provides a valuable insight when it is necessary to work with different unfoldings of a same tensor.

3.3.1 Uniqueness of the PARAFAC decomposition

The most remarkable advantage of the PARAFAC decomposition over the Tucker decomposition is its essential uniqueness property, which means that any triplet $(\bar{\mathbf{A}}^{(1)}, \bar{\mathbf{A}}^{(2)}, \bar{\mathbf{A}}^{(3)})$ is related to another triplet $(\mathbf{A}^{(1)}, \mathbf{A}^{(2)}, \mathbf{A}^{(3)})$ via the relation

$$\bar{\mathbf{A}}^{(i)} = \mathbf{A}^{(i)} \mathbf{\Pi} \mathbf{\Lambda}^{(i)}, \tag{3.21}$$

where $\mathbf{\Lambda}^{(i)}$ for i =1, 2 and 3 are diagonal matrices whose the product is equal to the identity matrix of order R, and $\mathbf{\Pi}$ is a permutation matrix. Therefore, essential uniqueness means that any triplet is unique up to arbitrary column scaling and permutation ambiguities of the factor matrices.

For the three-order tensor in (3.12), the uniqueness of its PARAFAC decomposition is satisfied under the Kruskal's sufficient condition, i.e.

$$k_{\mathbf{A}^{(1)}} + k_{\mathbf{A}^{(2)}} + k_{\mathbf{A}^{(3)}} \geqslant 2R + 2, \tag{3.22}$$

where the Kruskal rank was presented in Definition 1.

As the name reveals, this condition was proposed by Kruskal [67], and it is a widely adopted condition to ensure the uniqueness of the factors of the PARAFAC decomposition. Some works have discussed in which cases the condition (3.22) is necessary or only sufficient [82, 83].

3.4 PARATUCK2 decomposition

While any tensor can be decomposed following the Tucker and the PARAFAC models, the matrix factors obtained from these decompositions may not bring any evident meaning, whether due to the existence of inherent ambiguities on the solutions of the first model or by the over-simplicity of the second one to represent more complex scenarios.

The PARATUCK2 tensor decomposition was introduced by Harshman and Lundy in [62], and its name was derived from the presence of properties of both PARAFAC and Tucker2[3] tensor decompositions.

Definition 6. *(PARATUCK2 decomposition) The scalar form of the PARATUCK2 decomposition of a third-order tensor* $\mathcal{X} \in \mathbb{C}^{I_1 \times I_2 \times I_3}$ *is given by*

$$x_{i_1,i_2,i_3} = \sum_{r_1=1}^{R_1} \sum_{r_2=1}^{R_2} a^{(1)}_{i_1,r_1} a^{(2)}_{i_3,r_1} u_{r_1,r_2} b^{(2)}_{i_3,r_2} b^{(1)}_{i_2,r_2}, \tag{3.23}$$

where $\mathbf{A}^{(1)}$ *and* $\mathbf{B}^{(1)}$ *are denoted loading (factor) matrices,* $\mathbf{A}^{(2)}$ *and* $\mathbf{B}^{(2)}$ *are commonly called interaction matrices, and* $\mathbf{U}$ *is called core matrix.*

The block diagram of the PARATUCK2 model is given in Fig. 3.5. As done for the Tucker and the PARAFAC, the PARATUCK2 model was already extended to N^{th}-order tensors, being named PARATUCK-(N_1, N), where N_1 corresponds to the number of interaction matrices [63].

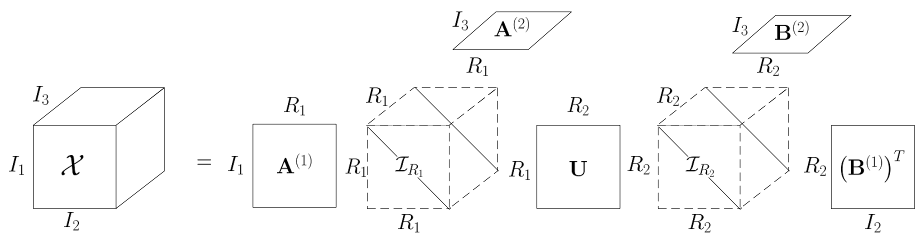

Figure 3.5: PARATUCK2 block representation

Frontal, horizontal and lateral slices of the PARATUCK2 model are given in order by

$$\mathbf{X}_{\cdot\cdot i_3} = \mathbf{A}^{(1)} D_{i_3}\left(\mathbf{A}^{(2)}\right) \mathbf{U} D_{i_3}\left(\mathbf{B}^{(2)}\right)\left(\mathbf{B}^{(1)}\right)^T \in \mathbb{C}^{I_1 \times I_2}, \tag{3.24}$$

$$\mathbf{X}_{i_1 \cdot\cdot} = \mathbf{B}^{(1)}\left[\left(\mathbf{I}_{R_2} \otimes \mathbf{A}^{(1)}_{i_1\cdot}\right) \diamond (\mathrm{vec}(\mathbf{U}))^T\right]\left(\left(\mathbf{B}^{(2)}\right)^T \diamond \left(\mathbf{A}^{(2)}\right)^T\right) \in \mathbb{C}^{I_2 \times I_3}, \tag{3.25}$$

$$\mathbf{X}_{\cdot i_2 \cdot} = \left(\left(\mathbf{B}^{(2)}\right)^T \diamond \left(\mathbf{A}^{(2)}\right)^T\right)^T \left[\left(\mathbf{B}^{(1)}_{i_2\cdot} \otimes \mathbf{I}_{R_1}\right) \diamond (\mathrm{vec}(\mathbf{U}))^T\right]^T \left(\mathbf{A}^{(1)}\right)^T \in \mathbb{C}^{I_3 \times I_1}, \tag{3.26}$$

[3]The Tucker2 decomposition corresponds to the Tucker3 model with one of its loading matrix as an identity.

and the mode-1, mode-2 and mode-3 unfoldings are respectively

$$\mathbf{X}_{I_2 I_3 \times I_1} = \left(\mathbf{I}_{I_3} \otimes \mathbf{B}^{(1)}\right) \mathbf{F}_1 \left(\mathbf{A}^{(1)}\right)^T, \tag{3.27}$$

$$\mathbf{X}_{I_3 I_1 \times I_2} = \left(\mathbf{I}_{I_1} \otimes \left(\left(\mathbf{B}^{(2)}\right)^T \diamond \left(\mathbf{A}^{(2)}\right)^T\right)^T\right) \mathbf{F}_2 \left(\mathbf{B}^{(1)}\right)^T, \tag{3.28}$$

$$\mathbf{X}_{I_1 I_2 \times I_3} = \left(\mathbf{I}_{I_2} \otimes \mathbf{A}^{(1)}\right) \mathbf{F}_3 \left(\left(\mathbf{B}^{(2)}\right)^T \diamond \left(\mathbf{A}^{(2)}\right)^T\right), \tag{3.29}$$

where

$$\mathbf{F}_1 = \begin{bmatrix} D_1\left(\mathbf{B}^{(2)}\right) \mathbf{U}^T D_1\left(\mathbf{A}^{(2)}\right) \\ \vdots \\ D_{I_3}\left(\mathbf{B}^{(2)}\right) \mathbf{U}^T D_{I_3}\left(\mathbf{A}^{(2)}\right) \end{bmatrix} \in \mathbb{C}^{R_2 I_3 \times R_1}, \tag{3.30}$$

$$\mathbf{F}_2 = \begin{bmatrix} \left[\left(\mathbf{I}_{R_2} \otimes \mathbf{A}^{(1)}_{1\cdot}\right) \diamond (\mathrm{vec}(\mathbf{U}))^T\right]^T \\ \vdots \\ \left[\left(\mathbf{I}_{R_2} \otimes \mathbf{A}^{(1)}_{I_1\cdot}\right) \diamond (\mathrm{vec}(\mathbf{U}))^T\right]^T \end{bmatrix} \in \mathbb{C}^{R_1 R_2 I_1 \times R_2}, \tag{3.31}$$

$$\mathbf{F}_3 = \begin{bmatrix} \left[\left(\mathbf{B}^{(1)}_{1\cdot} \otimes \mathbf{I}_{R_1}\right) \diamond (\mathrm{vec}(\mathbf{U}))^T\right] \\ \vdots \\ \left[\left(\mathbf{B}^{(1)}_{I_2\cdot} \otimes \mathbf{I}_{R_1}\right) \diamond (\mathrm{vec}(\mathbf{U}))^T\right] \end{bmatrix} \in \mathbb{C}^{R_1 I_2 \times R_1 R_2}. \tag{3.32}$$

The three unfoldings (3.27)-(3.29) can be used to estimate $\mathbf{A}^{(1)}$, $\mathbf{B}^{(1)}$ and the Khatri-Rao product $\left(\left(\mathbf{B}^{(2)}\right)^T \diamond \left(\mathbf{A}^{(2)}\right)^T\right)$ through a series of matrix-based methods, as in a Least Squares (LS) sense for example. The core matrix $\mathbf{U}$ can be found by resorting to the vectorized form

$$\mathbf{x}_{I_1 I_2 I_3} = \left[\left(\left(\mathbf{B}^{(2)}\right)^T \diamond \left(\mathbf{A}^{(2)}\right)^T\right)^T \diamond \left(\mathbf{B}^{(1)} \otimes \mathbf{A}^{(1)}\right)\right] \mathrm{vec}\left(\mathbf{U}\right), \tag{3.33}$$

and $\mathbf{A}^{(2)}$ and $\mathbf{B}^{(2)}$ can be solved independently by resorting to the vectorized form of each frontal slice, i.e. applying Property (A.13) on (3.24)

$$\mathrm{vec}(\mathbf{X}_{\cdot\cdot i_3}) = (\mathbf{X}_{I_1 I_2 \times I_3})_{\cdot i_3} = \left(\mathbf{B}^{(1)} \diamond \mathbf{A}^{(1)} D_{i_3}\left(\mathbf{A}^{(2)}\right) \mathbf{U}\right) \left(\mathbf{B}^{(2)}_{i_3\cdot}\right)^T, \tag{3.34}$$

$$= \left(\mathbf{B}^{(1)} D_{i_3}\left(\mathbf{B}^{(2)}\right) \mathbf{U}^T \diamond \mathbf{A}^{(1)}\right) \left(\mathbf{A}^{(2)}_{i_3\cdot}\right)^T. \tag{3.35}$$

The PARATUCK2 model, as already pointed out, share some similarities with the PARAFAC model. If $\mathbf{U}$ is a diagonal matrix, then it can be proved with some effort that from (3.27)-(3.29) it gives

$$\mathbf{X}_{I_2 I_3 \times I_1} = \left(\left(\mathbf{B}^{(2)} \odot \mathbf{A}^{(2)}\right) \mathbf{U} \diamond \mathbf{B}^{(1)}\right) \left(\mathbf{A}^{(1)}\right)^T, \tag{3.36}$$

$$\mathbf{X}_{I_3 I_1 \times I_2} = \left(\mathbf{A}^{(1)} \diamond \left(\mathbf{B}^{(2)} \odot \mathbf{A}^{(2)}\right) \mathbf{U}\right) \left(\mathbf{B}^{(1)}\right)^T, \tag{3.37}$$

$$\mathbf{X}_{I_1 I_2 \times I_3} = \left(\mathbf{B}^{(1)} \diamond \mathbf{A}^{(1)}\right) \mathbf{U}^T \left(\mathbf{B}^{(2)} \odot \mathbf{A}^{(2)}\right)^T, \tag{3.38}$$

and from correspondence with the unfoldings (3.18)-(3.20), we can deduce that the PARATUCK2 model becomes a PARAFAC model according to

$$\mathcal{X} = [\![\mathbf{A}^{(1)}, \mathbf{B}^{(1)}, (\mathbf{B}^{(2)} \odot \mathbf{A}^{(2)})\mathbf{U}]\!]. \tag{3.39}$$

3.4.1 Uniqueness of the PARATUCK2 decomposition

The PARATUCK2 model is interesting in situations where an intermediate flexibility between the PARAFACand Tucker decompositions is required [70, 84]. In other words, PARATUCK2 is suitable in a scenario where there are interactions between some components (loading matrices) that cannot be modeled by the PARAFAC model, but uniqueness of the model is still necessary.

Perhaps the most thorough study on the uniqueness of the PARATUCK2 model is still that one presented in its very introduction [62], whose main points are repeated in the following remark.

Remark 1. *The uniqueness properties of the PARATUCK2 decomposition is ensured under the following assumptions: i) All matrices of the model are full rank; ii)* $\mathbf{U}$ *with entries different from zero; iii) Matrices* $\mathbf{A}^{(2)}$ *and* $\mathbf{B}^{(2)}$ *with the same number of columns* ($R_1 = R_2 = R$)*. Uniqueness is then ensured up to column scaling and permutation ambiguities defined by means of the following equations*

$$\bar{\mathbf{A}}^{(1)} = \mathbf{A}^{(1)} \left(\mathbf{P}\mathbf{\Lambda}^{(A)}\right), \tag{3.40}$$

$$\bar{\mathbf{B}}^{(1)} = \mathbf{B}^{(1)} \left(\mathbf{Q}\mathbf{\Lambda}^{(B)}\right), \tag{3.41}$$

$$\bar{\mathbf{U}} = \left(\mathbf{\Lambda}^{(R_1)}\right)^{-1} \left(\mathbf{\Lambda}^{(A)}\right)^{-1} \mathbf{P}^T\mathbf{U}\mathbf{Q} \left(\mathbf{\Lambda}^{(B)}\right)^{-1} \left(\mathbf{\Lambda}^{(R_2)}\right)^{-1}, \tag{3.42}$$

where $\mathbf{P} \in \mathbb{R}^{R\times R}$ *and* $\mathbf{Q} \in \mathbb{R}^{R\times R}$ *are permutation matrices,* ($\mathbf{\Lambda}^{(A)}$,$\mathbf{\Lambda}^{(B)}$, $\mathbf{\Lambda}^{(R_1)}$, $\mathbf{\Lambda}^{(R_2)}$) *are diagonal matrices, and for any* $n \in \{1, \cdots, N\}$

$$D_n\left(\bar{\mathbf{A}}^{(2)}\right) = \left(z_n^{-1}\mathbf{P}^T\right) D_n(\mathbf{A}^{(2)}) \left(\mathbf{P}\mathbf{\Lambda}^{(R_1)}\right), \tag{3.43}$$

$$D_n\left(\bar{\mathbf{B}}^{(2)}\right) = \left(z_n\mathbf{Q}^T\right) D_n(\mathbf{B}^{(2)}) \left(\mathbf{Q}\mathbf{\Lambda}^{(R_2)}\right), \tag{3.44}$$

where z_n *is a scalar.*

In [56, 63] some theorems were deduced to ensure the uniqueness of PARATUCK2. The hypotheses therein are that $\mathbf{B}^{(2)}$, $\mathbf{A}^{(2)}$ and $\mathbf{U}$ are known, then consequently from (3.43) and (3.44) $\mathbf{P} = \mathbf{\Lambda}^{(R_1)} = \mathbf{I}_R$ and $\mathbf{Q} = \mathbf{\Lambda}^{(R_2)} = \mathbf{I}_R$, and from (3.42) $\mathbf{\Lambda}^{(A)} = \alpha\mathbf{I}_R$ and

$\mathbf{\Lambda}^{(B)} = (1/\alpha)\mathbf{I}_R$, where α is a scalar. Finally, $\bar{\mathbf{A}}^{(1)} = \alpha\mathbf{A}^{(1)}$ and $\bar{\mathbf{B}} = (1/\alpha)\mathbf{B}^{(1)}$. Although those theorems let one avoid all model ambiguities (apart from α) without the need to obey all those initial conditions presented in Remark 1, they are not useful for the communication models present in this thesis, where neither $\mathbf{B}^{(2)}$ nor $\mathbf{U}$ would be known. In the following, a new theorem is derived for the essential uniqueness of the PARATUCK2 decomposition.

Theorem 2. *Assuming that the three hypotheses in Remark 1 are valid, then admitting that $\mathbf{B}^{(1)}$, $\mathbf{A}^{(2)}$ and also a row of $\mathbf{B}^{(2)}$ are known, permutation ambiguities on all matrix factors of the PARATUCK2 model (3.23) are avoided if*

$$det(\mathbf{A}^{(2)}[n_1, n_2; i, j]) \neq 0 \ \ \forall i \ \ and \ \ j = 1, ..., R, \ \ i \neq j, \tag{3.45}$$

where $\mathbf{A}^{(2)}[n_1, n_2; i, j]$ is a 2×2 submatrix of $\mathbf{A}^{(2)}$ comprising its n_1^{th} and n_2^{th} rows and its i^{th} and j^{th} columns.

Proof. The initial hypothesis of Theorem 2 is that the PARATUCK2 model in (3.23) has a unique decomposition, with the aforementioned conditions stated in Remark 1. This means, in other words, that (3.40)-(3.44) are always valid. In addition, Theorem 2 adds the hypothesis that $\mathbf{B}^{(1)}$ and $\mathbf{A}^{(2)}$ are known, and from (3.41) we deduce that $\mathbf{Q} = \mathbf{\Lambda}^{(B)} = \mathbf{I}_R$. Furthermore, if a n^{th} row of $\mathbf{B}^{(2)}$ is also known, we deduce from (3.44) that $\mathbf{\Lambda}^{(R_2)} = (z_n)^{-1}\mathbf{I}_R$, and consequently $z_n = z$ for all $n = 1, ..., N$.

Assuming *a priori* that $\mathbf{P} = \mathbf{I}_R$, knowledge of $\mathbf{A}^{(2)}$ allows to deduce from Eq. (3.43) that $\mathbf{\Lambda}^{(R_1)} = z\mathbf{I}_R$. Equations (3.40) and (3.42) are then simplified as

$$\bar{\mathbf{A}}^{(1)} = \mathbf{A}^{(1)}\mathbf{\Lambda}^{(A)}$$
$$\bar{\mathbf{U}} = \left(\mathbf{\Lambda}^{(A)}\right)^{-1}\mathbf{U}.$$

Now, we show how to choose $\mathbf{A}^{(2)}$ so that the permutation matrix $\mathbf{P}$ be equal to the identity matrix. Eq. (3.43) can be rewritten in scalar form, for $i = 1, \cdots, R$, as

$$a^{(2)}_{n,i} = z^{-1}\delta_i^{(R_1)} \sum_{m_R=1}^{R} p^2_{m_R,i} a^{(2)}_{n,m_R} \tag{3.46}$$

where $p_{m_R,i}$ is the element (m_R, i) of $\mathbf{P}$, and $\delta_i^{(R_1)}$ is the i^{th} diagonal element of $\mathbf{\Lambda}^{(R_1)}$.

Let us consider a permutation of two columns (i, j) of $\mathbf{A}^{(2)}$ such that $p_{j,i} = 1$ with $i \neq j$. Application of this permutation to two rows n_1 and n_2 in (3.46) gives

$$\delta_i^{(R_1)} = z\frac{a^{(2)}_{n_1,i}}{a^{(2)}_{n_1,j}} = z\frac{a^{(2)}_{n_2,i}}{a^{(2)}_{n_2,j}},$$

leading to $det(\mathbf{A}^{(2)}[n_1, n_2; i, j]) = 0$, where $\mathbf{A}^{(2)}[n_1, n_2; i, j] = \begin{bmatrix} a^{(2)}_{n_1,i} & a^{(2)}_{n_1,j} \\ a^{(2)}_{n_2,i} & a^{(2)}_{n_2,j} \end{bmatrix}$. A sufficient condition to avoid such a permutation is

$$det(\mathbf{A}^{(2)}[n_1, n_2; i, j]) \neq 0. \tag{3.47}$$

Therefore, column permutations are avoided in $\mathbf{A}^{(2)}$ if the condition (3.47) is satisfied for any pair of rows (n_1, n_2) and all pairs of columns (i, j), which leads to the following general condition

$$\det(\mathbf{A}^{(2)}[n_1, n_2; i, j]) \neq 0 \;\; \forall i \;\text{ and }\; j = 1, ..., R, \;\; i \neq j.$$

□

3.5 Nested PARAFAC decomposition

The nested PARAFAC decomposition was recently introduced by de Almeida et al. [64] to model a space-time-frequency transmission scheme using a double Khatri-Rao coding. Due to its recent apparition, it is not known other works besides [64, 85, 69] that have approached this tensor decomposition, either from a theoretical point of view or in terms of its possible applications. Particularly in [69], representations of nested PARAFAC using mode-n products and also new unfoldings of this model for the estimation of all of its parameters were provided.

After the presentation of this model in this section, two new theorems about the uniqueness of the model will be derived. These theoretical contributions will be used directly in the modeling of the cooperative communication systems and its receivers in the following chapter.

Definition 7. *(Nested PARAFAC decomposition) The scalar form of the nested PARAFAC decomposition of a fourth-order tensor $\mathcal{X} \in \mathbb{C}^{I_1 \times I_2 \times I_3 \times I_4}$ is defined by means of the following equation*

$$x_{i_1,i_2,i_3,i_4} = \sum_{r_1=1}^{R_1} \sum_{r_2=1}^{R_2} b^{(1)}_{i_1,r_1} b^{(2)}_{i_2,r_1} u_{r_1,r_2} d^{(1)}_{i_3,r_2} d^{(2)}_{i_4,r_2}, \tag{3.48}$$

where $\mathbf{U} \in \mathbb{C}^{R_1 \times R_2}$ is the core matrix, and $\mathbf{B}^{(i)} \in \mathbb{C}^{I_i \times R_1}$ for $i \in \{1, 2\}$ and $\mathbf{D}^{(j-2)} \in \mathbb{C}^{I_j \times R_2}$ for $j \in \{3, 4\}$ are the loading (factor) matrices.

A number of useful equations can be derived for this tensor decomposition. Let us define the third-order tensors $\mathcal{W} \in \mathbb{C}^{R_1 \times I_3 \times I_4}$ and $\mathcal{Z} \in \mathbb{C}^{I_1 \times I_2 \times R_2}$ such as

$$w_{r_1,i_3,i_4} = \sum_{r_2=1}^{R_2} u_{r_1,r_2} d^{(1)}_{i_3,r_2} d^{(2)}_{i_4,r_2} \tag{3.49}$$

and

$$z_{i_1,i_2,r_2} = \sum_{r_1=1}^{R_1} b^{(1)}_{i_1,r_1} b^{(2)}_{i_2,r_1} u_{r_1,r_2}. \tag{3.50}$$

These tensors satisfy a PARAFAC decomposition with $(\mathbf{U}, \mathbf{D}^{(1)}, \mathbf{D}^{(2)})$ and $(\mathbf{B}^{(1)}, \mathbf{B}^{(2)}, \mathbf{U}^T)$ as matrix factors, respectively. They can be written in terms of mode-n products as

$$\mathcal{W} = \mathcal{I}_{R_2} \times_1 \mathbf{U} \times_2 \mathbf{D}^{(1)} \times_3 \mathbf{D}^{(2)}, \tag{3.51}$$

$$\mathcal{Z} = \mathcal{I}_{R_1} \times_1 \mathbf{B}^{(1)} \times_2 \mathbf{B}^{(2)} \times_3 \mathbf{U}^T. \tag{3.52}$$

According to the correspondences between these tensors and the PARAFAC model in (3.14), the mode-1, mode-2 and mode-3 unfoldings (3.18)-(3.20) of $\mathcal{W}$ become

$$\mathbf{W}_{I_3 I_4 \times R_1} = \left(\mathbf{D}^{(2)} \diamond \mathbf{D}^{(1)}\right) \mathbf{U}^T, \tag{3.53}$$

$$\mathbf{W}_{I_4 R_1 \times I_3} = \left(\mathbf{U} \diamond \mathbf{D}^{(2)}\right) \left(\mathbf{D}^{(1)}\right)^T, \tag{3.54}$$

$$\mathbf{W}_{R_1 I_3 \times I_4} = \left(\mathbf{D}^{(1)} \diamond \mathbf{U}\right) \left(\mathbf{D}^{(2)}\right)^T, \tag{3.55}$$

and the correspondent unfoldings for the tensor $\mathcal{Z}$ are

$$\mathbf{Z}_{I_2 R_2 \times I_1} = \left(\mathbf{U}^T \diamond \mathbf{B}^{(2)}\right) \left(\mathbf{B}^{(1)}\right)^T, \tag{3.56}$$

$$\mathbf{Z}_{R_2 I_1 \times I_2} = \left(\mathbf{B}^{(1)} \diamond \mathbf{U}^T\right) \left(\mathbf{B}^{(2)}\right)^T, \tag{3.57}$$

$$\mathbf{Z}_{I_1 I_2 \times R_2} = \left(\mathbf{B}^{(2)} \diamond \mathbf{B}^{(1)}\right) \mathbf{U}. \tag{3.58}$$

Consider the variable changes $k_1 = (i_4 - 1)I_3 + i_3$ and $k_2 = (i_2 - 1)I_1 + i_1$, with $k_1 \in \{1, 2, \cdots, K_1\}$ and $k_2 \in \{1, 2, \cdots, K_2\}$, where $K_1 = I_3 I_4$ and $K_2 = I_1 I_2$. Combining the last two modes of $\mathcal{X}$ and the first two ones, the nested PARAFAC decomposition (3.48) can be rewritten in terms of the following two PARAFAC decompositions, with $(\mathbf{B}^{(1)}, \mathbf{B}^{(2)}, \mathbf{W}_{I_3 I_4 \times R_1})$ and $(\mathbf{Z}_{I_1 I_2 \times R_2}, \mathbf{D}^{(1)}, \mathbf{D}^{(2)})$ as matrix factors

$$x_{i_1,i_2,k_1} = \sum_{r_1=1}^{R_1} b^{(1)}_{i_1,r_1} b^{(2)}_{i_2,r_1} w_{k_1,r_1} \tag{3.59}$$

and

$$x_{k_2,i_3,i_4} = \sum_{r_2=1}^{R_2} z_{k_2,r_2} d^{(1)}_{i_3,r_2} d^{(2)}_{i_4,r_2}. \tag{3.60}$$

Such third-order PARAFAC models obtained by combining two modes of $\mathcal{X}$ can be rewritten as

$$\mathcal{X}^{(1)} = \mathcal{I}_{R_1} \times_1 \mathbf{B}^{(1)} \times_2 \mathbf{B}^{(2)} \times_3 \mathbf{W}_{I_3 I_4 \times R_1}, \tag{3.61}$$

$$\mathcal{X}^{(2)} = \mathcal{I}_{R_2} \times_1 \mathbf{Z}_{I_1 I_2 \times R_2} \times_2 \mathbf{D}^{(1)} \times_3 \mathbf{D}^{(2)}. \tag{3.62}$$

These two equations highlight the nesting of the PARAFAC models $\mathcal{W}$ or $\mathcal{Z}$ into the nested PARAFAC model $\mathcal{X}$. The contracted forms $\mathcal{X}^{(1)}$ and $\mathcal{X}^{(2)}$ carry the same elements of $\mathcal{X}$.

Therefore, the mode-1 and mode-2 unfoldings of $\mathcal{X}^{(1)}$ leads to

$$\mathbf{X}_{I_2I_3I_4\times I_1} = \mathbf{X}^{(1)}_{I_2K_1\times I_1} = \left(\mathbf{W}_{I_3I_4\times R_1} \diamond \mathbf{B}^{(2)}\right)\left(\mathbf{B}^{(1)}\right)^T, \tag{3.63}$$

$$\mathbf{X}_{I_3I_4I_1\times I_2} = \mathbf{X}^{(1)}_{K_1I_1\times I_2} = \left(\mathbf{B}^{(1)} \diamond \mathbf{W}_{I_3I_4\times R_1}\right)\left(\mathbf{B}^{(2)}\right)^T, \tag{3.64}$$

and the mode-2 and mode-3 unfoldings of $\mathcal{X}^{(2)}$ leads to

$$\mathbf{X}_{I_4I_1I_2\times I_3} = \mathbf{X}^{(2)}_{I_4K_2\times I_3} = \left(\mathbf{Z}_{I_1I_2\times R_2} \diamond \mathbf{D}^{(2)}\right)\left(\mathbf{D}^{(1)}\right)^T, \tag{3.65}$$

$$\mathbf{X}_{I_1I_2I_3\times I_4} = \mathbf{X}^{(2)}_{K_2I_3\times I_4} = \left(\mathbf{D}^{(1)} \diamond \mathbf{Z}_{I_1I_2\times R_2}\right)\left(\mathbf{D}^{(2)}\right)^T. \tag{3.66}$$

Eqs. (3.63)-(3.66) are the mode-1, mode-2, mode-3 and mode-4 unfoldings of $\mathcal{X}$. As the matricisation of a third-order tensor usually consists in combining two of its modes, the passage from a fourth-order tensor to a third-order tensor to a matrix in this case is done by two sequential combination of two modes, e.g. (3.66) is obtained from $\mathcal{X}^{(2)}$, which is in its turn obtained from $\mathcal{X}$.

The unfolding $\mathbf{X}_{I_1I_2\times I_3I_4}$ of $\mathcal{X}$ can be deduced as a mode-3 unfolding of $\mathcal{X}^{(1)}$, or as a mode-1 unfolding of $\mathcal{X}^{(2)}$, which gives

$$\begin{aligned}\mathbf{X}_{I_1I_2\times I_3I_4} &= \left(\mathbf{B}^{(2)} \diamond \mathbf{B}^{(1)}\right)\left(\mathbf{W}_{I_3I_4\times R_1}\right)^T, &(3.67)\\ &= \mathbf{Z}_{I_1I_2\times R_2}\left(\mathbf{D}^{(2)} \diamond \mathbf{D}^{(1)}\right)^T. &(3.68)\end{aligned}$$

Replacing $\mathbf{W}_{I_3I_4\times R_1}$ and $\mathbf{Z}_{I_1I_2\times R_2}$ by their respective expressions (3.53) and (3.58) into (3.67) and (3.68), $\mathbf{X}_{I_1I_2\times I_3I_4}$ can be rewritten as

$$\mathbf{X}_{I_1I_2\times I_3I_4} = \left(\mathbf{B}^{(2)} \diamond \mathbf{B}^{(1)}\right)\mathbf{U}\left(\mathbf{D}^{(2)} \diamond \mathbf{D}^{(1)}\right)^T. \tag{3.69}$$

This unfolding (3.69) illustrates, once again, the nesting of the PARAFAC decompositions of $\mathcal{W}$ and $\mathcal{Z}$ into $\mathcal{X}$. The factors $\left(\mathbf{B}^{(2)} \diamond \mathbf{B}^{(1)}\right)$ and $\left(\mathbf{D}^{(2)} \diamond \mathbf{D}^{(1)}\right)$ results respectively from the combination of the first two modes of the tensor $\mathcal{Z}$ and of the last two modes of the tensor $\mathcal{W}$, while the central factor $\mathbf{U}$ is the common factor to the PARAFAC decompositions of these tensors.

The factor $\mathbf{U}$ can be isolated using its vectorized form $\mathrm{vec}\,(\mathbf{U})$ by applying Property (A.9) to (3.69), which gives

$$\mathrm{vec}\,(\mathbf{X}_{I_1I_2\times I_3I_4}) = \left(\left(\mathbf{D}^{(2)} \diamond \mathbf{D}^{(1)}\right) \otimes \left(\mathbf{B}^{(2)} \diamond \mathbf{B}^{(1)}\right)\right)\mathrm{vec}\,(\mathbf{U}). \tag{3.70}$$

3.5.1 Uniqueness of the nested PARAFAC decomposition

The nested PARAFAC and PARATUCK2 models belong to what is called PARAFAC-family of tensor decompositions, and thus the nested PARAFAC model, alike the PARAFACand PARATUCK2 models, presents the interesting property of essential uniqueness.

Indeed, given that nested PARAFAC model can be written in a PARAFACform, their properties of uniqueness can be obtained directly from the ones concerning this last model, which has well-known, established properties.

Two new theorems on the uniqueness of the nested PARAFAC model are proposed in the following.

Theorem 3. *Assuming that the elements of* $\mathbf{U}$ *are randomly drawn from a continuous distribution, then essential uniqueness of the nested PARAFAC decomposition (3.48) is ensured if both conditions*

$$k_{\mathbf{B}^{(1)}} + k_{\mathbf{B}^{(2)}} \geqslant \max(2R_1 - R_2, R_1) + 2, \tag{3.71}$$

$$k_{\mathbf{D}^{(1)}} + k_{\mathbf{D}^{(2)}} \geqslant \max(2R_2 - R_1, R_2) + 2 \tag{3.72}$$

are satisfied.

Proof. It is shown that the fourth-order nested PARAFAC model (3.48) can be rewritten as two third-order PARAFAC models (3.59) and (3.60), whose one of their matrix factors is a matrix unfolding of another third-order PARAFAC model ((3.49) or (3.50)). Sufficient conditions for uniqueness of the nested PARAFAC model can then be derived by applying the Kruskal's sufficient condition (3.22) to the associated third-order PARAFAC models (3.49) and (3.59), or (3.50) and (3.60).

Assuming that the elements of $\mathbf{U}$ are randomly drawn from a continuous distribution implies that $\mathbf{U}$ is full k-rank with probability one, i.e. $\mathrm{rank}(\mathbf{U}) = k_{\mathbf{U}} = k_{\mathbf{U}^T} = \min(R_1, R_2)$.

Let us first consider the case $R_2 \geqslant R_1$ for which we have $k_{\mathbf{U}} = k_{\mathbf{U}^T} = R_1$. Application of the Kruskal's condition to (3.49) and (3.59) gives respectively

$$k_{\mathbf{D}^{(1)}} + k_{\mathbf{D}^{(2)}} + k_{\mathbf{U}} \geqslant 2R_2 + 2 \tag{3.73}$$

and

$$k_{\mathbf{B}^{(1)}} + k_{\mathbf{B}^{(2)}} + k_{\mathbf{W}_{I_3 I_4 \times R_1}} \geqslant 2R_1 + 2. \tag{3.74}$$

Replacing $k_{\mathbf{U}}$ by R_1 in (3.73), we obtain

$$k_{\mathbf{D}^{(1)}} + k_{\mathbf{D}^{(2)}} \geqslant 2R_2 - R_1 + 2. \tag{3.75}$$

Since $2R_2 - R_1 + 2 \geqslant R_2 + 2$, and according to Property (1), this condition (3.75) implies that $\mathbf{D}^{(2)} \diamond \mathbf{D}^{(1)}$ is full column rank, and consequently, from (3.53) we deduce that $k_{\mathbf{W}_{I_3 I_4 \times R_1}} = k_{\mathbf{U}^T} = R_1$. The condition (3.74) then becomes

$$k_{\mathbf{B}^{(1)}} + k_{\mathbf{B}^{(2)}} \geqslant R_1 + 2. \tag{3.76}$$

In summary, the conditions (3.75) and (3.76) are sufficient to ensure essential uniqueness of the nested PARAFAC model when $R_2 \geqslant R_1$.

In the case $R_1 \geqslant R_2$, we have $k_{\mathbf{U}} = k_{\mathbf{U}^T} = R_2$, and application of the Kruskal's condition to the PARAFAC models (3.50) and (3.60) gives respectively

$$k_{\mathbf{B}^{(1)}} + k_{\mathbf{B}^{(2)}} + k_{\mathbf{U}^T} \geqslant 2R_1 + 2, k_{\mathbf{Z}_{I_1 I_2 \times R_2}} + k_{\mathbf{D}^{(1)}} + k_{\mathbf{D}^{(2)}} \qquad \geqslant 2R_2 + 2.$$

Following the same reasoning as in the previous case, it is easy to deduce the following sufficient conditions when $R_1 \geqslant R_2$

$$k_{\mathbf{B}^{(1)}} + k_{\mathbf{B}^{(2)}} \geqslant 2R_1 - R_2 + 2, \tag{3.77}$$

$$k_{\mathbf{D}^{(1)}} + k_{\mathbf{D}^{(2)}} \geqslant R_2 + 2, \tag{3.78}$$

The conditions (3.71) and (3.72) gather the conditions (3.75) and (3.76) obtained when $R_2 \geqslant R_1$, and the conditions (3.77) and (3.78) for the case $R_1 \geqslant R_2$. $\square$

Theorem 4. *When the sufficient conditions (3.71) and (3.72) are satisfied, essential uniqueness of the nested PARAFAC decomposition means that two quintuplets of matrix factors which are solutions of this decomposition, are linked by the following relations*

$$\bar{\mathbf{B}}^{(1)} = \mathbf{B}^{(1)}\mathbf{\Pi}^{(W)}\mathbf{\Lambda}^{(1)} \tag{3.79}$$

$$\bar{\mathbf{B}}^{(2)} = \mathbf{B}^{(2)}\mathbf{\Pi}^{(W)}\mathbf{\Lambda}^{(2)} \tag{3.80}$$

$$\bar{\mathbf{D}}^{(1)} = \mathbf{D}^{(1)}\mathbf{\Pi}^{(Z)}\mathbf{\Lambda}^{(3)} \tag{3.81}$$

$$\bar{\mathbf{D}}^{(2)} = \mathbf{D}^{(2)}\mathbf{\Pi}^{(Z)}\mathbf{\Lambda}^{(4)} \tag{3.82}$$

$$\bar{\mathbf{U}} = \left(\mathbf{\Pi}^{(W)}\mathbf{\Lambda}^{(2)}\mathbf{\Lambda}^{(1)}\right)^{-1}\mathbf{U}\left(\mathbf{\Pi}^{(Z)}\mathbf{\Lambda}^{(4)}\mathbf{\Lambda}^{(3)}\right)^{-T}, \tag{3.83}$$

where $\mathbf{\Pi}^{(W)}$ and $\mathbf{\Pi}^{(Z)}$ are permutation matrices of order R_1 and R_2, respectively, while $\mathbf{\Lambda}^{(1)}$ and $\mathbf{\Lambda}^{(2)}$ are diagonal matrices of dimensions (R_1, R_1), and $\mathbf{\Lambda}^{(3)}$ and $\mathbf{\Lambda}^{(4)}$ are diagonal matrices of dimensions (R_2, R_2).

Proof. Assuming that both PARAFAC decompositions (3.59) and (3.60) are essentially unique, and applying Property (3.21) to these decompositions, we have

$$\begin{aligned}
\bar{\mathbf{B}}^{(1)} &= \mathbf{B}^{(1)}\mathbf{\Pi}^{(W)}\mathbf{\Lambda}^{(1)}, \\
\bar{\mathbf{B}}^{(2)} &= \mathbf{B}^{(2)}\mathbf{\Pi}^{(W)}\mathbf{\Lambda}^{(2)}, \\
\overline{\mathbf{W}}_{I_3I_4\times R_1} &= \mathbf{W}_{I_3I_4\times R_1}\mathbf{\Pi}^{(W)}\mathbf{\Lambda}^{(5)}, \\
\bar{\mathbf{D}}^{(1)} &= \mathbf{D}^{(1)}\mathbf{\Pi}^{(Z)}\mathbf{\Lambda}^{(3)}, \\
\bar{\mathbf{D}}^{(2)} &= \mathbf{D}^{(2)}\mathbf{\Pi}^{(Z)}\mathbf{\Lambda}^{(4)}, \\
\bar{\mathbf{Z}}_{I_1I_2\times R_2} &= \mathbf{Z}_{I_1I_2\times R_2}\mathbf{\Pi}^{(Z)}\mathbf{\Lambda}^{(6)}.
\end{aligned} \tag{3.84}$$

Using the relations (3.79)-(3.82), we deduce that

$$\left(\bar{\mathbf{B}}^{(2)} \diamond \bar{\mathbf{B}}^{(1)}\right) = \left(\mathbf{B}^{(2)} \diamond \mathbf{B}^{(1)}\right)\mathbf{\Pi}^{(W)}\mathbf{\Lambda}^{(2)}\mathbf{\Lambda}^{(1)}, \tag{3.85}$$

$$\left(\bar{\mathbf{D}}^{(2)} \diamond \bar{\mathbf{D}}^{(1)}\right) = \left(\mathbf{D}^{(2)} \diamond \mathbf{D}^{(1)}\right)\mathbf{\Pi}^{(Z)}\mathbf{\Lambda}^{(4)}\mathbf{\Lambda}^{(3)}, \tag{3.86}$$

due to the fact that the same column permutation $\mathbf{\Pi}^{(W)}$ is applied to $\mathbf{B}^{(1)}$ and $\mathbf{B}^{(2)}$ on one hand, and $\mathbf{\Pi}^{(Z)}$ to $\mathbf{D}^{(1)}$ and $\mathbf{D}^{(2)}$ on the other hand.
Considering the unfolding (3.69) of $\mathcal{X}$ for the quintuplet $\left(\bar{\mathbf{B}}^{(1)}, \bar{\mathbf{B}}^{(2)}, \bar{\mathbf{D}}^{(1)}, \bar{\mathbf{D}}^{(2)}, \bar{\mathbf{U}}\right)$, we have

$$\mathbf{X}_{I_1I_2\times I_3I_4} = \left(\bar{\mathbf{B}}^{(2)} \diamond \bar{\mathbf{B}}^{(1)}\right)\bar{\mathbf{U}}\left(\bar{\mathbf{D}}^{(2)} \diamond \bar{\mathbf{D}}^{(1)}\right)^T.$$

Replacing the Khatri-Rao products by their expressions (3.85) and (3.86), and identifying the result with the unfolding (3.69) lead to the following relation between the factors $\bar{\mathbf{U}}$ and $\mathbf{U}$

$$\bar{\mathbf{U}} = \left(\mathbf{\Pi}^{(W)}\mathbf{\Lambda}^{(2)}\mathbf{\Lambda}^{(1)}\right)^{-1}\mathbf{U}\left(\mathbf{\Pi}^{(Z)}\mathbf{\Lambda}^{(4)}\mathbf{\Lambda}^{(3)}\right)^{-T},$$

which ends the proof of Theorem 4. □

Chapter 4

Tensor-based systems and their semi-blind receivers

Contents

This chapter firstly deals with two new transmission schemes for one-way two-hop AF relaying systems. Both feature a Khatri-Rao space-time coding (KRST) at the source node, but different forwarding strategies at the relay node. The chapter begins with the expression of the source coding, and then with the modeling of the signals received at the destination (via direct link) as a PARAFAC model. Following, the proposed transmission schemes namely *PARATUCK2-based amplify-and-forward relaying (PT2-AF)* and *nested PARAFAC-based amplify-and-forward relaying (NP-AF)* are presented, succeeded by the introduction of novel semi-blind receivers adapted for each transmission scheme. The sections comprising the receivers also include discussion on their intrinsic identifiability and uniqueness issues.

4.1 Source transmission

Consider the cooperative wireless system illustrated by means of Fig. 4.1, where M_S, M_R and M_D denote the numbers of antennas at the source (S), relay (R) and destination (D) nodes, respectively.

The *source-destination* channel $\mathbf{H}^{(SD)} \in \mathbb{C}^{M_D \times M_S}$, the *source-relay* channel $\mathbf{H}^{(SR)} \in \mathbb{C}^{M_R \times M_S}$ and the *relay-destination* channel $\mathbf{H}^{(RD)} \in \mathbb{C}^{M_D \times M_R}$ are assumed to be flat Rayleigh fading and constant during the transmission protocol, which is divided into two phases (two-hop). During the first one, each antenna m_S of the source transmits N information symbols to the relay, after a space-time coding. During the second hop, the source stays silent, and the relay amplifies the received signals before forwarding them to the destination.

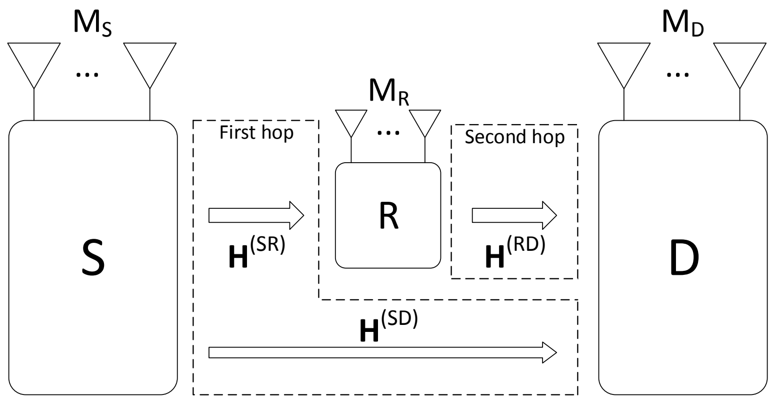

Figure 4.1: One-way model.

The source can be considered a single multi-antenna body, a set of M_S single-antenna elements or else a combination thereof. This flexibility of representation is possible because it is considered here the assumption of the independence (and absence of interference) among all source antennas. The same reasoning can be applied to the relay, where the exchange of received signals between two or more antennas is impeded. Indeed, the system shown in Fig. 4.1 may represent a broad class of realistic scenarios. For example, the case $M_S \gg M_R$ could be a scenario of a highly centralized relaying network, such as in cellular communication systems, where numerous users (source antennas) would share a few repeater stations (relay antennas) to let their messages be received by the base station (destination). The opposite case of $M_R \gg M_S$ would be perhaps suitable for ad hoc networks, where the transmission from one point (source) to another (destination) is in general assisted by several (relay) nodes.

Let $\mathbf{S} \in \mathbb{C}^{N \times M_S}$ be the matrix containing N data-streams of M_S symbols multiplexed to the M_S source antennas. A Khatri-Rao space-time (KRST) coding [61] is carried out by means of the source coding matrix $\mathbf{C} \in \mathbb{C}^{P \times M_S}$, which introduces time redundancy, with the code length P representing the number of repetitions of each data-stream. The coded signals to be transmitted are the result of the following Khatri-Rao operation

$$\widetilde{\mathbf{S}}_{M_S \times PN} = (\mathbf{S} \diamond \mathbf{C})^T, \tag{4.1}$$

which spreads the symbols on P symbol periods.

The matrix $\widetilde{\mathbf{S}}_{M_S \times PN}$ can be seen as a mode-1 unfolding of the virtual tensor $\widetilde{\mathcal{S}} \in \mathbb{C}^{M_S \times P \times N}$. More specifically, (4.1) comes from the transpose of (3.18) through the correspondence $(\mathcal{X}, \mathbf{A}^{(1)}, \mathbf{A}^{(2)}, \mathbf{A}^{(3)}) \Longleftrightarrow (\widetilde{\mathcal{S}}, \mathbf{I}_{M_S}, \mathbf{C}, \mathbf{S})$, and then according to (3.14) we can rewrite $\widetilde{\mathcal{S}}$ as

$$\widetilde{\mathcal{S}} = \mathcal{I}_{M_S} \times_1 \mathbf{I}_{M_S} \times_2 \mathbf{C} \times_3 \mathbf{S}. \tag{4.2}$$

In the last paragraph, the adjective virtual qualifies $\widetilde{\mathcal{S}}$ to denote that in practice there is no construction of this tensor, but it serves to represent the ensemble of coded signals at the source. In truth, the essential is that in the first hop of the communication protocol the columns of $\widetilde{\mathbf{S}}_{M_S \times PN}$ be sent, one by one, to the radio frequency (RF) chain (see Fig. 4.2), composed by digital-to-analog converters (DACs), RF modulators and others, and then finally be broadcast by the M_S antennas to the relay node and also to the destination node via a direct link.

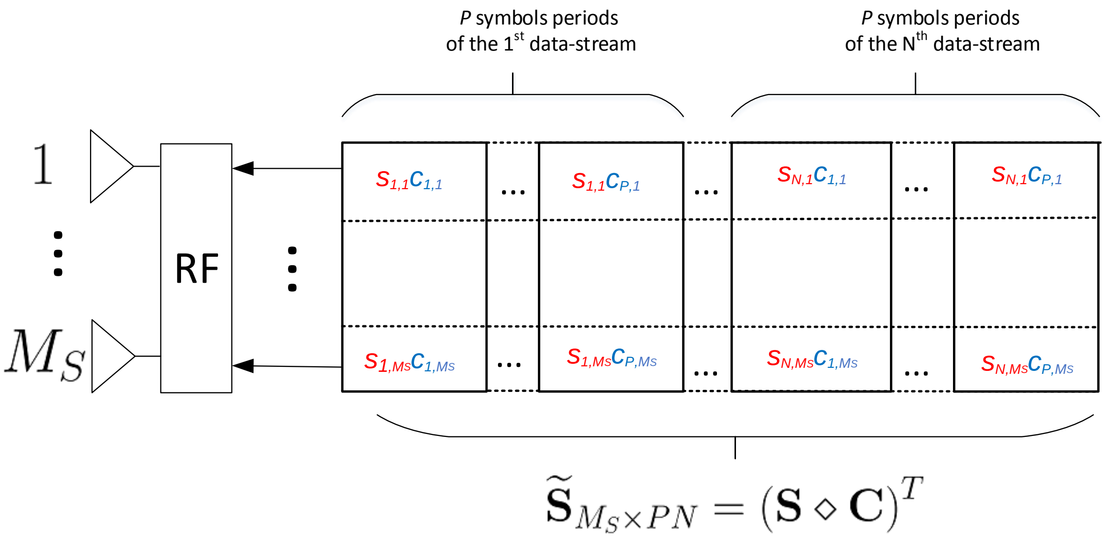

Figure 4.2: Source transmission

Although the transmission via direct link is not always possible or reliable, which in fact is one of the greatest motivations for using relaying stations, in this chapter some proposed receivers can exploit the existence of this link to improve their performances.

4.1.1 Model of the direct link (Source-Destination (SD))

The transmitted signals reaching the destination through the direct link channel $\mathbf{H}^{(SD)}$ are given by

$$\begin{aligned}\mathbf{X}^{(SD)}_{M_D \times PN} &= \mathbf{H}^{(SD)} \widetilde{\mathbf{S}}_{M_S \times PN} \\ &= \mathbf{H}^{(SD)} \left(\mathbf{S} \diamond \mathbf{C}\right)^T .\end{aligned} \tag{4.3}$$

Equation (4.3) represents, as (4.1), a mode-1 unfolding of a tensor that follows a PARAFAC model. In this case, it refers to the model of $\mathcal{X}^{(SD)} \in \mathbb{C}^{M_D \times P \times N}$, which captures the signals arriving at the M_D destination antennas during the total PN symbol periods. In the language of the multilinear algebra, the tensor $\mathcal{X}^{(SD)}$ is nothing but a mode-1 product between $\widetilde{\mathcal{S}}$ and $\mathbf{H}^{(SD)}$, i.e. from (4.2) it is obtained

$$\begin{aligned}\mathcal{X}^{(SD)} &= \widetilde{\mathcal{S}} \times_1 \mathbf{H}^{(SD)} \\ &= \mathcal{I}_{M_S} \times_1 \mathbf{H}^{(SD)} \times_2 \mathbf{C} \times_3 \mathbf{S}.\end{aligned} \tag{4.4}$$

The representation in (4.4) highlights the sequence of the symbol processing, executed from right to left. It can be drawn from (4.4) the straightforward conclusion that the symbols in $\mathbf{S}$ are first coded by $\mathbf{C}$, and then the signals are linear transformed by the channel matrix $\mathbf{H}^{(SD)}$. This disposition of the processing chain is valid in this thesis for all signal tensors decomposed as a PARAFAC.

Each entry of $\mathcal{X}^{(SD)}$ according to (3.12) is given by

$$x^{(SD)}_{m_D,p,n} = \sum_{m_S=1}^{M_S} h^{(SD)}_{m_D,m_S} c_{p,m_S} s_{n,m_S}. \tag{4.5}$$

Keeping the correspondence $(\mathcal{X}, \mathbf{A}^{(1)}, \mathbf{A}^{(2)}, \mathbf{A}^{(3)}) \iff (\mathcal{X}^{(SD)}, \mathbf{H}^{(SD)}, \mathbf{C}, \mathbf{S})$ between (3.12) and (4.5), the mode-2 and mode-3 unfoldings (3.19) and (3.20) of $\mathcal{X}^{(SD)}$ are given, respectively, by

$$\mathbf{X}^{(SD)}_{NM_D \times P} = \left(\mathbf{H}^{(SD)} \diamond \mathbf{S}\right) \mathbf{C}^T \tag{4.6}$$

and

$$\mathbf{X}^{(SD)}_{M_D P \times N} = (\mathbf{C} \diamond \mathbf{H}^{(SD)}) \mathbf{S}^T. \tag{4.7}$$

Besides interpreting (4.7) as the transformation of the symbol matrix $\mathbf{S}$ via the source coding $(\mathbf{C})$ and the transmission through the channel $\mathbf{H}^{(SD)}$, another interpretation consists in considering the Khatri-Rao product $\left(\mathbf{C} \diamond \mathbf{H}^{(SD)}\right) \in \mathbb{C}^{M_D P \times M_S}$ as a virtual channel with $M_D P$ destination antennas. Such equations of the direct link model was firstly derived by the original work on the Khatri-Rao codes [61].

The unfoldings (4.3), (4.6) and (4.7) can be used to jointly estimate the triplet ($\mathbf{H}^{(SD)}$,$\mathbf{C}$,$\mathbf{S}$), either through iterative or closed-form methods. Although symbol estimates can be obtained via direct link, in many cases the average SNR in this link is low, justifying the existence of a relay-assisted link.

4.2 Model of the relay-assisted link (SRD)

This section contains the two new schemes for transmission via the relay link: *PARATUCK2-based amplify-and-forward relaying (PT2-AF)* and *nested PARAFAC-based amplify-and-forward relaying (NP-AF)*. Both share the same transmission scheme shown in Fig. 4.3, only differing in the form of relay processing.

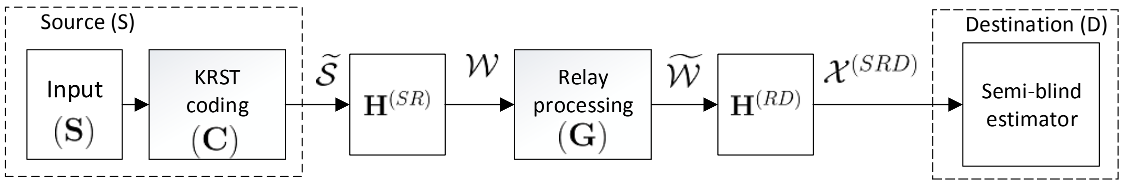

Figure 4.3: Block diagram of the relaying link

After transmission of the coded symbols (4.1) through the channel $\mathbf{H}^{(SR)}$, the signals received by the relay are given by

$$\begin{aligned}\mathbf{W}_{M_R \times PN} &= \mathbf{H}^{(SR)}\widetilde{\mathbf{S}}_{M_S \times PN} \\ &= \mathbf{H}^{(SR)} \left(\mathbf{S} \diamond \mathbf{C}\right)^T. \end{aligned} \tag{4.8}$$

The matrix $\mathbf{W}_{M_R \times PN}$ represents a mode-1 unfolding of the tensor $\mathcal{W} \in \mathbb{C}^{M_R \times P \times N}$, and it satisfies a PARAFAC model with $(\mathbf{H}^{(SR)}, \mathbf{C}, \mathbf{S})$ as factor matrices, i.e.

$$\mathcal{W} = \widetilde{\mathcal{S}} \times_1 \mathbf{H}^{(SR)} \tag{4.9}$$

$$= \mathcal{I}_{M_S} \times_1 \mathbf{H}^{(SR)} \times_2 \mathbf{C} \times_3 \mathbf{S}, \tag{4.10}$$

and thus mode-2 and mode-3 unfoldings of $\mathcal{W}$ are given respectively by

$$\mathbf{W}_{NM_R \times P} = \left(\mathbf{H}^{(SR)} \diamond \mathbf{S}\right) \mathbf{C}^T, \tag{4.11}$$

$$\mathbf{W}_{M_R P \times N} = \left(\mathbf{C} \diamond \mathbf{H}^{(SR)}\right) \mathbf{S}^T. \tag{4.12}$$

In Sections 4.2.1 and 4.2.2, the two proposed schemes of amplifying and forwarding the signals in the tensor $\mathcal{W}$ are presented.

4.2.1 PARATUCK2-based amplify-and-forward relaying (PT2-AF)

After the transmission through the channel $\mathbf{H}^{(SR)}$, the received signals in $\mathbf{W}_{M_R \times PN}$ (Eq. (4.8)) are transformed by means of an AF matrix $\mathbf{G} \in \mathbb{C}^{N \times M_R}$ at the relay. By the correspondences $(\mathcal{X}, \mathbf{A}^{(1)}, \mathbf{A}^{(2)}, \mathbf{A}^{(3)}) \Longleftrightarrow (\mathcal{W}, \mathbf{H}^{(SR)}, \mathbf{C}, \mathbf{S})$, from (3.15) we have the n^{th} frontal slice of $\mathcal{W}$ as

$$\mathbf{W}_{\cdot\cdot n} = \mathbf{H}^{(SR)} D_n\left(\mathbf{S}\right) \mathbf{C}^T, \tag{4.13}$$

and these signals are amplified according to

$$\begin{aligned} \widetilde{\mathbf{W}}_{\cdot\cdot n} &= D_n(\mathbf{G})\mathbf{W}_{\cdot\cdot n} \in \mathbb{C}^{M_R \times P} & (4.14)\\ &= D_n(\mathbf{G})\mathbf{H}^{(SR)} D_n(\mathbf{S})\mathbf{C}^T, & (4.15)\end{aligned}$$

where the diagonal matrix $D_n(\mathbf{G})$ contains the AF coefficients concerning the n^{th} data-stream. Thus, for each data-stream there is an associated set of coefficients at the relay, as shown at Fig 4.4.

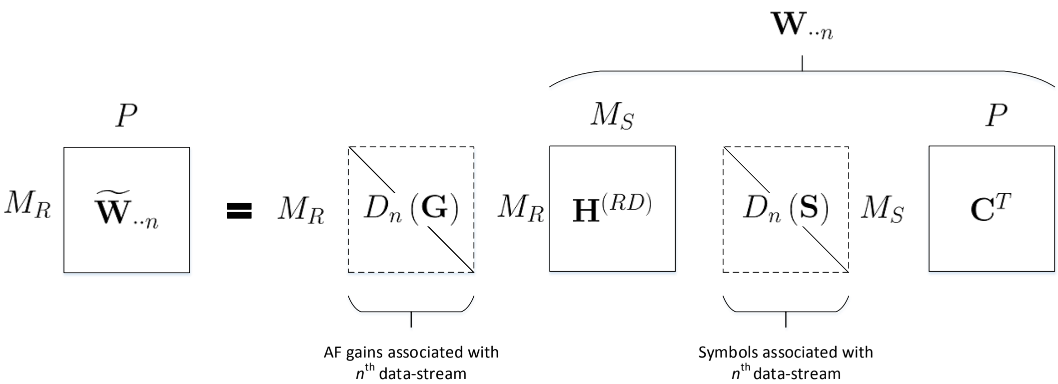

Figure 4.4: Block diagram of the PT2-AF scheme

This diagonal structure $D_n(\mathbf{G})$, besides applying for the m_r^{th} relay antenna, at the n^{th} data-stream, the gain g_{n,m_r} with $|g_{n,m_r}| \geqslant 1$, also avoids the mixing of the signals received by different antennas.

Equation (4.14) can be rewritten as

$$\widetilde{\mathbf{W}}_{\cdot\cdot n} = \mathbf{W}_{\cdot\cdot n} \circ \left(\mathbf{G}_{n\cdot} \otimes \mathbf{1}_{P\times 1}\right)^T, \tag{4.16}$$

where $\left(\mathbf{G}_{n\cdot} \otimes \mathbf{1}_{P\times 1}\right)^T \in \mathbb{C}^{M_R \times P}$ carries the M_R gains associated with the n^{th} data-stream repeated through all of its P symbol periods. Using (4.16) and the definition of the Khatri-

Rao product (A.10), the mode-1 unfolding of the tensor $\widetilde{\mathcal{W}} \in \mathbb{C}^{M_R \times P \times N}$ can be found by

$$\begin{aligned}
\widetilde{\mathbf{W}}_{M_R \times PN} &= \left[\widetilde{\mathbf{W}}_{..1} \quad \cdots \quad \widetilde{\mathbf{W}}_{..N}\right] \\
&= \left[\mathbf{W}_{..1} \circ (\mathbf{G}_{1.} \otimes \mathbf{1}_{P\times 1})^T \quad \cdots \quad \mathbf{W}_{..N} \circ (\mathbf{G}_{N.} \otimes \mathbf{1}_{P\times 1})^T\right] \\
&= [\mathbf{W}_{..1} \quad \cdots \quad \mathbf{W}_{..N}] \circ \left[(\mathbf{G}_{1.} \otimes \mathbf{1}_{P\times 1})^T \quad \cdots \quad (\mathbf{G}_{N.} \otimes \mathbf{1}_{P\times 1})^T\right] \\
&= \mathbf{W}_{M_R \times PN} \circ (\mathbf{G} \diamond \mathbf{1}_{P\times M_R})^T . \qquad (4.17)
\end{aligned}$$

The signals received at destination after the passage through $\mathbf{H}^{(RD)}$ form a third-order tensor $\mathcal{X}^{(SRD)} \in \mathbb{C}^{M_D \times P \times N}$, whose n^{th} frontal slice, using (4.14), is given by

$$\begin{aligned}
\mathbf{X}^{(SRD)}_{..n} &= \mathbf{H}^{(RD)} \widetilde{\mathbf{W}}_{..n} \in \mathbb{C}^{M_D \times P} \\
&= \mathbf{H}^{(RD)} D_n(\mathbf{G}) \mathbf{H}^{(SR)} D_n(\mathbf{S}) \mathbf{C}^T . \qquad (4.18)
\end{aligned}$$

The Eq. (4.18) corresponds to a frontal slice (3.24) of the tensor $\mathcal{X}^{(SRD)}$ following a PARATUCK2 decomposition with $\mathbf{H}^{(RD)}$ and $\mathbf{C}$ as matrix factors, $\mathbf{H}^{(SR)}$ as the core matrix, and $\mathbf{G}$ and $\mathbf{S}$ as interaction matrices, i.e. following the correspondences

$$(\mathcal{X}, \mathbf{A}^{(1)}, \mathbf{A}^{(2)}, \mathbf{B}^{(1)}, \mathbf{B}^{(2)}, \mathbf{U}) \Longleftrightarrow (\mathcal{X}^{(SRD)}, \mathbf{H}^{(RD)}, \mathbf{G}, \mathbf{C}, \mathbf{S}, \mathbf{H}^{(SR)}) \qquad (4.19)$$

and

$$(I_1, I_2, I_3, R_1, R_2) \Longleftrightarrow (M_D, P, N, M_R, M_S) \qquad (4.20)$$

with the model in (3.23). Therefore, the tensor $\mathcal{X}^{(SRD)}$ can be rewritten in its scalar form (3.23) as

$$x^{(SRD)}_{m_D,p,n} = \sum_{m_R=1}^{M_R} \sum_{m_S=1}^{M_S} h^{(RD)}_{m_D,m_R} g_{n,m_R} h^{(SR)}_{m_R,m_S} c_{p,m_S} s_{n,m_S} .$$

By the correspondences in (4.19), the mode-1, mode-2 and mode-3 unfoldings (3.27)-(3.29) are given respectively by

$$\begin{aligned}
\mathbf{X}^{(SRD)}_{PN \times M_D} &= (\mathbf{I}_N \otimes \mathbf{C}) \, \mathbf{F}_1 \left(\mathbf{H}^{(RD)}\right)^T , \qquad (4.21) \\
\mathbf{X}^{(SRD)}_{NM_D \times P} &= \left(\mathbf{I}_{M_D} \otimes \left(\mathbf{S}^T \diamond \mathbf{G}^T\right)^T\right) \mathbf{F}_2 \mathbf{C}^T , \qquad (4.22) \\
\mathbf{X}^{(SRD)}_{M_D P \times N} &= \left(\mathbf{I}_P \otimes \mathbf{H}^{(RD)}\right) \mathbf{F}_3 \left(\mathbf{S}^T \diamond \mathbf{G}^T\right) , \qquad (4.23)
\end{aligned}$$

where the auxiliary matrix

$$\mathbf{F}_1 = \begin{bmatrix} D_1(\mathbf{S}) \left(\mathbf{H}^{(SR)}\right)^T D_1(\mathbf{G}) \\ \vdots \\ D_N(\mathbf{S}) \left(\mathbf{H}^{(SR)}\right)^T D_N(\mathbf{G}) \end{bmatrix} \in \mathbb{C}^{M_S N \times M_R} \qquad (4.24)$$

can be obtained from (3.30) also with the correspondences in (4.19). Matrices $\mathbf{F}_2$ and $\mathbf{F}_3$ could be obtained by using the same correspondences, but they are not necessary in the development of the semi-blind receivers. In addition, the transpose of (4.21) can be alternatively given by

$$\mathbf{X}^{(SRD)}_{M_D \times PN} = \mathbf{H}^{(RD)} \widetilde{\mathbf{W}}_{M_R \times PN}, \tag{4.25}$$

with $\widetilde{\mathbf{W}}_{M_R \times PN}$ defined in (4.17).

The unfolding (4.21) can be used to estimate $\mathbf{H}^{(RD)}$ in a LS sense. From (3.33) the core matrix $\mathbf{H}^{(SR)}$ can be isolated in its vectorized form by

$$\mathbf{x}^{(SRD)}_{M_D PN} = \left[\left(\mathbf{S}^T \diamond \mathbf{G}^T \right)^T \diamond \left(\mathbf{C} \otimes \mathbf{H}^{(RD)} \right) \right] \mathbf{h}^{(SR)}, \tag{4.26}$$

where $\mathbf{h}^{(SR)} = \text{vec}\left(\mathbf{H}^{(SR)}\right)$, and $\mathbf{G}$ and $\mathbf{S}$ can be solved independently by resorting to the vectorized form of each frontal slices, i.e. from (3.34) and (3.35) we get

$$\mathbf{x}^{(SRD)}_{n} \triangleq \text{vec}(\mathbf{X}^{(SRD)}_{\cdot\cdot n}) = \left(\mathbf{C} \diamond \mathbf{Z}_n \right) \mathbf{S}^T_{n\cdot}, \tag{4.27}$$

$$= \left(\mathbf{W}^T_{\cdot\cdot n} \diamond \mathbf{H}^{(RD)} \right) \mathbf{G}^T_{n\cdot}. \tag{4.28}$$

The matrix slice $\mathbf{W}_{\cdot\cdot n}$ was defined in (4.13) and

$$\mathbf{Z}_n = \mathbf{H}^{(RD)} D_n(\mathbf{G}) \mathbf{H}^{(SR)} \in \mathbb{C}^{M_D \times M_S} \tag{4.29}$$

can be interpreted as the effective channel of the Source-Relay-Destination (SRD) link concerning the n^{th} data-stream.

4.2.2 Nested PARAFAC-based amplify-and-forward relaying (NP-AF)

This section presents the alternative transmission scheme called NP-AF. Its difference from PT2-AF begins at its relaying process, where the signals $\mathbf{W}_{M_R \times PN}$ in (4.8) are processed in a different fashion from the aforementioned scheme.

The relay performs a new space-time coding, which consists in repeating the block of signals $\mathbf{W}_{M_R \times PN}$ through J sequential time-frames[1]. This repetition is carried out using a second KRST coding with the relay matrix $\mathbf{G} \in \mathbb{C}^{J \times M_R}$. That gives the following matrix containing the signals coded at the relay

$$\widetilde{\mathbf{W}}_{M_R \times JPN} = \left(\mathbf{W}_{PN \times M_R} \diamond \mathbf{G} \right)^T, \tag{4.30}$$

whose form resembles the source coding at (4.1). In other words, the NP-AF scheme is composed by a double KRST coding, one at the source by the code matrix $\mathbf{C}$ and another at the relay by the code matrix $\mathbf{G}$.

[1] The term *time-frame* is also employed by [24], and it is named *time-block* in [20]

After the transmission through the channel $\mathbf{H}^{(RD)}$, the signals received by the M_D destination antennas are given by

$$\mathbf{X}^{(SRD)}_{M_D \times JPN} = \mathbf{H}^{(RD)} \widetilde{\mathbf{W}}_{M_R \times JPN}, \tag{4.31}$$

and combining the expression (4.30) and (4.8) in (4.31) gives

$$\begin{aligned} \mathbf{X}^{(SRD)}_{M_D \times JPN} &= \mathbf{H}^{(RD)} \left(\mathbf{W}_{PN \times M_R} \diamond \mathbf{G}\right)^T & (4.32) \\ &= \mathbf{H}^{(RD)} \left((\mathbf{S} \diamond \mathbf{C}) \left(\mathbf{H}^{(SR)}\right)^T \diamond \mathbf{G} \right)^T . & (4.33) \end{aligned}$$

The concatenation of the two Khatri-Rao operations in Eq. (4.33) reflects the double Khatri-Rao coding at the source and relay nodes, as illustrated in Fig. 4.5.

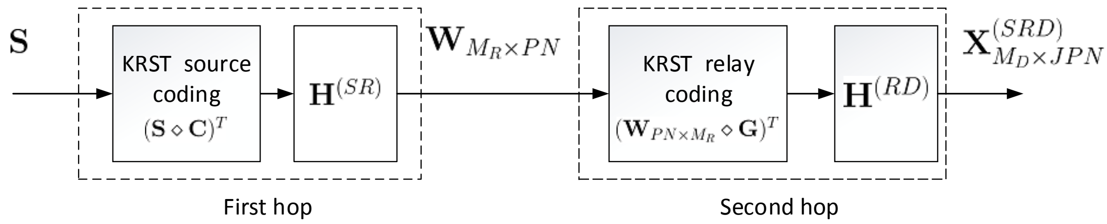

Figure 4.5: Block diagram of NP-AF scheme

This expression (4.33) can be interpreted as a mode-1 unfolding of the fourth-order signal tensor $\mathcal{X}^{(SRD)} \in \mathbb{C}^{M_D \times J \times N \times P}$. Comparing (4.33) with (3.63) after transposing its two members, we can conclude that $\mathcal{X}^{(SRD)}$ satisfies a nested PARAFAC model (3.48), with the following correspondences

$$(\mathcal{X}, \mathbf{B}^{(1)}, \mathbf{B}^{(2)}, \mathbf{D}^{(1)}, \mathbf{D}^{(2)}, \mathbf{U}) \Longleftrightarrow (\mathcal{X}^{(SRD)}, \mathbf{H}^{(RD)}, \mathbf{G}, \mathbf{C}, \mathbf{S}, \mathbf{H}^{(SR)}) \tag{4.34}$$

and

$$(I_1, I_2, I_3, I_4, R_1, R_2) \Longleftrightarrow (M_D, J, P, N, M_R, M_S). \tag{4.35}$$

From (3.48) we deduce the scalar form of the received signal tensor $\mathcal{X}^{(SRD)}$

$$x^{(SRD)}_{m_D,j,n,p} = \sum_{m_R=1}^{M_R} \sum_{m_S=1}^{M_S} h^{(RD)}_{m_D,m_R} g_{j,m_R} h^{(SR)}_{m_R,m_S} c_{p,m_S} s_{n,m_S}, \tag{4.36}$$

and from (3.61) and (3.62) one gets

$$\begin{aligned} \mathcal{X}^{(1)} &= \mathcal{I}_{M_R} \times_1 \mathbf{H}^{(RD)} \times_2 \mathbf{G} \times_3 \mathbf{W}_{PN \times M_R} \in \mathbb{C}^{M_D \times J \times PN}, & (4.37) \\ \mathcal{X}^{(2)} &= \mathcal{I}_{M_S} \times_1 \mathbf{Z}_{M_D J \times M_S} \times_2 \mathbf{C} \times_3 \mathbf{S} \in \mathbb{C}^{M_D J \times P \times N}. & (4.38) \end{aligned}$$

These two contracted forms of $\mathcal{X}^{(SRD)}$, following two different PARAFAC decompositions, bring interesting interpretations of the NP-AF transmission scheme. From right to left, (4.37) and (4.38) highlight respectively the processing of the signals $\mathbf{W}_{PN\times M_R}$ and $\mathbf{S}$. More precisely, (4.37) shows the KRST coding of the signals $\mathbf{W}_{PN\times M_R}$ by $\mathbf{G}$, followed by their transmission through the channel $\mathbf{H}^{(RD)}$, while (4.38) presents the KRST coding of the symbols at source by the matrix $\mathbf{C}$ and its transmission through the effective channel $\mathbf{Z}_{M_D J\times M_S}$. Such observations could also be drawn from the expressions corresponding to (3.67) and (3.68), i.e.

$$\mathbf{X}^{(SRD)}_{M_D J\times PN} = \left(\mathbf{G}\diamond\mathbf{H}^{(RD)}\right)\mathbf{W}_{M_R\times PN}, \tag{4.39}$$

$$= \mathbf{Z}_{M_D J\times M_S}\left(\mathbf{S}\diamond\mathbf{C}\right)^T. \tag{4.40}$$

The tensor $\mathcal{Z}\in\mathbb{C}^{M_D\times J\times M_S}$ can be deduced from (3.50) using the correspondences (4.34) and (4.35)

$$z_{m_D,j,m_S} = \sum_{m_R=1}^{M_R} h^{(RD)}_{m_D,m_R} g_{j,m_R} h^{(SR)}_{m_R,m_S}, \tag{4.41}$$

with the following mode-1, mode-2 and mode-3 unfoldings

$$\mathbf{Z}_{JM_S\times M_D} = \left((\mathbf{H}^{(SR)})^T\diamond\mathbf{G}\right)(\mathbf{H}^{(RD)})^T, \tag{4.42}$$

$$\mathbf{Z}_{M_S M_D\times J} = \left(\mathbf{H}^{(RD)}\diamond(\mathbf{H}^{(SR)})^T\right)\mathbf{G}^T. \tag{4.43}$$

$$\mathbf{Z}_{M_D J\times M_S} = \left(\mathbf{G}\diamond\mathbf{H}^{(RD)}\right)\mathbf{H}^{(SR)}. \tag{4.44}$$

Finally, the vector unfolding (3.70) becomes

$$\mathbf{x}^{(SRD)}_{M_D JPN} = \left[(\mathbf{S}\diamond\mathbf{C})\otimes(\mathbf{G}\diamond\mathbf{H}^{(RD)})\right]\mathbf{h}^{(SR)}, \tag{4.45}$$

where $\mathbf{h}^{(SR)} = \mathrm{vec}(\mathbf{H}^{(SR)})$, and from (3.64)-(3.66) the mode-2, mode-3 and mode-4 unfoldings of $\mathcal{X}^{(SRD)}$ are given by

$$\mathbf{X}^{(SRD)}_{PNM_D\times J} = \left(\mathbf{H}^{(RD)}\diamond(\mathbf{S}\diamond\mathbf{C})\,\mathbf{H}^{(SR)^T}\right)\mathbf{G}^T, \tag{4.46}$$

$$\mathbf{X}^{(SRD)}_{NM_D J\times P} = \left(\left(\mathbf{G}\diamond\mathbf{H}^{(RD)}\right)\mathbf{H}^{(SR)}\diamond\mathbf{S}\right)\mathbf{C}^T, \tag{4.47}$$

$$\mathbf{X}^{(SRD)}_{M_D JP\times N} = \left(\mathbf{C}\diamond\left(\mathbf{G}\diamond\mathbf{H}^{(RD)}\right)\mathbf{H}^{(SR)}\right)\mathbf{S}^T. \tag{4.48}$$

In spite of the possibility of estimating all matrix factors exploiting directly the unfoldings of $\mathcal{X}^{(SRD)}$, the NP-AF scheme lets the channels be extracted from the tensor $\mathcal{Z}$, which in general shall be estimated from the contracted model (4.38) of $\mathcal{X}^{(SRD)}$.

A comparison between the NP-AF transmission scheme with PT2-AF, in terms of their coding and transmission processes, is given in Table 4.1. Regarding the signals processed at the relay, for the NP-AF scheme it is possible to see the time-spreading caused by the Khatri-Rao product between the incoming signals and $\mathbf{G}$, which in turn is replaced by the entry-wise product for PT2-AF.

	PT2-AF	NP-AF
Signals coded at the source	$\widetilde{\mathbf{S}}_{M_S \times PN} = (\mathbf{S} \diamond \mathbf{C})^T$	
Signals arriving at the relay	$\mathbf{W}_{M_R \times PN} = \mathbf{H}^{(SR)} \widetilde{\mathbf{S}}_{M_S \times PN}$	
Relay matrix	$\mathbf{G} \in \mathbb{C}^{N \times M_R}$	$\mathbf{G} \in \mathbb{C}^{J \times M_R}$
Signals processed at the relay	$\widetilde{\mathbf{W}}_{M_R \times PN} = (\mathbf{W}_{PN \times M_R} \circ (\mathbf{G} \diamond \mathbf{1}_{P \times M_R}))^T$	$\widetilde{\mathbf{W}}_{M_R \times JPN} = (\mathbf{W}_{PN \times M_R} \diamond \mathbf{G})^T$
Signals arriving at the destination	$\mathbf{X}^{(SRD)}_{M_D \times PN} = \mathbf{H}^{(RD)} \widetilde{\mathbf{W}}_{M_R \times PN}$	$\mathbf{X}^{(SRD)}_{M_D \times JPN} = \mathbf{H}^{(RD)} \widetilde{\mathbf{W}}_{M_R \times JPN}$

Table 4.1: Comparison between PT2-AF and NP-AF

4.3 Noise degradation

The accuracy of the estimates of the matrix factors (e.g. symbol and channel matrices) is linked not only to the adopted estimation process itself, but also to the generation of the data in the input of the respective estimator. In other words, the quality of the estimates depends strongly on the proximity of the observed data to the original theoretical model. In wireless communication systems, the degradation of the signals is caused by several factors, such as unwanted interferences and the presence of additive noises.

Disregarding interferences of any sort, the presence of additive noises is illustrated by Fig. ??, where $\mathcal{V}^{(R)} \sim \mathcal{CN}\left(0, \left(\sigma^{(R)}\right)^2\right)$ and $\mathcal{V}^{(D)} \sim \mathcal{CN}\left(0, \left(\sigma^{(D)}\right)^2\right)$ are the respective white measurement noises at the relay and the destination, and $\left(\sigma^{(R)}\right)^2$ and $\left(\sigma^{(D)}\right)^2$ are their variances.

The channel matrix $\mathbf{H}^{(RD)}$ is a linear process, and thus we can write the equations relating to the presence of noise in the following way

$$\mathcal{Y}^{(SRD)} = \mathcal{X}^{(SRD)} + \mathcal{V}^{(SRD)}, \tag{4.49}$$

$$\mathcal{V}^{(SRD)} = \mathcal{V}^{(RD)} + \mathcal{V}^{(D)}, \tag{4.50}$$

$$\mathcal{V}^{(RD)} = \widetilde{\mathcal{V}}^{(R)} \times_1 \mathbf{H}^{(RD)}. \tag{4.51}$$

Due to the superposition property of linear systems, the amplified noise tensor $\widetilde{\mathcal{V}}^{(R)}$ (and its derivatives) can be obtained, for both PT2-AF and NP-AF, by replacing the noise-free $\mathcal{W}$ by the tensor $\mathcal{V}^{(R)}$ in the equations that generate $\widetilde{\mathcal{W}}$ (and eventually $\mathcal{X}^{(SRD)}$). For each transmission scheme, the tensor $\widetilde{\mathcal{W}}$ is generated in a different fashion, and thus so it is $\widetilde{\mathcal{V}}^{(R)}$. The derivation of the noise tensors for PT2-AF and NP-AF are presented in the following:

- PT2-AF: Replacing $\mathbf{W}_{M_R \times PN}$ in (4.17) by the the noise matrix $\mathbf{V}^{(R)}_{M_R \times PN}$:

$$\widetilde{\mathbf{V}}^{(R)}_{M_R \times PN} = \mathbf{V}^{(R)}_{M_R \times PN} \circ (\mathbf{G} \diamond \mathbf{1}_{P \times M_R})^T . \tag{4.52}$$

Consequently, inserting $\widetilde{\mathbf{V}}^{(R)}_{M_R \times PN}$ in the place of $\widetilde{\mathbf{W}}_{M_R \times PN}$ in (4.25) gives

$$\mathbf{V}^{(RD)}_{M_D \times PN} = \mathbf{H}^{(RD)} \left(\mathbf{V}^{(R)}_{M_R \times PN} \circ (\mathbf{G} \diamond \mathbf{1}_{P \times M_R})^T \right). \tag{4.53}$$

- NP-AF: Replacing $\mathbf{W}_{PN \times M_R}$ by $\mathbf{V}^{(R)}_{PN \times M_R}$ in (4.30) gives

$$\widetilde{\mathbf{V}}^{(R)}_{M_R \times JPN} = \left(\mathbf{V}^{(R)}_{PN \times M_R} \diamond \mathbf{G} \right)^T, \tag{4.54}$$

leading from (4.31) to

$$\mathbf{V}^{(RD)}_{M_D \times JPN} = \mathbf{H}^{(RD)} \left(\mathbf{V}^{(R)}_{PN \times M_R} \diamond \mathbf{G} \right)^T. \tag{4.55}$$

4.4 Semi-blind receivers

For the transmission schemes presented in this chapter, including the transmission via direct link, the semi-blind estimation of the triplet $\left(\mathbf{S}, \mathbf{H}^{(RD)}, \mathbf{H}^{(SR)}\right)$ is viable due to the uniqueness properties of the PARAFAC, PARATUCK2 and nested PARAFAC decompositions discussed in sections 3.3.1, 3.4.1 and 3.5.1.

The semi-blind receivers proposed in this thesis are classified into two types: those of the iterative solution, using the ALS method; and those of closed-solution, using a Singular Value Decomposition (SVD)-based procedure known as Least Squares Khatri-Rao Factorization (LSKRF).

We assume that the code ($\mathbf{C}$ and $\mathbf{G}$) matrices are known by any receiver. In addition, the first row of the symbol matrix is also assumed known and formed of ones, which means $\mathbf{S}_{1\cdot} = \mathbf{1}_{1 \times M_S}$. This choice is compatible with most of the modulation standards (e.g. Phase-Shift Keying (PSK), Quadrature Amplitude Modulation (QAM), Frequency-Shift Keying (FSK)), and it has the main goal of eliminating column scaling ambiguities on the solution of $\mathbf{S}$.

4.4.1 Iterative receivers (ALS-based)

The principle of the ALS algorithm applied to tensor models is simple. In each of its steps it seeks to minimize, in the LS sense, a reconstruction error of the given data tensor with respect to one of its matrix factors. Such minimization is conditioned to the estimates of the other matrix factors, obtained from previous minimization steps. Therefore, a matrix estimated in one step feeds the subsequent minimization step to update another matrix factor.

Thanks to its simplicity, ALS is widely used for a broad variety of tensor models. For the trilinear PARAFAC model, the ALS algorithm applied to estimate its three matrix factors corresponds to minimize in the LS sense the three cost functions

$$\widehat{\mathbf{A}}_i^{(1)} \triangleq \underset{\mathbf{A}^{(1)}}{\arg\min} \left\| \mathbf{Y}_{I_2 I_3 \times I_1} - \left(\widehat{\mathbf{A}}_{i-1}^{(3)} \diamond \widehat{\mathbf{A}}_{i-1}^{(2)} \right) \left(\mathbf{A}^{(1)} \right)^T \right\|_2^2, \tag{4.56}$$

$$\widehat{\mathbf{A}}_i^{(2)} \triangleq \underset{\mathbf{A}^{(2)}}{\arg\min} \left\| \mathbf{Y}_{I_3 I_1 \times I_2} - \left(\widehat{\mathbf{A}}_{i}^{(1)} \diamond \widehat{\mathbf{A}}_{i-1}^{(3)} \right) \left(\mathbf{A}^{(2)} \right)^T \right\|_2^2, \tag{4.57}$$

$$\widehat{\mathbf{A}}_i^{(3)} \triangleq \underset{\mathbf{A}^{(3)}}{\arg\min} \left\| \mathbf{Y}_{I_1 I_2 \times I_3} - \left(\widehat{\mathbf{A}}_{i}^{(2)} \diamond \widehat{\mathbf{A}}_{i}^{(1)} \right) \left(\mathbf{A}^{(3)} \right)^T \right\|_2^2, \tag{4.58}$$

deduced from (3.18), (3.19) and (3.20), respectively. After minimizing these cost functions, the iteration i is incremented, and the process is repeated with the new estimates, until convergence is accepted. The tensor $\mathcal{Y}$ is the observed (noisy) version of $\mathcal{X}$.

4.4.2 Non-iterative receivers (SVD-based)

Another base algorithm used by the receivers in this chapter is called LSKRF. This method proposes a non-iterative, algebraic solution for the decomposition of a Khatri-Rao product between two matrices. Although it is a fully matrix-based method, and therefore there is no need of working with different unfoldings of a tensor, the very factorization of the Khatri-Rao product makes it suitable for the solution of some PARAFAC-family decompositions.

This algorithm has already been used by other works [24, 86, 18], and it is based on the rank-one approximations of Kronecker products [87], more specifically through truncating SVD decompositions of supposedly rank-one matrices. The LSKRF method is highlighted in Remark 2.

Remark 2. *(**LSKRF**[87]) Given the matrix* $\mathbf{X}_{I_2 I_1 \times R} = \left(\mathbf{A}^{(1)} \diamond \mathbf{A}^{(2)} \right)$, *where* $\mathbf{A}^{(1)} \in \mathbb{C}^{I_2 \times R}$ *and* $\mathbf{A}^{(2)} \in \mathbb{C}^{I_2 \times R}$, *then from the definition of the Khatri-Rao product* $\mathbf{X}_{I_2 I_1 \times R} = \left[\mathbf{a}_1^{(1)} \otimes \mathbf{a}_1^{(2)} \ \cdots \ \mathbf{a}_R^{(1)} \otimes \mathbf{a}_R^{(2)} \right]$, *where* $\mathbf{a}_r^{(1)} = \mathbf{A}_{\cdot r}^{(1)} \in \mathbb{C}^{I_1 \times 1}$ *and* $\mathbf{a}_r^{(2)} = \mathbf{A}_{\cdot r}^{(2)} \in \mathbb{C}^{I_2 \times 1}$ *are column vectors. The LSKRF procedure consists of:*

For $1 \leqslant r \leqslant R$*:*

1: *Reshape the column vector* $(\mathbf{X}_{I_2 I_1 \times R})_{\cdot r} = \hat{\mathbf{a}}_r^{(1)} \otimes \hat{\mathbf{a}}_r^{(2)}$ *into a rank-one matrix* $\bar{\mathbf{X}} \in \mathbb{C}^{I_2 \times I_1}$, *so from property (A.8) we have* $\bar{\mathbf{X}} = \hat{\mathbf{a}}_r^{(2)} \left(\hat{\mathbf{a}}_r^{(1)} \right)^T$*;*

2: *Compute the Singular Value Decomposition* $\bar{\mathbf{X}} = \mathbf{U} \boldsymbol{\Xi} \mathbf{V}^H$, *where* $\mathbf{U}$ *and* $\mathbf{V}$ *are orthogonal matrices, and* $\boldsymbol{\Xi}$ *is diagonal matrix with singular values in decreasing order.*

3: *Find* $\hat{\mathbf{a}}_r^{(2)} = \sqrt{\boldsymbol{\Xi}_{1,1}} \mathbf{U}_{\cdot 1}$ *and* $\hat{\mathbf{a}}_r^{(1)} = \sqrt{\boldsymbol{\Xi}_{1,1}} \mathbf{V}_{\cdot 1}^*$

4.5 Direct link: SVD-based receiver (PARAFAC-SVD)

For all proposed transmission schemes (including via direct link), the noise-free symbol vector $\bar{\mathbf{x}}_n$ arriving at the destination node can be given by

$$\bar{\mathbf{x}}_n \triangleq \left(\mathbf{C} \diamond \bar{\mathbf{Z}}\right) \mathbf{s}_n, \tag{4.59}$$

where $\mathbf{s}_n = (\mathbf{S}_{n\cdot})^T$ and $\bar{\mathbf{Z}}$ is the effective channel between the source and the destination. Equation (4.59) concerns the n^{th} data-stream arriving at the destination antennas. In othe words, from (4.7), (4.27) or (4.48) we can deduce the following correspondences

$$\begin{aligned}
(\bar{\mathbf{x}}_n, \bar{\mathbf{Z}}) &\Longleftrightarrow \left(\left(\mathbf{X}^{(SD)}_{M_D P\times N}\right)_{\cdot n}, \mathbf{H}^{(SD)}\right) && \text{(via direct link)} && (4.60)\\
&\Longleftrightarrow \left(\left(\mathbf{X}^{(SRD)}_{M_D P\times N}\right)_{\cdot n}, \mathbf{H}^{(RD)} D_n(\mathbf{G})\mathbf{H}^{(SR)}\right) && \text{(via PT2-AF)} && (4.61)\\
&\Longleftrightarrow \left(\left(\mathbf{X}^{(SRD)}_{M_D JP\times N}\right)_{\cdot n}, \left(\mathbf{G} \diamond \mathbf{H}^{(RD)}\right)\mathbf{H}^{(SR)}\right) && \text{(via NP-AF)} && (4.62)
\end{aligned}$$

for each transmission protocol.

Due to the same KRST coding at the source, it is natural that the direct and relay links may be jointly exploited to enhance symbol estimation. The direct link is particularly easy to be exploited in conjunction with such relaying schemes because their signals arrive at the destination in distinct moments (hops). Among the receivers to be introduced throughout this chapter, variants that include utilization of the direct link are also developed. More than just treating the signals arriving from the direct link in independent, separated processes, most of these receiver variants exploit the direct link model internally in their estimation frameworks.

Assuming that $\mathbf{C}$ is full-column rank and post-multiplying (4.6) by $(\mathbf{C}^T)^\dagger$ gives $\mathbf{A} = \mathbf{X}^{(SD)}_{NM_D\times P}(\mathbf{C}^T)^\dagger = \mathbf{H}^{(SD)} \diamond \mathbf{S} \in \mathbb{C}^{NM_D\times M_S}$. So, we can use LSKRF to estimate $\mathbf{S}$ and $\mathbf{H}^{(SD)}$ from this Khatri-Rao product, which leads to the following closed-form solution:

I For $m_S = 1, \cdots, M_S$

II Apply the *unvec(.)* operator to reshape the m_S^{th}-column vector of $\mathbf{A}$ into a matrix $\mathbf{B}(m_S) \in \mathbb{C}^{N\times M_D}$ such as:

$$\begin{aligned}
\mathbf{B}(m_S) &= unvec(\mathbf{A}_{.m_S}) = unvec(\mathbf{H}^{(SD)}_{.m_S} \otimes \mathbf{S}_{.m_S})\\
&= \mathbf{S}_{.m_S}\mathbf{H}^{(SD)T}_{.m_S}.
\end{aligned}$$

III Compute the SVD of $\mathbf{B}(m_S)$, with the singular values $\sigma_i\ \forall\ i \in \{1, \cdots, \max(N, M_D)\}$ ordered in a decreasing order on the diagonal of $\mathbf{\Sigma}$, i.e. $\sigma_1 \geqslant \sigma_2 \geqslant \cdots \geqslant \sigma_{\max(N,M_D)}$.

IV Assuming that $s_{1,m_S} = 1$ for $m_S = 1, \cdots, M_S$, we deduce the following estimated values $\hat{\mathbf{S}}_{.m_S} = \mathbf{U}_{.1}/u_{1,1}$ and $\hat{\mathbf{H}}^{(SD)}_{.m_S} = \mathbf{V}^*_{.1}u_{1,1}\sigma_1$.

Step IV is modified from step 3 in Remark 2 by the knowledge of the first row of $\mathbf{S}$. Such knowledge let us remove the scaling ambiguities on the columns of this matrix and $\mathbf{H}^{(SD)}$.

4.5.1 Uniqueness of the direct link model

The signals arriving at the destination through the direct link follows a PARAFAC models, as shown in (4.4), and thus one may resort to the Kruskal's condition (Eq. (3.22)) to ensure the uniqueness of the model, i.e.

$$k_{\mathbf{H}^{(SD)}} + k_{\mathbf{C}} + k_{\mathbf{S}} \geqslant 2M_S + 2, \tag{4.63}$$

and consequently we can directly state the straightforward theorem.

Theorem 5. *If the source-destination channel $\mathbf{H}^{(SD)}$ models a rich-scattering environment (i.e. its entries are independent and identically distributed (i.i.d.)), the essential uniqueness of the triplet $(\mathbf{H}^{(SD)}, \mathbf{C}, \mathbf{S})$ is ensured if*

$$k_{\mathbf{C}} + k_{\mathbf{S}} \geqslant max(2M_S - M_D, M_S) + 2. \tag{4.64}$$

Proof. If $\mathbf{H}^{(SD)}$ is a i.i.d. matrix, then with probability one $k_{\mathbf{H}^{(SD)}} = \min(M_D, M_S)$. Eq. (4.63) then becomes $k_{\mathbf{C}} + k_{\mathbf{S}} \geqslant 2M_S - \min(M_D, M_S) + 2$, which is equal to (4.64), proving Theorem 5. $\square$

The hypothesis that $\mathbf{H}^{(SD)}$ is rich scattering does not necessarily mean that the direct link is reliable. In many cases, a direct link is feeble due to a strong signal attenuation, caused for example by a high path loss between the source and the destination.

In the case where the PARAFAC model of the direct link has a unique solution, we may propose the additional theorem.

Theorem 6 (Semi-blind estimation using the direct link)**.** *Supposing the knowledge of the code matrix $\mathbf{C}$ and of the n^{th} row of the symbol matrix $\mathbf{S}$, joint estimation of $\mathbf{S}$ and $\mathbf{H}^{(SD)}$ using the SD link can be solved without any arbitrary ambiguities, i.e.*

$$\bar{\mathbf{S}} = \mathbf{S}\boldsymbol{\Lambda}^{(S)} \tag{4.65}$$

$$\bar{\mathbf{H}}^{(SD)} = \mathbf{H}^{(SD)} \left(\boldsymbol{\Lambda}^{(S)}\right)^{-1}, \tag{4.66}$$

with the known matrix $\boldsymbol{\Lambda}^{(S)} = D_n\left(\bar{\mathbf{S}}\right) D_n^{-1}\left(\mathbf{S}\right)$.

Proof. If $\mathbf{C}$ is known, then from (3.21) we know that $\bar{\mathbf{C}} = \mathbf{C}\mathbf{\Pi}\mathbf{\Lambda}^{(C)} = \mathbf{C}$, where $\mathbf{\Lambda}^{(C)}$ carries the scaling ambiguities on the columns of $\mathbf{C}$ and $\mathbf{\Pi}$ is the permutation matrix. Thus, simply $\mathbf{\Lambda}^{(C)} = \mathbf{\Pi} = \mathbf{I}_{M_S}$, and the knowledge of $\mathbf{C}$ is responsible for the absence of column permutations on the matrix factors of $\mathcal{X}^{(SD)}$. Therefore, $\bar{\mathbf{S}} = \mathbf{S}\mathbf{\Lambda}^{(S)}$ and $\bar{\mathbf{H}}^{(SD)} = \mathbf{H}^{(SD)}(\mathbf{\Lambda}^{(SD)})^{-1}$ remain to be solved.

Given that the n^{th} rows of $\mathbf{S}$ and $\bar{\mathbf{S}}$ are also known, thus the scaling ambiguities on the columns of $\mathbf{S}$ can be calculated. It can be inferred that the known matrix $\mathbf{\Lambda}^{(S)} = D_n\left(\bar{\mathbf{S}}\right) D_n^{-1}\left(\mathbf{S}\right)$ leads to $\bar{\mathbf{S}}_{n\cdot} = \mathbf{S}_{n\cdot}$, justifying the last line of Theorem 6 and thus finally proving it. □

4.6 PT2-AF receivers

In this section, we propose three different ALS-based receivers to estimate the system parameters with the PT2-AF transmission scheme. These receivers combine differently the tensor models of the direct link (i.e. PARAFAC) and of the relay-assisted link (i.e. PARATUCK2).

4.6.1 PARATUCK2-ALS (PT2-ALS)

The first receiver, called PT2-ALS, uses only the PARATUCK2 model for estimating the channel ($\mathbf{H}^{(SR)}$ and $\mathbf{H}^{(RD)}$) and symbol ($\mathbf{S}$) matrices, with a random initialization ($\widehat{\mathbf{S}}_0$, $\widehat{\mathbf{H}}_0^{(RD)}$).

Once the estimation of $\mathbf{C}$ and $\mathbf{G}$ are unnecessary, the equations of the model to be exploited are recalled in the following:

$$\mathbf{x}_{M_DPN}^{(SRD)} = \mathbf{\Omega}_1\mathbf{h}^{(SR)}, \qquad (4.26) \text{ revisited}$$

$$\mathbf{X}_{PN\times M_D}^{(SRD)} = \mathbf{\Omega}_2\left(\mathbf{H}^{(RD)}\right)^T, \qquad (4.21) \text{ revisited}$$

$$\mathbf{x}_{n}^{(SRD)} = \mathbf{\Omega}_3\mathbf{S}_{n\cdot}^T, \qquad (4.27) \text{ revisited}$$

where

$$\mathbf{\Omega}_1 = \left[\left(\mathbf{S}^T \diamond \mathbf{G}^T\right)^T \diamond \left(\mathbf{C}\otimes\mathbf{H}^{(RD)}\right)\right] \in \mathbb{C}^{M_DPN\times M_RM_S}, \tag{4.67}$$

$$\mathbf{\Omega}_2 = \left(\mathbf{I}_N\otimes\mathbf{C}\right)\mathbf{F}_1 \in \mathbb{C}^{PN\times M_R}, \tag{4.68}$$

$$\mathbf{\Omega}_3 = \left(\mathbf{C}\diamond\mathbf{Z}_n\right) \in \mathbb{C}^{M_DP\times M_S}. \tag{4.69}$$

The channel ($\mathbf{H}^{(SR)}, \mathbf{H}^{(RD)}$) and symbol ($\mathbf{S}$) matrices are jointly estimated by alternately minimizing the following conditional least squares (LS) criteria deduced from these equations of the PT2-AF model:

$$J\left(\mathbf{h}^{(SR)}\right) = \left\|\mathbf{y}^{(SRD)}_{M_D PN} - (\widehat{\mathbf{\Omega}}_1)_{i-1}\mathbf{h}^{(SR)}\right\|_2^2 \tag{4.70}$$

$$\Rightarrow \quad \widehat{\mathbf{h}}^{(SR)}_i = (\widehat{\mathbf{\Omega}}_1)^{\dagger}_{i-1}\mathbf{y}^{(SRD)}_{M_D PN}, \tag{4.71}$$

$$J\left(\mathbf{H}^{(RD)}\right) = \left\|\mathbf{Y}^{(SRD)}_{PN\times M_D} - (\widehat{\mathbf{\Omega}}_2)_i\left(\mathbf{H}^{(RD)}\right)^T\right\|_F^2 \tag{4.72}$$

$$\Rightarrow \quad \left(\widehat{\mathbf{H}}^{(RD)}_i\right)^T = (\widehat{\mathbf{\Omega}}_2)^{\dagger}_i\mathbf{Y}^{(SRD)}_{PN\times M_D}, \tag{4.73}$$

$$J\left(\mathbf{S}^T_{n\cdot}\right) = \left\|\mathbf{y}^{(SRD)}_n - (\widehat{\mathbf{\Omega}}_3)_i\mathbf{S}^T_{n\cdot}\right\|_2^2 \tag{4.74}$$

$$\Rightarrow \quad \left(\widehat{\mathbf{S}}^T_{n\cdot}\right)_i = (\widehat{\mathbf{\Omega}}_3)^{\dagger}_i\mathbf{y}^{(SRD)}_n \tag{4.75}$$

where i denotes the iteration number, $\mathbf{Y}^{(SRD)}_{PN\times M_D}$, $\mathbf{y}^{(SRD)}_{M_D PN}$ and $\mathbf{y}^{(SRD)}_n$ are the correspondent forms of the noisy tensor $\mathcal{Y}^{(SRD)}$ discussed in Sec. 4.3, and

$$(\widehat{\mathbf{\Omega}}_1)_{i-1} = \left(\widehat{\mathbf{S}}^T_{i-1} \diamond \mathbf{G}^T\right)^T \diamond \left(\mathbf{C} \otimes \widehat{\mathbf{H}}^{(RD)}_{i-1}\right), \tag{4.76}$$

$$(\widehat{\mathbf{\Omega}}_2)_i = (\mathbf{I}_N \otimes \mathbf{C})\left(\widehat{\mathbf{F}_1}\right)_i, \tag{4.77}$$

$$(\widehat{\mathbf{\Omega}}_3)_i = \mathbf{C} \diamond (\widehat{\mathbf{Z}}_n)_i, \tag{4.78}$$

with

$$\left(\widehat{\mathbf{F}_1}\right)_i = \begin{bmatrix} D_1\left(\widehat{\mathbf{S}}_{i-1}\right)\left(\widehat{\mathbf{H}}^{(SR)}_i\right)^T D_1(\mathbf{G}) \\ \vdots \\ D_N\left(\widehat{\mathbf{S}}_{i-1}\right)\left(\widehat{\mathbf{H}}^{(SR)}_i\right)^T D_N(\mathbf{G}) \end{bmatrix}, \tag{4.79}$$

$$\left(\widehat{\mathbf{Z}}_n\right)_i = \widehat{\mathbf{H}}^{(RD)}_i D_n(\mathbf{G})\widehat{\mathbf{H}}^{(SR)}_i. \tag{4.80}$$

The receiver is described in Alg. 1. The Normalized Reconstruction Error (NRE) ε_i is based on an updated version of (4.70)

$$\varepsilon_i = \left\|\mathbf{y}^{(SRD)}_{M_D PN} - \left(\widehat{\mathbf{S}}^T_i \diamond \mathbf{G}^T\right)^T \diamond \left(\mathbf{C} \otimes \widehat{\mathbf{H}}^{(RD)}_i\right)\mathbf{h}^{(SR)}_i\right\|_2^2, \tag{4.81}$$

and $\delta = 10^{-6}$ is usually the stopping criterion.

4.6.2 PT2-AF with direct link: SPP-ALS and CPP-ALS receivers

Concerning the presence of the direct link, it can be exploited along the PT2-AF protocol in two ways: the symbol estimates from direct link are used to initialize the PT2-ALS receiver or else the two links are combined to provide an alternative updating equation to (4.75).

The two possibilities lead to the formulation of two hybrid receivers, respectively called Sequential PARAFAC/PARATUCK2 (SPP-ALS) and Combined PARAFAC/PARATUCK2

Algorithm 1 PARATUCK2-ALS (PT2-ALS)

1: Initialize $\widehat{\mathbf{S}}_0$ and $\widehat{\mathbf{H}}_0^{(RD)}$

2: $i = 1$

3: **while** $|1 - \frac{\varepsilon_i}{\varepsilon_{i-1}}| \geqslant \delta$ **do** estimate $\widehat{\mathbf{h}}_i^{(SR)}$, $\widehat{\mathbf{H}}_i^{(RD)}$ and $\widehat{\mathbf{S}}_i$ minimizing in a LS sense (4.70), (4.72) and (4.74):

$$\begin{aligned}
\widehat{\mathbf{h}}_i^{(SR)} &= (\widehat{\boldsymbol{\Omega}}_1)_{i-1}^{\dagger}\mathbf{y}_{M_DPN}^{(SRD)} \\
\left(\widehat{\mathbf{H}}_i^{(RD)}\right)^T &= (\widehat{\boldsymbol{\Omega}}_2)_i^{\dagger}\mathbf{Y}_{PN\times M_D}^{(SRD)} \\
\left(\widehat{\mathbf{S}}_{n\cdot}^T\right)_i &= (\widehat{\boldsymbol{\Omega}}_3)_i^{\dagger}\mathbf{y}_n^{(SRD)}
\end{aligned} \tag{4.82}$$

4: Compute ε_i according to (4.81)

5: $i = i + 1$, return to Step 3

6: Eliminate scaling ambiguities by doing $\widehat{\mathbf{S}} \leftarrow \widehat{\mathbf{S}}_\infty(\widehat{\boldsymbol{\Lambda}}^{(S)})^{-1}$, $\widehat{\mathbf{H}}^{(RD)} \leftarrow \widehat{\mathbf{H}}_\infty^{(RD)}(\widehat{\boldsymbol{\Lambda}}^{(RD)})^{-1}$ and $\widehat{\mathbf{H}}^{(SR)} \leftarrow \widehat{\boldsymbol{\Lambda}}^{(RD)}\widehat{\mathbf{H}}_\infty^{(SR)}\widehat{\boldsymbol{\Lambda}}^{(S)}$. See (4.103) and (4.104) in Sec. 4.6.4 for further details.

(CPP-ALS), both using the PARAFAC and the PARATUCK2 models. For the SPP-ALS receiver, the direct link is used for initializing $\widehat{\mathbf{S}}_0$ as the solution of the PARAFAC-SVD algorithm presented in subsection 4.5, and then the system parameters are also estimated using Eq. (4.71), (4.73) and (4.75).

Defining $\mathbf{x}_n^{(SD)} \triangleq \left(\mathbf{X}_{M_DP\times N}^{(SD)}\right)_{\cdot n} = \left(\mathbf{C}\diamond\mathbf{H}^{(SD)}\right)\mathbf{S}_{n\cdot}^T$ from (4.7), the symbols can also be estimated by combining $\left\|\mathbf{y}_n^{(SD)} - \left(\mathbf{C}\diamond\mathbf{H}_{i-1}^{(SD)}\right)\mathbf{S}_{n\cdot}^T\right\|_2^2$ with (4.74) to form the following cost function

$$\begin{aligned}
J(\mathbf{S}_{n\cdot}^T) &= \left\|\mathbf{y}_n^{(C)} - \begin{bmatrix} \mathbf{C}\diamond\widehat{\mathbf{H}}_{i-1}^{(SD)} \\ \mathbf{C}\diamond(\widehat{\mathbf{Z}}_n^{(SRD)})_i \end{bmatrix}\mathbf{S}_{n\cdot}^T\right\|_2^2 \\
\Rightarrow\ (\widehat{\mathbf{S}}_{n\cdot}^T)_i &= \begin{bmatrix} \mathbf{C}\diamond\widehat{\mathbf{H}}_{i-1}^{(SD)} \\ \mathbf{C}\diamond(\widehat{\mathbf{Z}}_n^{(SRD)})_i \end{bmatrix}^{\dagger}\mathbf{y}_n^{(C)},
\end{aligned} \tag{4.83}$$

where

$$\mathbf{y}_n^{(C)} = \begin{bmatrix} \mathbf{y}_n^{(SD)} \\ \mathbf{y}_n^{(SRD)} \end{bmatrix} \in \mathbb{C}^{(M_DP+M_DP)\times 1}. \tag{4.84}$$

For the CPP-ALS receiver, the initial values $\widehat{\mathbf{S}}_0$ and $\widehat{\mathbf{H}}_0^{(SD)}$ are also calculated from the PARAFAC-SVD algorithm, and the symbol vector $\mathbf{S}_{n\cdot}$ is estimated using Eq. (4.83)-(4.85), i.e. by jointly exploiting the signals received from the direct link and the link via relay. Concatenating the signals received via direct link and relay link in (4.84) is possible because their acquisition is done at different instants, i.e. at the first ($\mathbf{y}_n^{(SD)}$) and at second ($\mathbf{y}_n^{(SRD)}$) hops.

The estimate $\widehat{\mathbf{H}}_{i-1}^{(SD)}$ used in (4.83) is updated at each iteration by the following equation, deduced from Eq. (4.3)

$$\left(\widehat{\mathbf{H}}_i^{(SD)}\right)^T = \left(\widehat{\mathbf{S}}_i \diamond \mathbf{C}\right)^{\dagger} \mathbf{Y}_{PN \times M_D}^{(SD)}. \tag{4.85}$$

The summary of PT2-AF receivers is show at Table 4.2. It is important to note that the three receivers differ only in the initialization (step 1) and the symbol estimation (steps 2.2 and 2.3).

Table 4.2: PT2-AF hybrid receivers

<table>
<tr><th></th><th>PT2-ALS</th><th>SPP-ALS</th><th>CPP-ALS</th></tr>
<tr><td rowspan="3">Step 1
Initialization
($i = 0$)</td><td rowspan="2">$\widehat{\mathbf{S}}_0$ random</td><td colspan="2">PARAFAC-SVD
Section 4.5</td></tr>
<tr><td>$\widehat{\mathbf{S}}_0 \leftarrow \widehat{\mathbf{S}}_{SVD}$</td><td>$\widehat{\mathbf{S}}_0 \leftarrow \widehat{\mathbf{S}}_{SVD}$
$\widehat{\mathbf{H}}_0^{(SD)} \leftarrow \widehat{\mathbf{H}}_{SVD}^{(SD)}$</td></tr>
<tr><td colspan="3">$\widehat{\mathbf{H}}_0^{(RD)}$ random</td></tr>
<tr><td>Step 2
Iteration</td><td colspan="3">$i \leftarrow i + 1$</td></tr>
<tr><td>2.1 Channel estimation</td><td colspan="3">Calculation of $\widehat{\mathbf{h}}_i^{(SR)}$ using Eq. (4.71) and (4.76)
Calculation of $\widehat{\mathbf{H}}_i^{(RD)}$ using Eq. (4.73), (4.77) and (4.79)</td></tr>
<tr><td rowspan="2">2.2 Symbol estimation</td><td colspan="3">Calculation of $(\widehat{\mathbf{S}}_{n\cdot}^T)_i$ for $n = 1, \cdots, N$</td></tr>
<tr><td colspan="2">Eq. (4.75), (4.78), and (4.80)</td><td>Eq. (4.83)-(4.84)</td></tr>
<tr><td>2.3 Refinement of $\widehat{\mathbf{H}}^{(SD)}$</td><td colspan="2"></td><td>Eq. (4.85)</td></tr>
<tr><td>Step 3</td><td colspan="3">Go to step 2 until convergence</td></tr>
</table>

4.6.3 Identifiability conditions of the PT2-AF receiver

Necessary and sufficient conditions for system identifiability with the PT2-ALS receiver are directly linked to the full column-rank condition to be satisfied by the arguments of the pseudo-inverse operators that result from the minimization of the LS cost functions (4.70), (4.72) and (4.74). That leads to the following theorems.

Theorem 7 (Necessary conditions for identifiability using PT2-ALS)**.** *The necessary condition to employ the PARATUCK2-ALS is*

$$P \geqslant \left\lceil max\left(\frac{M_R M_S}{M_D N}, \frac{M_R}{N}, \frac{M_S}{M_D}\right)\right\rceil. \tag{4.86}$$

Proof. From (4.26), (4.21) and (4.27) we have $\mathbf{x}^{(SRD)}_{M_D PN} = \mathbf{\Omega}_1 \mathbf{h}^{(SR)}$, $\mathbf{X}^{(SRD)}_{PN\times M_D} = \mathbf{\Omega}_2 \left(\mathbf{H}^{(RD)}\right)^T$ and $\mathbf{x}^{(SRD)}_{n} = \mathbf{\Omega}_3 \mathbf{S}^T_{n\cdot}$. We deduce that the system identifiability in the LS sense requires that $\mathbf{\Omega}_1$, $\mathbf{\Omega}_2$ and $\mathbf{\Omega}_3$ be full column rank.

The first necessary condition to ensure that $\mathbf{\Omega}_1 \in \mathbb{C}^{M_D PN\times M_R M_S}$, $\mathbf{\Omega}_2 \in \mathbb{C}^{PN\times M_R}$ and $\mathbf{\Omega}_3 \in \mathbb{C}^{M_D P\times M_S}$ are full column rank is that all matrices have more rows than columns. Based on the external dimensions of such matrices, the necessary conditions are respectively

$$M_D PN \geqslant M_R M_S \quad \text{and} \quad PN \geqslant M_R \quad \text{and} \quad M_D P \geqslant M_S,$$

which are transcribed in (4.86). □

Remark 3. *The condition (4.86) is necessary for both PT2-ALS and SPP-ALS. Due to the presence of the direct link to estimate* $\mathbf{S}$ *in CPP-ALS, its necessary condition to estimate the symbols is* $2M_D P \geqslant M_S$ *(see (4.83)). Therefore, for the CPP-ALS receiver the necessary condition is slightly modified to*

$$P \geqslant \left\lceil max\left(\frac{M_R M_S}{M_D N}, \frac{M_R}{N}, \frac{M_S}{2M_D}\right)\right\rceil. \tag{4.87}$$

Theorem 8 (Sufficient conditions for identifiability using PT2-AF receivers)**.** *Assuming that* $\mathbf{H}^{(RD)}$ *and* $\mathbf{H}^{(SR)}$ *have independent and identically distributed (i.i.d.) entries drawn from a continuous distribution (rich scattering assumption), joint identifiability of the channel (*$\mathbf{H}^{(RD)}$*,* $\mathbf{H}^{(SR)}$*) and symbol (*$\mathbf{S}$*) matrices with the PT2-AF receivers is guaranteed if* $\mathbf{S}$ *and* $\mathbf{G}$ *do not contain zero element, and if the code* $\mathbf{C}$ *and the channel* $\mathbf{H}^{(RD)}$ *matrices are full column rank, and the channel matrix* $\mathbf{H}^{(SR)}$ *is full row rank, which implies the following inequalities*

$$P \geqslant M_S \quad \text{and} \quad \mathrm{Min}(M_S, M_D) \geqslant M_R. \tag{4.88}$$

Proof. Applying the lemma 1, Chapter 3, which establishes that the Khatri-Rao product of $\mathbf{A} \in \mathbb{C}^{I\times R}$ and $\mathbf{B} \in \mathbb{C}^{J\times R}$ is full column rank if $k_{\mathbf{A}} + k_{\mathbf{B}} \geqslant R + 1$, we can conclude that $\mathbf{\Omega}_1$ defined in (4.67) is full column rank if

$$k_{(\mathbf{S}^T \diamond \mathbf{G}^T)^T} + k_{\mathbf{C}\otimes\mathbf{H}^{(RD)}} \geqslant M_R M_S + 1. \tag{4.89}$$

Assuming that $\mathbf{S}$ and $\mathbf{G}$ do not contain zero element ($k_{\mathbf{S}} \geqslant 1$ and $k_{\mathbf{G}} \geqslant 1$), we have $k_{(\mathbf{S}^T \diamond \mathbf{G}^T)^T} \geqslant 1$. Moreover, under the assumptions enounced in Theorem 1 ($\mathbf{C}$ and $\mathbf{H}^{(RD)}$ full column rank), we can conclude that the Kronecker product $\mathbf{C}\otimes\mathbf{H}^{(RD)}$ is full column rank, i.e. $k_{\mathbf{C}\otimes\mathbf{H}^{(RD)}} = M_R M_S$, and consequently (4.89) is satisfied, which implies that $\mathbf{\Omega}_1$ is full column rank.

From (4.68), we can deduce that $\mathbf{\Omega}_2$ is full column rank if $\mathbf{C}$ and $\mathbf{F}_1$ are also full column rank, which is the case of $\mathbf{C}$ by assumption. Considering the first row block of $\mathbf{F}_1$ in (4.24), it is easy to verify that the assumptions of Theorem 1 ensure that this block, and consequently $\mathbf{F}_1$ is full column rank. Finally, by applying again the lemma 1, Chapter 3, with $k_{\mathbf{C}} = M_S$ and $k_{\mathbf{Z}_n^{(SRD)}} \geqslant 1$, we deduce that $\mathbf{\Omega}_3$ defined in (4.69) is full column rank. That concludes the proof of Theorem 1. □

Remark 4. *When the assumptions of Theorem 8 are satisfied, implying that* $\mathbf{C}$ *is full column rank, the PARAFAC-SVD receiver described in subsection 4.5 can be applied for estimating* $\mathbf{S}$ *and* $\mathbf{H}^{(SD)}$*, i.e. initializing the SPP-ALS and CPP-ALS receivers (see step 1 in Table I).*

4.6.4 Uniqueness conditions for the PT2-AF receivers

The starting point for asserting the uniqueness of the estimated parameters in the PT2-AF transmission protocol is to ensure that the PARATUCK2 decomposition of the receiving tensor $\mathcal{X}^{(SRD)}$ has a unique solution. This is done by obeying the three conditions described in Remark 1 (Chapter 3, Sec. 3.4.1), which are restated here with the appropriate correspondences (4.19) and (4.20):

1. All matrices of the model are full rank:
2. $\mathbf{H}^{(SR)}$ has entries different from zero;
3. The number of antennas $M_R = M_S = M$;

The Remark 1 can be contextualized for the PT2-AF scheme by the following theorem.

Theorem 9. *Suppose that the channel matrices $\mathbf{H}^{(SR)}$ and $\mathbf{H}^{(RD)}$ model rich-scattering environments, and the coding matrices $\mathbf{C}$ and $\mathbf{G}$ are designed a priori to be full rank. Also assume that $\mathbf{S}$ is a full rank matrix.*

If the number of relay and source antennas are the same, i.e.

$$M_R = M_S = M, \tag{4.90}$$

and all channel coefficients of $\mathbf{H}^{(SR)}$ are different from zero, then in this case there is a triplet $\left(\mathbf{H}^{(RD)}, \mathbf{H}^{(SR)}, \mathbf{S}\right)$ such that any alternative solution $\left(\bar{\mathbf{H}}^{(RD)}, \bar{\mathbf{H}}^{(SR)}, \bar{\mathbf{S}}\right)$ satisfies the following equations

$$\bar{\mathbf{H}}^{(RD)} = \mathbf{H}^{(RD)}\left(\mathbf{P}\boldsymbol{\Lambda}^{(RD)}\right), \tag{4.91}$$

$$\bar{\mathbf{H}}^{(SR)} = \left(\boldsymbol{\Lambda}^{(G)}\right)^{-1}\left(\boldsymbol{\Lambda}^{(RD)}\right)^{-1}\mathbf{P}^T\mathbf{H}^{(SR)}\left(\boldsymbol{\Lambda}^{(S)}\right)^{-1}, \tag{4.92}$$

$$D_n\left(\bar{\mathbf{S}}\right) = z_n D_n(\mathbf{S})\boldsymbol{\Lambda}^{(S)} \quad \forall\, n \in \{1, \cdots, N\}, \tag{4.93}$$

where $\boldsymbol{\Lambda}^{(RD)} \in \mathbb{C}^{M\times M}$, $\boldsymbol{\Lambda}^{(G)} \in \mathbb{C}^{M\times M}$ and $\boldsymbol{\Lambda}^{(S)} \in \mathbb{C}^{M\times M}$ are complex diagonal matrices, $\mathbf{P} \in \mathbb{C}^{M\times M}$ is a permutation matrix and z_n is a scale factor.

Proof. The first condition to ensure the uniqueness of the PARATUCK2 decomposition according to Remark 1 is that all matrices of the model are full rank, which according to Theorem 9 is already a design rule to construct both $\mathbf{G}$ and $\mathbf{C}$. Since the channels are rich-scattering, then they can be admitted to have full rank with probability one. Besides, $\mathbf{S}$ is already assumed to be full rank, satisfying the first condition.

The second and third conditions require respectively that $M_R = M_S$ and $h^{(SR)}_{m_R,m_S} \neq 0$, for any m_r, m_S. Therefore, the three conditions in Remark 1 are indeed contextualized to the PT2-AF transmission scheme through the hypotheses stated in Theorem 9. Under its hypotheses, (3.40)-(3.44) are valid with the correspondences in (4.19) and

$$(\boldsymbol{\Lambda}^{(A)}, \boldsymbol{\Lambda}^{(B)}, \boldsymbol{\Lambda}^{(R_1)}, \boldsymbol{\Lambda}^{(R_2)}) \Longleftrightarrow (\boldsymbol{\Lambda}^{(RD)}, \boldsymbol{\Lambda}^{(C)}, \boldsymbol{\Lambda}^{(G)}, \boldsymbol{\Lambda}^{(S)}). \tag{4.94}$$

In addition, since $\mathbf{C}$ is known, then $\bar{\mathbf{C}} = \mathbf{C}\mathbf{Q}\boldsymbol{\Lambda}^{(C)} = \mathbf{C}$, and thus $\mathbf{Q} = \boldsymbol{\Lambda}^{(C)} = \mathbf{I}_{M_S}$. Therefore, (4.91)-(4.93) are proved directly from (3.40), (3.42) and (3.44). □

In Theorem 9, one of the hypotheses is that $\mathbf{S}$ is a full rank matrix. Although the symbols are sorted out from a finite alphabet, $\mathbf{S}$ being full rank is plausible if the sequences of N symbols transmitted by the M_S source antennas are statistically independent, i.e. there is no transmit diversity introduced by the multiple source antennas. In this case, the probability of full-rank increases with the number of symbols and with the modulation cardinality. The likelihood that $\mathbf{S}$ is full-rank is greater for 8-PSK than for BPSK, so for the latter modulation it may be advisable to use a greater number of transmitted symbols.

Besides, although the condition $M_R = M_S$ requires from the relaying network the same number of source and relay antennas, it does not mean that all antennas have to be active during the whole transmission, i.e. both $\mathbf{S}$ and $\mathbf{G}$ may have zero elements, as long as they do not have zero rows or zero columns.

Moreover, the hypotheses stated in Theorem 9 are sufficient to ensure the uniqueness of the model, they are not necessary, as numerous simulations with $M_S \neq M_R$ have proved.

Remark 5. *If the condition (4.90) is true, which is required to ensure the uniqueness of the PARATUCK2 model in Theorem (9), the sufficient identifiability condition (4.88) comes down to*

$$\text{Min}(P, M_D) \geqslant M. \tag{4.95}$$

The permutation matrix $\mathbf{P}$ in (4.91) and (4.92) and the ambiguities $\mathbf{\Lambda}^{(G)}$ and $\mathbf{\Lambda}^{(S)}$ can be eliminated according to the following theorem.

Theorem 10 (Semi-blind estimation using PT2-AF)**.** *Assume that all hypotheses in Theorem 9 are satisfied, such that equations (4.91)-(4.93) are always true. If the n^{th} row of $\mathbf{S}$ is known and $\mathbf{G}$ is designed accordingly to*

$$\mathbf{G} = \begin{bmatrix} 1 & 1 & \cdots & 1 \\ e^{j\phi_1} & e^{j\phi_2} & \cdots & e^{j\phi_M} \\ e^{j2\phi_1} & e^{j2\phi_2} & \cdots & e^{j2\phi_M} \\ \vdots & \vdots & \ddots & \vdots \\ e^{j(N-1)\phi_1} & e^{j(N-1)\phi_2} & \cdots & e^{j(N-1)\phi_M} \end{bmatrix}, \tag{4.96}$$

with random generators ϕ_m, $m = 1, \cdots, M$, representing phase shifts introduced by the relay antennas and known at the destination, then (4.91)-(4.93) become

$$\bar{\mathbf{H}}^{(RD)} = \mathbf{H}^{(RD)}\mathbf{\Lambda}^{(RD)}, \tag{4.97}$$

$$\bar{\mathbf{H}}^{(SR)} = \left(\mathbf{\Lambda}^{(RD)}\right)^{-1}\mathbf{H}^{(SR)}\left(\mathbf{\Lambda}^{(S)}\right)^{-1}, \tag{4.98}$$

$$\bar{\mathbf{S}} = \mathbf{S}\mathbf{\Lambda}^{(S)}. \tag{4.99}$$

with the known matrix $\mathbf{\Lambda}^{(S)} = D_n\left(\bar{\mathbf{S}}\right)D_n^{-1}\left(\mathbf{S}\right)$.

Proof. For the PARATUCK2 model, it is shown in Theorem 2 (Chapter 3, Sec. 3.4.1) that a simple design of $\mathbf{G}$ sets $\mathbf{P} = \mathbf{I}_M$ in (4.91) and (4.92), given that $\mathbf{C}$, $\mathbf{G}$ and a row of $\mathbf{S}$ are known, which are hypotheses present in theorems 9 and 10.

Besides being a full rank known matrix, $\mathbf{G}$ is also assumed *a priori* to be the Vandermonde (VD) matrix in (4.96). Applying the condition (3.47) to the first two rows of $\mathbf{G}$ defined in (4.96) gives $\phi_j \neq \phi_i + 2m\pi$ for $i \neq j$. As the phase shifts are randomly drawn, this condition is satisfied with a probability one. Indeed, inequality (3.45) is always true using $\mathbf{G}$ defined in (4.96).

Once $\mathbf{P} = \mathbf{I}_M$ and $\mathbf{Q} = \mathbf{I}_M$, since $\mathbf{G}$ is known, then from (3.43) with proper correspondence in (4.94) we have that $\mathbf{\Lambda}^{(G)} = \mathbf{I}_M$ and $z_n = 1$. In addition, given that the n^{th} row of $\mathbf{S}$ is known, then consequently from (4.93) it is calculated that $\mathbf{\Lambda}^{(S)} = D_n\left(\bar{\mathbf{S}}\right) D_n^{-1}(\mathbf{S})$.

Replacing the new expressions found for $\mathbf{\Lambda}^{(S)}$, $\mathbf{\Lambda}^{(G)}$ and $\mathbf{P}$ in (4.91)-(4.93) we prove Theorem 10. □

In Theorem 10 it was proposed a design of $\mathbf{G}$ such that at the convergence of the PT2-AF receivers their solution $\left(\hat{\mathbf{S}}_\infty, \hat{\mathbf{H}}_\infty^{(RD)}, \hat{\mathbf{H}}_\infty^{(SR)}\right)$ satisfies the following equations

$$\hat{\mathbf{S}}_\infty = \mathbf{S}\mathbf{\Lambda}^{(S)}, \tag{4.100}$$

$$\hat{\mathbf{H}}_\infty^{(RD)} = \mathbf{H}^{(RD)}\mathbf{\Lambda}^{(RD)}, \tag{4.101}$$

$$\hat{\mathbf{H}}_\infty^{(SR)} = \left(\mathbf{\Lambda}^{(RD)}\right)^{-1}\mathbf{H}^{(SR)}\left(\mathbf{\Lambda}^{(S)}\right)^{-1}, \tag{4.102}$$

where $\mathbf{\Lambda}^{(RD)} \in \mathbb{C}^{M\times M}$ is a complex diagonal matrix. From the same theorem, $\mathbf{\Lambda}^{(S)} \in \mathbb{C}^{M\times M}$ can be estimated by

$$\hat{\mathbf{\Lambda}}^{(S)} = D_1(\mathbf{S})D_1^{-1}(\hat{\mathbf{S}}_\infty), \tag{4.103}$$

due to the knowledge of the first row of $\mathbf{S}$.

This scaling ambiguity $\mathbf{\Lambda}^{(RD)}$ can be eliminated using the knowledge of one row of $\mathbf{H}^{(RD)}$ or one column of $\mathbf{H}^{(SR)}$, as mentioned in [20, 26]. In practice, such a knowledge can be obtained by means of a simple supervised procedure which consists in sending a training sequence from the relay to destination and applying the standard LS algorithm to estimate the channel $\mathbf{H}^{(RD)}$ that can be used to calculate the scaling ambiguity matrix $\mathbf{\Lambda}^{(RD)}$. This procedure is more detailed in Appendix B. When an individual channel estimation is not needed, it is important to notice that the PT2-AF receivers are robust to channel ambiguities due to the fact that symbol estimation by means of (4.75) or (4.83) only depends on the effective channel defined in (4.29), which is without scaling ambiguity since $\hat{\mathbf{H}}^{(RD)}D_n(\mathbf{G})\hat{\mathbf{H}}^{(SR)} = \mathbf{H}^{(RD)}D_n(\mathbf{G})\mathbf{H}^{(SR)}$.

Therefore, if we know the first row of $\mathbf{H}^{(RD)}$, the remaining scaling ambiguities can be eliminated by means of

$$\widehat{\boldsymbol{\Lambda}}^{(RD)} = D_1(\mathbf{H}^{(RD)})D_1^{-1}(\widehat{\mathbf{H}}_{\infty}^{(RD)}). \tag{4.104}$$

4.7 NP-AF receivers

As shown previously, the transmission scheme NP-AF provides a greater flexibility in relation to PT2-AF due to the possibility of writing the 4^{th}-order nested PARAFAC model of $\mathcal{Y}^{(SRD)}$ through different combinations of 3^{rd}-order PARAFAC models. Consequently, the NP-AF scheme allows a greater variety of receivers for symbol and channel estimation.

In this section, it is presented two classes of such receivers: one that relies on a single estimation iterative and those that employ two sequential processes. Within the first class, the NPALS receiver is developed. For the second class, a greater number of receivers are obtained due to the possibility to exploit the PARAFAC model either by ALS- or by SVD-based algorithms.

4.7.1 Nested PARAFAC using ALS (NPALS)

The receiver namely NPALS estimates all unknown parameters with a single run of the ALS algorithm. The model equations to be exploited are recalled in the following:

$$\mathbf{x}_{M_DJPN}^{(SRD)} = \left[(\mathbf{S} \diamond \mathbf{C}) \otimes (\mathbf{G} \diamond \mathbf{H}^{(RD)})\right] \mathbf{h}^{(SR)}, \qquad \text{(4.45) revisited}$$

$$\mathbf{X}_{JPN \times M_D}^{(SRD)} = \left((\mathbf{S} \diamond \mathbf{C})\, \mathbf{H}^{(SR)^T} \diamond \mathbf{G}\right) \left(\mathbf{H}^{(RD)}\right)^T, \qquad \text{(4.33) transposed}$$

$$\mathbf{X}_{M_DJP \times N}^{(SRD)} = \left(\mathbf{C} \diamond \left(\mathbf{G} \diamond \mathbf{H}^{(RD)}\right) \mathbf{H}^{(SR)}\right) \mathbf{S}^T. \qquad \text{(4.48) revisited}$$

Therefore, the NPALS receiver minimizes sequentially at its i^{th} iteration the following cost functions

$$J(\mathbf{h}^{(SR)}) = \|\mathbf{y}_{M_DJPN}^{(SRD)} - \left[(\widehat{\mathbf{S}}_{i-1} \diamond \mathbf{C}) \otimes (\mathbf{G} \diamond \widehat{\mathbf{H}}_{i-1}^{(RD)})\right] \mathbf{h}^{(SR)}\|_2^2, \tag{4.105}$$

$$J(\mathbf{H}^{(RD)}) = \|\mathbf{Y}_{JPN \times M_D}^{(SRD)} - \left[(\widehat{\mathbf{W}}_{PN \times M_R})_i \diamond \mathbf{G}\right] (\mathbf{H}^{(RD)})^T\|_F^2, \tag{4.106}$$

$$J(\mathbf{S}) = \|\mathbf{Y}_{M_DJP \times N}^{(SRD)} - \left[\mathbf{C} \diamond \left(\widehat{\mathbf{Z}}_{M_DJ \times M_S}\right)_i\right] \mathbf{S}^T\|_F^2, \tag{4.107}$$

where

$$(\widehat{\mathbf{W}}_{PN \times M_R})_i = \left(\widehat{\mathbf{S}}_{i-1} \diamond \mathbf{C}\right) (\widehat{\mathbf{H}}_i^{(SR)})^T, \tag{4.108}$$

$$\left(\widehat{\mathbf{Z}}_{M_DJ \times M_S}\right)_i = \left(\mathbf{G} \diamond \widehat{\mathbf{H}}_i^{(RD)}\right) \widehat{\mathbf{H}}_i^{(SR)}, \tag{4.109}$$

are derived from (4.8) and (4.44).

The NPALS algorithm is presented in Alg. 2. The NRE ε_i is based on an updated version of (4.105), i.e.

$$\varepsilon_i = \left\| \mathbf{y}^{(SRD)}_{M_D JPN} - \left[(\hat{\mathbf{S}}_i \diamond \mathbf{C}) \otimes (\mathbf{G} \diamond \hat{\mathbf{H}}^{(RD)}_i) \right] \hat{\mathbf{h}}^{(SR)}_i \right\|^2_F, \tag{4.110}$$

and once again $\delta = 10^{-6}$ is usually the stopping criterion.

Algorithm 2 NPALS

1: Initialize $\hat{\mathbf{S}}_0$ and $\hat{\mathbf{H}}^{(RD)}_0$

2: $i = 1$

3: **while** $|1 - \frac{\varepsilon_i}{\varepsilon_{i-1}}| \geqslant \delta$ **do** estimate $\hat{\mathbf{h}}^{(SR)}_i$, $\hat{\mathbf{H}}^{(RD)}_i$ and $\hat{\mathbf{S}}_i$ minimizing in a LS sense (4.105), (4.106) and (4.107):

$$\begin{aligned}
\hat{\mathbf{h}}^{(SR)}_i &= \left[(\hat{\mathbf{S}}_{i-1} \diamond \mathbf{C}) \otimes (\mathbf{G} \diamond \hat{\mathbf{H}}^{(RD)}_{i-1}) \right]^{\dagger} \mathbf{y}^{(SRD)}_{M_D JPN} \\
(\hat{\mathbf{H}}^{(RD)}_i)^T &= \left[(\hat{\mathbf{S}}_{i-1} \diamond \mathbf{C}) (\hat{\mathbf{H}}^{(SR)}_i)^T \diamond \mathbf{G} \right]^{\dagger} \mathbf{Y}^{(SRD)}_{JPN \times M_D} \\
\hat{\mathbf{S}}^T_i &= \left[\mathbf{C} \diamond (\mathbf{G} \diamond \hat{\mathbf{H}}^{(RD)}_i) \hat{\mathbf{H}}^{(SR)}_i \right]^{\dagger} \mathbf{Y}^{(SRD)}_{M_D JP \times N}
\end{aligned} \tag{4.111}$$

4: Compute ε_i according to (4.110)

5: $i = i + 1$, return to Step 3

6: Using (4.157) and (4.156) eliminate scaling ambiguities by doing $\hat{\mathbf{S}} \leftarrow \hat{\mathbf{S}}_\infty (\hat{\mathbf{\Lambda}}^{(S)})^{-1}$, $\hat{\mathbf{H}}^{(RD)} \leftarrow \hat{\mathbf{H}}^{(RD)}_\infty (\hat{\mathbf{\Lambda}}^{(RD)})^{-1}$ and $\hat{\mathbf{H}}^{(SR)} \leftarrow \hat{\mathbf{\Lambda}}^{(RD)} \hat{\mathbf{H}}^{(SR)}_\infty \hat{\mathbf{\Lambda}}^{(S)}$. See Sec. 4.7.5 for further details.

4.7.2 NP-AF two-step receivers

On the contrary to the single-stage, three-steps NPALS receiver, now it is presented two two-steps semi-blind receivers. The convenience of this approach is the partition of the estimation into likely faster procedures. Iterative algorithms dedicated to minimization of square errors, such as the ALS itself, may not behave well for a great number of parameters, mainly due to the often present inverse operations.

In order to estimate all parameters (channel and symbol matrices) in two stages, we define here the DALS and DKRF receivers. DALS stands for *Double Alternating Least Squares*, since it is composed by two sequential ALS-based methods, named ALS-X and ALS-Z routines. The DKRF receiver is composed sequentially by the methods named KRF-X and KRF-Z, which uses the SVD-based algorithm presented in Remark 2.

For both receivers, in the first stage the symbol matrix $\mathbf{S}$ and an unfolding of the effective channel tensor $\mathcal{Z}$ are estimated, and then from the reconstruction of this tensor $\mathbf{H}^{(SR)}$ and

$\mathbf{H}^{(RD)}$ are estimated. Therefore, the first step comprises the symbol estimation procedure, while the second one is dedicated to the joint estimation of the individual channels.

4.7.2.1 Double Alternating Least Squares (DALS) receiver

In the ALS-X routine of the DALS receiver, $\mathbf{S}$ and $\mathcal{Z}$ are estimated by exploiting the following equations

$$\begin{aligned}
\mathbf{X}^{(SRD)}_{PN\times M_D J} &= (\mathbf{S} \diamond \mathbf{C})\, \mathbf{Z}_{M_S\times M_D J}, && \text{(4.40) transposed}\\
\mathbf{X}^{(SRD)}_{M_D JP\times N} &= (\mathbf{C} \diamond \mathbf{Z}_{M_D J\times M_S})\, \mathbf{S}^T. && \text{(4.48) revisited}
\end{aligned}$$

Therefore, the ALS-X step estimates $\mathbf{Z}_{M_D J\times M_S}$ and $\mathbf{S}$ by minimizing the respective cost functions

$$\left\| \mathbf{Y}^{(SRD)}_{PN\times M_D J} - \left(\hat{\mathbf{S}}_{i-1} \diamond \mathbf{C}\right) \mathbf{Z}_{M_S\times M_D J} \right\|_F^2, \tag{4.112}$$

$$\left\| \mathbf{Y}^{(SRD)}_{M_D JP\times N} - \left(\mathbf{C} \diamond \left(\hat{\mathbf{Z}}_{M_D J\times M_S}\right)_i\right) \mathbf{S}^T \right\|_F^2. \tag{4.113}$$

Once $\hat{\mathcal{Z}}$ is obtained in the form of its unfolding $\hat{\mathbf{Z}}_{M_D J\times M_S}$, then ALS-Z estimates $\mathbf{H}^{(SR)}$ and $\mathbf{H}^{(RD)}$ minimizing the cost functions in a LS sense

$$\left\| \hat{\mathbf{Z}}_{M_D J\times M_S} - \left(\mathbf{G} \diamond \hat{\mathbf{H}}^{(RD)}_{i-1}\right) \mathbf{H}^{(SR)} \right\|_F^2, \tag{4.114}$$

$$\left\| \hat{\mathbf{Z}}_{JM_S\times M_D} - \left((\hat{\mathbf{H}}^{(SR)})^T_i \diamond \mathbf{G}\right) (\mathbf{H}^{(RD)})^T \right\|_F^2, \tag{4.115}$$

derived respectively from

$$\begin{aligned}
\mathbf{Z}_{M_D J\times M_S} &= \left(\mathbf{G} \diamond \mathbf{H}^{(RD)}\right) \mathbf{H}^{(SR)}, && \text{(4.44) revisited}\\
\mathbf{Z}_{JM_S\times M_D} &= \left(\left(\mathbf{H}^{(SR)}\right)^T \diamond \mathbf{G}\right) (\mathbf{H}^{(RD)})^T. && \text{(4.42) revisited}
\end{aligned}$$

The DALS algorithm is better explained through its steps in Algs. 3 and 4. The stopping criteria ε_i and $\varepsilon_i^{(1)}$ for DALS are calculated respectively by (4.110) and

$$\varepsilon_i^{(1)} = \left\| \mathbf{Y}^{(SRD)}_{PN\times M_D J} - \left(\hat{\mathbf{S}}_i \diamond \mathbf{C}\right) \left(\hat{\mathbf{Z}}_{M_D J\times M_S}\right)_i^T \right\|_F^2. \tag{4.116}$$

4.7.2.2 Double Khatri-Rao Factorization (DKRF) receiver

We assume that $\mathbf{C}$ and $\mathbf{G}$ are known, full column-rank matrices, thus the LSKRF method described in Remark 2 can be used to estimate at the same time both terms of the Khatri-Rao products from the respective tensor unfoldings:

Algorithm 3 ALS-X: Symbol estimation step

Input $\mathbf{Y}^{(SRD)}_{NM_DJ\times P}$ and $\mathbf{C}$

1: Initialize $\widehat{\mathbf{S}}_0$

2: $i = 1$

3: **while** $|1 - \frac{\varepsilon_i^{(1)}}{\varepsilon_{i-1}^{(1)}}| \geqslant \delta$ **do** estimate $\widehat{\mathbf{Z}}_{M_DJ\times M_S}$ and $\widehat{\mathbf{S}}$ minimizing in a LS sense (4.112) and (4.113) :

$$(\widehat{\mathbf{Z}}_{M_S\times M_DJ})_i = \left(\widehat{\mathbf{S}}_{i-1}\diamond\mathbf{C}\right)^{\dagger}\mathbf{Y}^{(SRD)}_{PN\times M_DJ}$$
$$\widehat{\mathbf{S}}_i^T = \left(\mathbf{C}\diamond(\widehat{\mathbf{Z}}_{M_DJ\times M_S})_i\right)^{\dagger}\mathbf{Y}^{(SRD)}_{M_DJP\times N} \tag{4.117}$$

4: Compute $\varepsilon_i^{(1)}$ according to (4.116)

5: $i = i + 1$, return to Step 3

6: Using (4.157) eliminate column ambiguities by doing $\widehat{\mathbf{S}} \leftarrow \widehat{\mathbf{S}}_\infty(\widehat{\boldsymbol{\Lambda}}^{(S)})^{-1}$ and $\widehat{\mathbf{Z}}_{M_DJ\times M_S} \leftarrow (\widehat{\mathbf{Z}}_{M_DJ\times M_S})_\infty\widehat{\boldsymbol{\Lambda}}^{(S)}$.

Output $\widehat{\mathbf{S}}$ and $\widehat{\mathbf{Z}}^{(SRD)}_{M_DJ\times M_S}$

Algorithm 4 ALS-Z: Channel estimation step

Input $\widehat{\mathbf{Z}}^{(SRD)}_{M_DJ\times M_S}$ and $\mathbf{G}$

1: Initialize $\widehat{\mathbf{H}}_0^{(RD)}$

2: $i = 1$

3: **while** $|1 - \frac{\varepsilon_i}{\varepsilon_{i-1}^{(2)}}| \geqslant \delta$ **do** estimate $\widehat{\mathbf{H}}^{(SR)}$ and $\widehat{\mathbf{H}}^{(RD)}$ minimizing in a LS sense (4.114) and (4.115):

$$\widehat{\mathbf{H}}_i^{(SR)} = \left(\mathbf{G}\diamond\widehat{\mathbf{H}}_{i-1}^{(RD)}\right)^{\dagger}\widehat{\mathbf{Z}}_{M_DJ\times M_S}$$
$$(\widehat{\mathbf{H}}_i^{(RD)})^T = \left((\widehat{\mathbf{H}}_i^{(SR)})^T\diamond\mathbf{G}\right)^{\dagger}\widehat{\mathbf{Z}}_{JM_S\times M_D} \tag{4.118}$$

4: Compute ε_i according to (4.110)

5: $i = i + 1$, return to Step 3

6: Using (4.156) eliminate scaling ambiguities by doing $\widehat{\mathbf{H}}^{(RD)} \leftarrow \widehat{\mathbf{H}}_\infty^{(RD)}(\widehat{\boldsymbol{\Lambda}}^{(RD)})^{-1}$ and $(\widehat{\mathbf{H}}^{(SR)})^T \leftarrow (\widehat{\mathbf{H}}_\infty^{(SR)})^T\widehat{\boldsymbol{\Lambda}}^{(RD)}$.

Output $\widehat{\mathbf{H}}^{(SR)}$ and $\widehat{\mathbf{H}}^{(RD)}$

$$\mathbf{X}^{(SRD)}_{NM_DJ\times P} = \left(\mathbf{Z}_{M_DJ\times M_S} \diamond \mathbf{S}\right)\mathbf{C}^T, \qquad \text{(4.47) revisited}$$

$$\mathbf{Z}_{M_SM_D\times J} = \left(\mathbf{H}^{(RD)} \diamond (\mathbf{H}^{(SR)})^T\right)\mathbf{G}^T. \qquad \text{(4.43) revisited}$$

The sequential procedures KRF-X and KRF-Z are summarized in Algs. 5 and 6, respectively.

Algorithm 5 KRF-X: Symbol estimation step

Input $\mathbf{Y}^{(SRD)}_{NM_DJ\times P}$ and $\mathbf{C}$

1. $\mathbf{A} = \mathbf{Y}^{(SRD)}_{NM_DJ\times P}\left(\mathbf{C}^T\right)^{\dagger} \in \mathbb{C}^{NM_DJ\times M_S}$
2. For $m_S \in \{1, \cdots, M_S\}$:
   - i Reshape $\mathbf{A}_{\cdot m_S}$ into matrix $\text{unvec}(\mathbf{A}_{\cdot m_S}) \in \mathbb{C}^{N\times M_DJ}$
   - ii Compute the SVD of $\text{unvec}(\mathbf{A}_{\cdot m_S})$.
   - iii $\hat{\mathbf{S}}_{\cdot m_S} = \mathbf{u}/u_1$ and $\left(\hat{\mathbf{Z}}^{(SRD)}_{M_DJ\times M_S}\right)_{\cdot m_S} = \mathbf{v}^* u_1\sigma_1$, where σ_1 is the greatest singular value, and $\mathbf{u}$ and $\mathbf{v}$ are respectively the associated left-singular and right-singular vectors.

Output $\hat{\mathbf{S}}$ and $\hat{\mathbf{Z}}^{(SRD)}_{M_DJ\times M_S}$

Algorithm 6 KRF-Z: Channel estimation step

Input $\hat{\mathbf{Z}}^{(SRD)}_{M_DJ\times M_S}$ and $\mathbf{G}$

1. Reorder $\hat{\mathbf{Z}}^{(SRD)}_{M_DJ\times M_S}$ into $\hat{\mathbf{Z}}^{(SRD)}_{M_SM_D\times J}$
2. $\mathbf{B} = \hat{\mathbf{Z}}^{(SRD)}_{M_SM_D\times J}\left(\mathbf{G}^T\right)^{\dagger} \in \mathbb{C}^{M_SM_D\times M_R}$
3. For $m_R \in \{1, \cdots, M_R\}$:
   - i Reshape $\mathbf{B}_{\cdot m_R}$ into matrix $\text{unvec}(\mathbf{B}_{\cdot m_R}) \in \mathbb{C}^{M_S\times M_D}$
   - ii Compute the SVD of $\text{unvec}(\mathbf{B}_{\cdot m_R})$.
   - iii $\left(\hat{\mathbf{H}}^{(SR)}_{m_R\cdot}\right)^T = \mathbf{u}\sqrt{\sigma_1}$ and $\hat{\mathbf{H}}^{(RD)}_{\cdot m_R} = \mathbf{v}^*\sqrt{\sigma_1}$, where σ_1 is the greatest singular value, and $\mathbf{u}$ and $\mathbf{v}$ are respectively the associated left-singular and right-singular vectors.

Output $\hat{\mathbf{H}}^{(SR)}$ and $\hat{\mathbf{H}}^{(RD)}$

The ALS-X and KRF-X steps estimate the same parameters ($\hat{\mathbf{S}}$ and $\hat{\mathbf{Z}}_{M_DJ\times M_S}$), while ALS-Z and KRF-Z also have the same function of estimating $\hat{\mathbf{H}}^{(SR)}$ and $\hat{\mathbf{H}}^{(RD)}$. Indeed, there is some modularity within the proposed algorithms, as ALS-X (or KRF-X) could be followed by either ALS-Z or KRF-Z, as shown in the scheme that follows

$$\begin{array}{ccccl} \text{ALS-X} & + & \text{ALS-Z} & \Rightarrow \text{DALS} \\ \text{ALS-X} & + & \text{KRF-Z} & \\ \text{KRF-X} & + & \text{ALS-Z} & \\ \text{KRF-X} & + & \text{KRF-Z} & \Rightarrow \text{DKRF} \\ \underbrace{\qquad\qquad}_{\substack{\text{Symbol}\\ \text{estimation}}} & & \underbrace{\qquad\qquad}_{\substack{\text{Channel}\\ \text{estimation}}} & \end{array}$$

The advantage of each combination lies mainly on the identifiability issues (discussed in §4.7.4) and on the computational complexities (discussed in §4.8). For a greater cohesion with the works [69, 85] that firstly introduced DALS and DKRF, the other possible combinations (i.e. ALS-X+KRF-Z and KRF-X +ALS-Z) are left aside in favor of emphasizing the difference between ALS- and SVD-based strategies through the use of these two receivers.

Prior to the study of the conditions for the use of the just proposed NP-AF receivers, it is convenient to introduce some variants that can exploit the presence of a direct link.

4.7.3 NP-AF with direct link

Similarly to the case of using the direct link with the PT2-AF protocol in §4.6.2, to which the SPP-ALS and CPP-ALS receivers have been developed, the direct link can also be combined with NP-AF, thus opening the possibility of new strategies for semi-blind estimation .

For the NPALS and DALS receivers it is clear that the symbols estimated via direct link can be directly used as an initialization for their iterative algorithm, likewise in SPP-ALS. For DKRF this sort of initialization is irrelevant, since the estimation is done in a non-iterative fashion. For any proposed NP-AF receiver the direct link can be used in combination with the relay link to improve symbol estimation, as in CPP-ALS.

Let us combine the signals received from the two links such as

$$\mathbf{X}^{(c)} = \begin{bmatrix} \mathbf{X}^{(SD)}_{M_D P \times N} \\ \mathbf{X}^{(SRD)}_{M_D JP \times N} \end{bmatrix} \in \mathbb{C}^{(M_D P + M_D JP) \times N}, \tag{4.119}$$

so that the vertical staking of signals received via both links, obtained from (4.7) and (4.48), be expressed by

$$\mathbf{X}^{(c)} = \begin{bmatrix} \mathbf{C} \diamond \mathbf{H}^{(SD)} \\ \mathbf{C} \diamond \mathbf{Z}_{M_D J \times M_S} \end{bmatrix} \mathbf{S}^T \tag{4.120}$$

$$= \begin{bmatrix} \mathbf{C} \diamond \mathbf{H}^{(SD)} \\ \mathbf{C} \diamond \left(\mathbf{G} \diamond \mathbf{H}^{(RD)}\right) \mathbf{H}^{(SR)} \end{bmatrix} \mathbf{S}^T \tag{4.121}$$

The following three variants of receivers are proposed to combine the symbol estimation using the two available links. For both NPALS and ALS-X, symbol estimation is updated at each iteration, so we can define their respective variants CNPALS and CALS-X, both minimizing in the LS sense the following cost function

$$\left\| \mathbf{Y}^{(c)} - \begin{bmatrix} \mathbf{C} \diamond \hat{\mathbf{H}}^{(SD)}_{i-1} \\ \mathbf{C} \diamond \left(\hat{\mathbf{Z}}_{M_D J \times M_S} \right)_i \end{bmatrix} \mathbf{S}^T \right\|_F^2 . \tag{4.122}$$

The estimated channel at i^{th} iteration $\left(\hat{\mathbf{Z}}_{M_D J \times M_S} \right)_i$ are exploited differently by each algorithm. For CNPALS such matrix is calculated using the estimates of $\mathbf{H}^{(RD)}$ and $\mathbf{H}^{(SR)}$, whereas CALS-X finds $\hat{\mathbf{Z}}_{M_D J \times M_S}$ to be used in ALS-Z to estimate such individual channels. Indeed, this is a fundamental difference between the NPALS and DALS (and DKRF) receivers, since their processes of joint channel estimation are conceptually opposite to each other. In the former receiver the effective channel can be determined after its explicit constituents ($\mathbf{H}^{(RD)}$ and $\mathbf{H}^{(SR)}$), while the two-step receivers segment the effective channel in the aforementioned channels. Whether $\left(\hat{\mathbf{Z}}_{M_D J \times M_S} \right)_i$ is calculated or simply estimated, the updating equations for symbol estimation using CNPALS or CALS-X, derived from (4.122), are respectively

$$\mathbf{S}_i^T = \begin{bmatrix} \mathbf{C} \diamond \hat{\mathbf{H}}^{(SD)}_{i-1} \\ \mathbf{C} \diamond \left(\mathbf{G} \diamond \hat{\mathbf{H}}^{(RD)}_i \right) \hat{\mathbf{H}}^{(SR)}_i \end{bmatrix}^{\dagger} \mathbf{Y}^{(c)} \tag{4.123}$$

and

$$\mathbf{S}_i^T = \begin{bmatrix} \mathbf{C} \diamond \hat{\mathbf{H}}^{(SD)}_{i-1} \\ \mathbf{C} \diamond \left(\hat{\mathbf{Z}}_{M_D J \times M_S} \right)_i \end{bmatrix}^{\dagger} \mathbf{Y}^{(c)}. \tag{4.124}$$

These equations may replace the original equations in NPALS and ALS-X, as described in Table 4.3. As for CPP-ALS, this new symbol estimation can be used to refine the direct channel estimate at the end of each iteration using (4.85).

A variant to KRF-X is obtained in a different way, since the non-iterative algorithms explore different unfoldings of the input tensors ($\mathcal{Y}^{(SRD)}$ and $\mathcal{Z}$). Defining the compound channel

$$\mathbf{Z}^{(c)} = \begin{bmatrix} \mathbf{H}^{(SD)} \\ \mathbf{Z}_{M_D J \times M_S} \end{bmatrix} \in \mathbb{C}^{(M_D + M_D J) \times M_S} \Rightarrow \hat{\mathbf{Z}}^{(c)} = \begin{bmatrix} \hat{\mathbf{H}}^{(SD)} \\ \hat{\mathbf{Z}}_{M_D J \times M_S}, \end{bmatrix} \tag{4.125}$$

then from (4.6) and (4.47) one obtains

$$\mathbf{X}^{(a)} \triangleq \begin{bmatrix} \mathbf{X}^{(SD)}_{NM_D \times P} \\ \mathbf{X}^{(SRD)}_{NM_D J \times P} \end{bmatrix} = \left(\mathbf{Z}^{(c)} \diamond \mathbf{S} \right) \mathbf{C}^T \in \mathbb{C}^{(NM_D + NM_D J) \times P}. \tag{4.126}$$

Therefore, the variant CKRF-X corresponds to replacing in KRF-X the input $\mathbf{Y}^{(SRD)}_{NM_D J \times P}$ by $\mathbf{Y}^{(a)}$, the noisy observation of (4.126), such that in the output of this algorithm one may obtain $\hat{\mathbf{S}}$ and $\hat{\mathbf{Z}}^{(c)}$, this last one obtained in the place of the original outcome $\hat{\mathbf{Z}}_{M_D J \times M_S}$.

From $\hat{\mathbf{Z}}^{(c)}$ both $\hat{\mathbf{Z}}_{M_D J \times M_S}$ and $\hat{\mathbf{H}}^{(SD)}$ can be found as its submatrices from (4.125). The CKRF-X procedure is also summarized in Table 4.3.

Table 4.3: NP-AF hybrid receivers

CNPALS	Run NPALS (Alg. 2) with the following modifications : i. Initialize $\hat{\mathbf{S}}_0 \leftarrow \hat{\mathbf{S}}_{SVD}$ and $\hat{\mathbf{H}}_0^{(SD)} \leftarrow \hat{\mathbf{H}}_{SVD}^{(SD)}$ from PARAFAC-SVD (§4.5) ii. Replace the symbol estimation in (4.82) by (4.123). iii. Refine $\hat{\mathbf{H}}^{(SD)}$ at i^{th} iteration using Eq. (4.85).
CALS-X	Run ALS-X (Alg. 3) with the following modifications : i. Initialize $\hat{\mathbf{S}}_0 \leftarrow \hat{\mathbf{S}}_{SVD}$ and $\hat{\mathbf{H}}_0^{(SD)} \leftarrow \hat{\mathbf{H}}_{SVD}^{(SD)}$ from PARAFAC-SVD (§4.5) ii. Replace the symbol estimation in (4.117) by (4.124). iii. Refine $\hat{\mathbf{H}}^{(SD)}$ at i^{th} iteration using Eq. (4.85).
CKRF-X	Run KRF-X (Alg. 5) with the following modifications : i. Replace $\mathbf{Y}_{NM_DJ\times P}^{(SRD)}$ by $\mathbf{Y}^{(a)}$, the noisy observation of (4.126) ii. Replace $\mathbf{Z}_{M_DJ\times M_S}$ by $\mathbf{Z}^{(c)}$ iii. Estimate $\hat{\mathbf{H}}^{(SD)}$ and $\hat{\mathbf{Z}}_{M_DJ\times M_S}$ from $\hat{\mathbf{Z}}^{(c)}$, according to (4.125).

4.7.4 Identifiability conditions of NP-AF receivers

The following theorems present necessary and sufficient conditions for system identifiability with the proposed NP-AF receivers.

Theorem 11. *(Necessary identifiability conditions for the NPALS and DALS receivers) Necessary conditions for system identifiability in the LS sense with the NPALS receiver are*

$$
\begin{aligned}
P &\geqslant \lceil M_S/N \rceil, \\
J &\geqslant \lceil M_R/M_D \rceil, \\
PJ &\geqslant \left\lceil \max\left(\frac{M_S}{M_D}, \frac{M_R}{N}\right)\right\rceil,
\end{aligned}
$$

while for the DALS receiver these necessary conditions are

$$
\begin{aligned}
P &\geqslant \lceil M_S/\min(N, M_DJ) \rceil, \\
J &\geqslant \lceil M_R/\min(M_D, M_S) \rceil.
\end{aligned}
$$

Proof. To minimize the cost functions proposed by the NPALS and DALS receivers in a LS sense is necessary that all matrices to be left-inverted have full column-rank.

For the NPALS receiver we need from (4.105), (4.106) and (4.107) that

$$\text{rank}\left((\mathbf{S}\diamond\mathbf{C})\otimes(\mathbf{G}\diamond\mathbf{H}^{(RD)})\right) = M_R M_S, \tag{4.127}$$

$$\text{rank}\left(\mathbf{W}_{PN\times M_R}\diamond\mathbf{G}\right) = M_R, \tag{4.128}$$

$$\text{rank}\left(\mathbf{C}\diamond\mathbf{Z}_{M_D J\times M_S}\right) = M_S. \tag{4.129}$$

Due to the property that $\text{rank}\left((\mathbf{S}\diamond\mathbf{C})\otimes(\mathbf{G}\diamond\mathbf{H}^{(RD)})\right) = \text{rank}\left((\mathbf{S}\diamond\mathbf{C})\right)\text{rank}\left(\mathbf{G}\diamond\mathbf{H}^{(RD)})\right)$, then (4.127) is only satisfied if

$$\text{rank}\left(\mathbf{S}\diamond\mathbf{C}\right) = M_S, \tag{4.130}$$

$$\text{rank}\left(\mathbf{G}\diamond\mathbf{H}^{(RD)}\right) = M_R. \tag{4.131}$$

Eqs. (4.130), (4.131), (4.128) and (4.129) are necessary and sufficient conditions for system identifiability using the NPALS receiver. Therefore, for these conditions to be true we need at least that $\mathbf{S}\diamond\mathbf{C}\in\mathbb{C}^{PN\times M_S}$, $\mathbf{G}\diamond\mathbf{H}^{(RD)}\in\mathbb{C}^{M_D J\times M_R}$, $\mathbf{W}_{PN\times M_R}\diamond\mathbf{G}\in\mathbb{C}^{JPN\times M_R}$ and $\mathbf{C}\diamond\mathbf{Z}_{M_D J\times M_S}\in\mathbb{C}^{M_D JP\times M_S}$ be tall matrices. Based on the dimensions of these matrices, we need respectively that $PN\geqslant M_S$, $M_D J\geqslant M_R$, $JPN\geqslant M_R$ and $M_D JP\geqslant M_S$. The necessary identifiability conditions for NPALS can be grouped as

$$P\geqslant\lceil M_S/N\rceil, \tag{4.132}$$

$$J\geqslant\lceil M_R/M_D\rceil, \tag{4.133}$$

$$PJ\geqslant\left\lceil\max\left(\frac{M_S}{M_D},\frac{M_R}{N}\right)\right\rceil. \tag{4.134}$$

Using the same logic, the necessary conditions for the DALS receiver are obtained from (4.112)–(4.115). For the ALS-X routine to minimize (4.112) and (4.113) both $\mathbf{S}\diamond\mathbf{C}\in\mathbb{C}^{PN\times M_S}$ and $\mathbf{C}\diamond\mathbf{Z}_{M_D J\times M_S}\in\mathbb{C}^{M_D JP\times M_S}$ must have more rows than columns, and thus

$$P\geqslant\lceil M_S/\min(N,M_D J)\rceil. \tag{4.135}$$

For the ALS-Z routine, such reasoning is made on the dimensions of $\mathbf{G}\diamond\mathbf{H}^{(RD)}\in\mathbb{C}^{M_D J\times M_R}$ and of $(\mathbf{H}^{(SR)})^T\diamond\mathbf{G}\in\mathbb{C}^{JM_S\times M_R}$ present in (4.114) and (4.115), respectively. Therefore, these conditions lead to

$$J\geqslant\lceil M_R/\min(M_D,M_S)\rceil. \tag{4.136}$$

□

Theorem 11 does not concern specific conditions on the matrix factors to assure identifiability using the proposed receivers.

In the following theorem, sufficient conditions are presented for that matter.

Theorem 12. *(Sufficient identifiability conditions for NPALS, DALS and DKRF receivers) Assuming that channels $\mathbf{H}^{(SR)}$ and $\mathbf{H}^{(RD)}$ have i.i.d. entries drawn from a continuous complex Gaussian distribution and symbol matrix $\mathbf{S}$ does not have zero columns, then the identifiability of channels and symbol matrices using the NPALS, DALS and DKRF receivers is ensured if both source and relay coding matrices $\mathbf{C}$ and $\mathbf{G}$ have full column-rank (i.e. rank$(\mathbf{C}) = k_{\mathbf{C}} = M_S$ and rank$(\mathbf{G}) = k_{\mathbf{G}} = M_R$), which implies the following inequalities*

$$P \geqslant M_S \quad \text{and} \quad J \geqslant M_R. \tag{4.137}$$

Condition (4.137) is also a necessary identifiability condition for the DKRF receiver.

Proof. As previously stated in the proof of Theorem 11, the identifiability conditions for the NPALS and DALS receivers are linked to the condition of full column-rank of the arguments of the pseudo-inverse operations. Using the lemma 1, Chapter 3, then the necessary and sufficient conditions (4.130), (4.131), (4.128) and (4.129) for the NPALS algorithm are always satisfied if

$$k_{\mathbf{S}} + k_{\mathbf{C}} \geqslant M_S + 1, \tag{4.138}$$

$$k_{\mathbf{G}} + k_{\mathbf{H}^{(RD)}} \geqslant M_R + 1, \tag{4.139}$$

$$k_{\mathbf{W}_{PN\times M_R}} + k_{\mathbf{G}} \geqslant M_R + 1, \tag{4.140}$$

$$k_{\mathbf{C}} + k_{\mathbf{Z}_{M_D J\times M_S}} \geqslant M_S + 1. \tag{4.141}$$

From the hypotheses presented in Theorem 12 we have that $k_{\mathbf{C}} = M_S$ and $k_{\mathbf{G}} = M_R$, then the conditions (4.138)-(4.141) are always satisfied if $k_{\mathbf{S}}$, $k_{\mathbf{H}^{(RD)}}$, $k_{\mathbf{W}_{PN\times M_R}}$ and $k_{\mathbf{Z}_{M_D J\times M_S}}$ are different from zero, where the k-rank of a matrix is only zero if and only if such matrix has a zero column. It is stated in Theorem 12 that $\mathbf{S}$ does not have zero columns and $\mathbf{H}^{(RD)}$ is full rank, thus $k_{\mathbf{S}} \geqslant 1$ and $k_{\mathbf{H}^{(RD)}} \geqslant 1$, and conditions (4.138) and (4.139) are always satisfied. Concerning $k_{\mathbf{W}_{PN\times M_R}}$ and $k_{\mathbf{Z}_{M_D J\times M_S}}$, we can inferred from (4.8) and (4.44) that $\mathbf{W}_{PN\times M_R}$ and $\mathbf{Z}_{M_D J\times M_S}$ have a zero column if

$$(\mathbf{W}_{PN\times M_R})_{\cdot m_R} = (\mathbf{S} \diamond \mathbf{C}) \left(\mathbf{H}^{(SR)}_{m_R \cdot}\right)^T = \mathbf{0}_{PN\times 1}, \tag{4.142}$$

$$(\mathbf{Z}_{M_D J\times M_S})_{\cdot m_S} = \left(\mathbf{G} \diamond \mathbf{H}^{(RD)}\right) \mathbf{H}^{(SR)}_{\cdot m_S} = \mathbf{0}_{M_D J\times 1}. \tag{4.143}$$

Satisfied (4.138) and (4.139), and thus $(\mathbf{S} \diamond \mathbf{C})$ and $\left(\mathbf{G} \diamond \mathbf{H}^{(RD)}\right)$ are full column-rank, (4.142) and (4.143) are true if and only if $\left(\mathbf{H}^{(SR)}_{m_R \cdot}\right)^T = \mathbf{0}_{M_S\times 1}$ and $\mathbf{H}^{(SR)}_{\cdot m_S} = \mathbf{0}_{M_R\times 1}$ (that would be the trivial solutions of such linear systems (4.142) and (4.143)). Once the channel matrices are assumed to have i.i.d. entries, this is clearly not likely, and then we may admit that $k_{\mathbf{W}_{PN \times M_R}} \geqslant 1$ and $k_{\mathbf{Z}_{M_D J \times M_S}} \geqslant 1$, and (4.140) and (4.141) are satisfied. Therefore, the hypotheses introduced in Theorem 12 let us satisfy the identifiability for the NPALS receiver.

To derive the set of identifiability conditions of the DALS receiver, one may start by looking at (4.112)-(4.115). The necessary and sufficient conditions based on the cost functions (4.112), (4.113) and (4.114) are exactly (4.130), (4.129) and (4.131), respectively. As proved in the last paragraph, such conditions are always satisfied if (4.138), (4.141) and (4.139) are true, so the hypotheses made on Theorem 12 do satisfy these identifiability conditions.

The only sufficient identifiability condition for the DALS receiver that is not shared by the NPALS receiver is based on the minimization of (4.115). To identify $\mathbf{H}^{(RD)}$ we need that $(\mathbf{H}^{(SR)})^T \diamond \mathbf{G}$ be full column-rank. Using the lemma 1, Chapter 3, we have that

$$k_{(\mathbf{H}^{(SR)})^T} + k_{\mathbf{G}} \geqslant M_R + 1, \tag{4.144}$$

which is always satisfied, since $k_{(\mathbf{H}^{(SR)})^T} \geqslant 1$ and $k_{\mathbf{G}} = M_R$.

For the DKRF receiver, the only necessary and sufficient condition is that both $\mathbf{G}$ and $\mathbf{C}$ be full column rank, and thus the condition (4.137). This ends the proof of Theorem 12. $\square$

Remark 6. *Although the presence of the direct link in the equations of CNPALS and CALS-X tends to increase the spatial diversity at the destination, which could relax the necessary conditions on P and J, the use of the PARAFAC-SVD algorithm determines that the necessary (and sufficient) condition for these receivers, subject to the same hypotheses of Theorem 11, is*

$$P \geqslant M_S.$$

Evidently, this condition is also necessary and sufficient for CKRF-X, as it is for KRF-X algorithm.

4.7.5 Uniqueness conditions for the NP-AF receivers

The sufficient conditions for the uniqueness of the parameters in the NP-AF system are drawn from Sec. 3.5.1 using the correspondences in (4.34) and (4.35).

Theorem 13. *Assuming that the entries of the channels* $\mathbf{H}^{(SR)}$ *and* $\mathbf{H}^{(RD)}$ *are drawn from a continuous distribution, and the symbol matrix* $\mathbf{S}$ *does not have zero columns, which implies* $k_{\mathbf{S}} \geqslant 1$*, then identifiability of channels and symbol matrices using the NP-AF transmission scheme is ensured if both source and relay coding matrices* $\mathbf{C}$ *and* $\mathbf{G}$ *have full column-rank (i.e. rank*$(\mathbf{C}) = k_{\mathbf{C}} = M_S$ *and rank*$(\mathbf{G}) = k_{\mathbf{G}} = M_R$*), which implies*

$$min(M_D, M_R) \geqslant max(M_R - M_S + 2, 2), \tag{4.145}$$

$$k_{\mathbf{S}} \geqslant max(M_S - M_R + 2, 2). \tag{4.146}$$

Proof. The first hypothesis of this theorem is that the channels are drawn from a continuous distribution, which means $k_{\mathbf{H}^{(RD)}} = \min(M_D, M_R)$ and $k_{\mathbf{H}^{(SR)}} = \min(M_R, M_S)$. In addition, the Theorem states that $k_{\mathbf{G}} = M_R$ and $k_{\mathbf{C}} = M_S$. Therefore, under all hypotheses of Theorem 13, one can translate (3.71) and (3.72) of Theorem 3 into

$$\min(M_D, M_R) \geqslant \max(M_R - M_S + 2, 2),$$

$$k_{\mathbf{S}} \geqslant \max(M_S - M_R, +2),$$

proving Theorem 13. □

The exact $k_{\mathbf{S}}$ is unknown for $\mathbf{S}$ is a random variable. However, by definition of the Kruskal rank, it is possible to assure that at least $k_{\mathbf{S}} \geqslant 2$ if every subset of two columns of $\mathbf{S}$ is linearly independent. The probability of this occurring increases as N and/or the cardinality of the modulation alphabet increases.

The next theorem addresses the removal of column permutation ambiguities on the symbol and channel matrices through the semi-blind channel estimation using the NP-AF scheme.

Theorem 14 (Semi-blind estimation using NP-AF)**.** *If the code* $\mathbf{C}$ *and* $\mathbf{G}$ *matrices and the* n^{th} *row of the symbol matrix* $\mathbf{S}$ *are known at the destination, then symbol and channel matrices can be estimated without any column ambiguity, i.e.*

$$\bar{\mathbf{H}}^{(RD)} = \mathbf{H}^{(RD)}\mathbf{\Lambda}^{(RD)}, \tag{4.147}$$

$$\bar{\mathbf{S}} = \mathbf{S}\mathbf{\Lambda}^{(S)}, \tag{4.148}$$

$$\bar{\mathbf{H}}^{(SR)} = \left(\mathbf{\Lambda}^{(RD)}\right)^{-1} \mathbf{H}^{(SR)} \left(\mathbf{\Lambda}^{(S)}\right)^{-1}, \tag{4.149}$$

where $\mathbf{\Lambda}^{(S)} = D_n\left(\bar{\mathbf{S}}\right) D_n^{-1}\left(\mathbf{S}\right)$ *is known.*

Proof. Taking into account the knowledge of the code matrix $\mathbf{G}$, from the correspondences (4.34) and (4.35), the ambiguity relation (3.80) gives $\boldsymbol{\Pi}^{(W)} = \boldsymbol{\Lambda}^{(G)} = \mathbf{I}_{M_R}$, and the three ambiguity relations (3.79), (3.82), and (3.83) then become

$$\bar{\mathbf{H}}^{(RD)} = \mathbf{H}^{(RD)}\boldsymbol{\Lambda}^{(RD)}, \tag{4.150}$$

$$\bar{\mathbf{S}} = \mathbf{S}\boldsymbol{\Pi}^{(Z)}\boldsymbol{\Lambda}^{(S)}, \tag{4.151}$$

$$\bar{\mathbf{H}}^{(SR)} = \left(\boldsymbol{\Lambda}^{(RD)}\right)^{-1}\mathbf{H}^{(SR)}\left(\boldsymbol{\Pi}^{(Z)}\boldsymbol{\Lambda}^{(S)}\boldsymbol{\Lambda}^{(C)}\right)^{-1}. \tag{4.152}$$

The remaining ambiguities consist in the permutation matrix $\boldsymbol{\Pi}^{(Z)}$ and the diagonal matrices $\boldsymbol{\Lambda}^{(RD)}$, $\boldsymbol{\Lambda}^{(S)}$ and $\boldsymbol{\Lambda}^{(C)}$.

If $\mathbf{C}$ is known, then $\boldsymbol{\Pi}^{(Z)} = \boldsymbol{\Lambda}^{(C)} = \mathbf{I}_{M_S}$, and thus from (4.151) and (4.152) we have $\bar{\mathbf{S}} = \mathbf{S}\boldsymbol{\Lambda}^{(S)}$ and $\bar{\mathbf{H}}^{(SR)} = \left(\boldsymbol{\Lambda}^{(RD)}\right)^{-1}\mathbf{H}^{(SR)}\left(\boldsymbol{\Lambda}^{(S)}\right)^{-1}$, equalities stated in (4.148) and (4.149);

In addition, if the n^{th} row of $\mathbf{S}$ is known, then $\boldsymbol{\Lambda}^{(S)} = D_n\left(\bar{\mathbf{S}}\right)D_n^{-1}\left(\mathbf{S}\right)$ can be calculated at the receiver. □

Furthermore, given that the code matrices $\mathbf{G}$ and $\mathbf{C}$ are known, then we have from Theorem 14 that

$$\widehat{\mathbf{H}}_{\infty}^{(RD)} = \mathbf{H}^{(RD)}\boldsymbol{\Lambda}^{(RD)}, \tag{4.153}$$

$$\widehat{\mathbf{S}}_{\infty} = \mathbf{S}\boldsymbol{\Lambda}^{(S)}, \tag{4.154}$$

$$\widehat{\mathbf{H}}_{\infty}^{(SR)} = \left(\boldsymbol{\Lambda}^{(RD)}\right)^{-1}\mathbf{H}^{(SR)}\left(\boldsymbol{\Lambda}^{(S)}\right)^{-T}, \tag{4.155}$$

where once again $(\widehat{\mathbf{H}}_{\infty}^{(RD)}, \widehat{\mathbf{S}}_{\infty}, \widehat{\mathbf{H}}_{\infty}^{(SR)})$ denotes the solution of any of the receivers after the convergence to a global minimum.

Therefore, all ambiguities can be solved if $\boldsymbol{\Lambda}^{(RD)}$ and $\boldsymbol{\Lambda}^{(S)}$ are known. If we know *a priori* the first rows of $\mathbf{H}^{(RD)}$ and $\mathbf{S}$, then consequently we can estimate these ambiguities by using

$$\widehat{\boldsymbol{\Lambda}}^{(RD)} = D_1(\widehat{\mathbf{H}}_{\infty}^{(RD)})D_1^{-1}(\mathbf{H}^{(RD)}), \tag{4.156}$$

$$\widehat{\boldsymbol{\Lambda}}^{(S)} = D_1(\widehat{\mathbf{S}}_{\infty})D_1^{-1}(\mathbf{S}), \tag{4.157}$$

where $\widehat{\mathbf{H}}_{\infty}^{(RD)}$ and $\widehat{\mathbf{S}}_{\infty}$ are the estimates after convergence of any of the NP-AF receivers. Again, when an individual channel estimation is not needed, the NP-AF receivers are robust to this ambiguity due to the fact that estimates of the symbols (Eq. (4.154)) is independent of $\boldsymbol{\Lambda}^{(RD)}$.

4.8 Computational cost

Many factors contribute to the complexity of a given estimator. More importantly, the number of mathematical operation and how they are realistically performed, since there is a wide range of arithmetic libraries for an even larger selection of dedicated hardware.

For the sake of simplicity, the expressions presented in the discussion here approximate the number of floating-point operations in considering the dominant cost associated with the SVD computation, which is used to calculate the matrix pseudo-inverses [88, 89]. Note that, for a matrix of dimension $I_1 \times I_2$, the overall SVD computational cost is $\mathrm{O}(I_1 I_2 \min(I_1, I_2))$.

The computational cost needed at each iteration of the proposed single-stage iterative receivers is given in Table 4.4. We can see from it that the complexity O(.) per iteration of

Receiver	No. of floating-point operations O(.) by iteration
PT2-ALS	$PNM_R^2 + M_D PN(M_R M_S)^2 + NM_D PM_S^2$
NPALS	$PNJM_R^2 + M_D JPN(M_R M_S)^2 + PM_D JM_S^2$

Table 4.4: Computational costs of iterative algorithms

PT2-ALS scales similarly to that of the NPALS receiver with the number of source and relay antennas, the difference being on the choice of the coding parameters. One can note that for the processes of channel estimation (two first terms of the each cost) the NPALS is J times heavier, per iteration, than PT2-ALS, thanks once gain to the KRST relay coding of the former. However, this computational gain per iteration becomes J/N for symbol estimation, since PT2-AF has the inconvenience of inverting (4.78) for each data-stream.

Remark 7. *The computational costs of the so-called hybrid variants of PT2-ALS and of NPALS are slightly modified from those of Table 4.4.*

Due to the combination of the direct and relay link models, which virtually doubles the number of destination antennas for symbol estimation, then the computational costs for this task becomes $2NM_D PM_S^2$ in the CPP-ALS receiver and $2PM_D JM_S^2$ in the NPALS receiver.

For DALS and DKRF receivers it is appropriate to identify the complexity for each one of its two steps. Comparing ALS-X with KRF-X via Table 4.5, one can see that the former presents a quadratic dependence on M_S, while the complexity of the latter is quadratic in $M_D J$ or N. Regarding the channel estimation step, the ALS-Z algorithm is quadratic in M_R and linear in M_S and M_D, while for KRF-Z it is the opposite, i.e. linear in M_R and quadratic in M_S or M_D. Therefore, the complexity of the DKRF is linear in M_S for both symbol and channel estimation steps, while the complexity of DALS is quadratic in this parameter only for symbol estimation. Thus, for a large number of source antennas a relevant gain in complexity for symbol estimation is expected by choosing the DKRF receiver over its iterative rival, while the opposite effect may be seen for the channel estimation step.

In addition, since $P \geqslant M_S$ and $J \geqslant M_R$ are sufficient identifiability conditions for both receivers (cf. Theorem 12), as either M_S or M_R increases, the iterative receiver may tend

Table 4.5: Computational cost of the two-step receivers

	Alg.	O(.)
I	KRF-X	$O_A = M_D J N \min(M_D J, N) M_S$
	ALS-X	$O_B = l_1 \left(M_D J P M_S^2 + N P M_S^2\right)$
II	KRF-Z	$O_C = M_S M_D \min(M_S, M_D) M_R$
	ALS-Z	$O_D = l_2 \left(M_D J M_R^2 + M_S J M_R^2\right)$
I: Symbol estimation; II: Channel estimation		
l_1,l_2: Number of iterations		

to be further penalized, given the fact that DKRF is independent of P, and likely linear in J for symbol estimation, while DALS is linear in P for symbol estimation and in J for both steps.

4.9 Summary of the chapter

This chapter have proposed the PT2-AF and NP-AF transmission schemes, based on the tensor decompositions presented in Chapter 3. Such schemes have the same source coding, but differ in the signal processing by the relay. For each of the systems a series of semi-blind receivers have been proposed, as shown in Fig. 4.6.

All PT2-AF receivers offer iterative ALS solutions for the joint estimation of symbols and channels, while the NP-AF receivers fall into a larger number of categories: of iterative (e.g. NPALS and DALS) or closed-form solution (e.g. DKRF), and of single-step (i.e. NPALS) or two-step (i.e. DALS and DKRF) structure. In addition, some of the PT2-AF and NP-AF receivers have hybrid variants (e.g. CNPALS and CKRF-X), where the direct link model is combined with the relay link model to improve estimation. Particularly in this case, the solution of the direct link by the PARAFAC-SVD algorithm requires that the length P of the source code be greater than or equal to the number of transmit antennas M_S, which sets a necessary and sufficient condition on P for this class of receivers. This and other conclusions on the proposed receivers can be drawn from the summary displayed in Table 4.6.

With regard to the study of the uniqueness properties of the PT2-AF and NP-AF protocols done in this chapter, the latter also had advantages over the former. Concerning the column ambiguities in the matrix factors of the two models, there is no difference between them, and ambiguities can be solved in the same way (Secs. 4.6.4 and 4.7.5). However, the sufficient uniqueness conditions for NP-AF are more relaxed than for PT2-AF, particularly due to the possibility of using different numbers of source and relay antennas. For instance, if $M_S = M_R$, then the uniqueness conditions for NP-AF become simply $M_D \geqslant M_R$ and

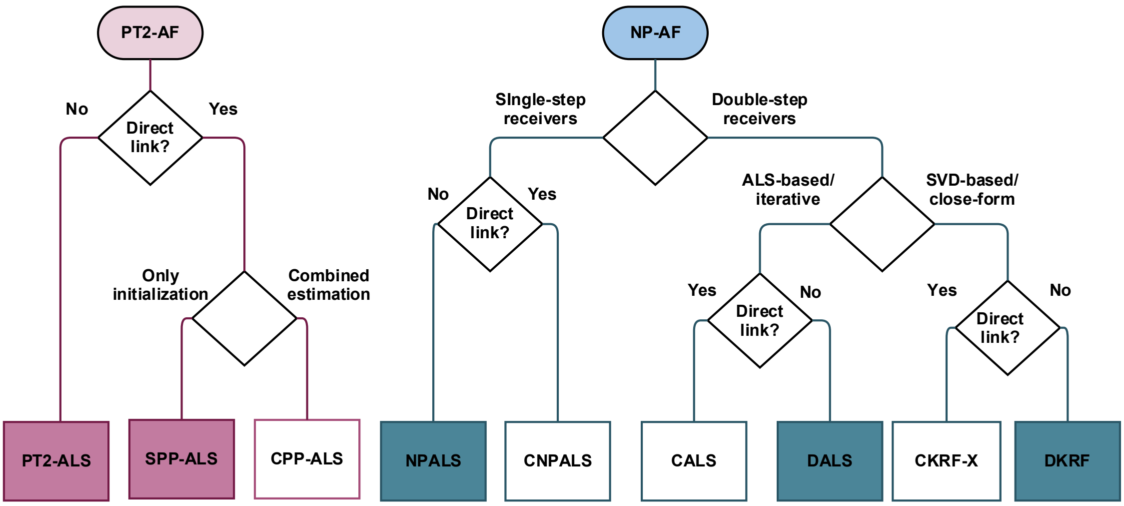

Figure 4.6: Proposed semi-blind receivers

<table>
<tr><th>Receiver</th><th>Direct link</th><th>Necessary condition</th><th>Sufficient condition</th></tr>
<tr><td>PT2-ALS</td><td>No</td><td rowspan="2">$P \geqslant \left\lceil \max\left(\frac{M_R M_S}{M_D N}, \frac{M_R}{N}, \frac{M_S}{M_D}\right)\right\rceil$</td><td rowspan="3">$P \geqslant M_S$
$\min(M_S, M_D) \geqslant M_R$</td></tr>
<tr><td>SPP-ALS</td><td rowspan="2">Yes</td></tr>
<tr><td>CPP-ALS</td><td>$P \geqslant \left\lceil \max\left(\frac{M_R M_S}{M_D N}, \frac{M_R}{N}, \frac{M_S}{2M_D}\right)\right\rceil$</td></tr>
<tr><td>NPALS</td><td>No</td><td>$P \geqslant \lceil M_S/N \rceil$
$J \geqslant \lceil M_R/M_D \rceil$
$PJ \geqslant \left\lceil \max\left(\frac{M_S}{M_D}, \frac{M_R}{N}\right)\right\rceil$</td><td rowspan="6">$P \geqslant M_S$
$J \geqslant M_R$</td></tr>
<tr><td>CNPALS</td><td>Yes</td><td>$P \geqslant M_S$
$J \geqslant \lceil M_R/M_D \rceil$
$PJ \geqslant \lceil M_R/N \rceil$</td></tr>
<tr><td>DALS
(ALS-X+ALS-Z)</td><td>No</td><td>$P \geqslant \lceil M_S/\min(N, M_D J) \rceil$
$J \geqslant \lceil M_R/\min(M_D, M_S) \rceil$</td></tr>
<tr><td>CALS-X+ALS-Z</td><td>Yes</td><td>$P \geqslant M_S$
$J \geqslant \lceil M_R/\min(M_D, M_S) \rceil$</td></tr>
<tr><td>DKRF
(KRF-X+KRF-Z)</td><td>No</td><td>$P \geqslant M_S$
$J \geqslant M_R$</td></tr>
<tr><td>CKRF-X+KRF-Z</td><td>Yes</td><td>$P \geqslant M_S$
$J \geqslant M_R$</td></tr>
</table>

Table 4.6: Summary of identifiability conditions

$k_{\mathbf{S}} \geqslant 2$. These conclusions can be drawn from Table 4.7.

Transm.	Sufficient uniqueness condition	Ambiguities for semi-blind estimation
SD link	$k_{\mathbf{C}} + k_{\mathbf{S}} \geqslant \max(2M_S - M_D, M_S) + 2$ (Theorem 5, Sec. 4.5.1)	$\bar{\mathbf{S}} = \mathbf{S}\boldsymbol{\Lambda}^{(S)}$ $\bar{\mathbf{H}}^{(SD)} = \mathbf{H}^{(SD)}\left(\boldsymbol{\Lambda}^{(S)}\right)^{-1}$ (Theorem 6, Sec. 4.5.1)
PT2-AF	i) All matrices are full rank: ii) $\mathbf{h}^{(SR)}_{m_r,m_S} \neq 0$, for all m_R, m_S ; iii) $M_R = M_S$; (Theorems 9, Sec. 4.6.4)	$\bar{\mathbf{S}} = \mathbf{S}\boldsymbol{\Lambda}^{(S)}$, $\bar{\mathbf{H}}^{(RD)} = \mathbf{H}^{(RD)}\boldsymbol{\Lambda}^{(RD)}$ $\bar{\mathbf{H}}^{(SR)} = \left(\boldsymbol{\Lambda}^{(RD)}\right)^{-1}\mathbf{H}^{(SR)}\left(\boldsymbol{\Lambda}^{(S)}\right)^{-1}$ (Theorem 10, Sec. 4.6.4)
NP-AF	$\min(M_D, M_R) \geqslant \max(M_R - M_S + 2, 2)$ and $k_{\mathbf{S}} \geqslant \max(M_S - M_R + 2, 2)$ (Theorem 13, Sec. 4.7.5)	$\bar{\mathbf{S}} = \mathbf{S}\boldsymbol{\Lambda}^{(S)}$, $\bar{\mathbf{H}}^{(RD)} = \mathbf{H}^{(RD)}\boldsymbol{\Lambda}^{(RD)}$ $\bar{\mathbf{H}}^{(SR)} = \left(\boldsymbol{\Lambda}^{(RD)}\right)^{-1}\mathbf{H}^{(SR)}\left(\boldsymbol{\Lambda}^{(S)}\right)^{-1}$ (Theorem 14, Sec. 4.7.5)

If the n^{th} row of $\mathbf{S}$ is known, then $\boldsymbol{\Lambda}^{(S)} = D_n\left(\bar{\mathbf{S}}\right)D_n^{-1}\left(\mathbf{S}\right)$.

Table 4.7: Summary of uniqueness conditions

Chapter 5

Simulation analysis of the semi-blind receivers

Contents

This chapter covers the analysis of the two-hop one-way semi-blind receivers proposed in Chapter 4 via computational simulations. Bearing in mind the impact of the system parameters on the complexity (Sec. 4.8), firstly the simulations take into account the influence of each individual parameter (e.g. number of relay antennas) on the symbol estimation with the proposed tensor-based transmission schemes (§5.2). This section is important to investigate some of the particularities of the tensor-based schemes introduced in the previous chapter, as well as to delimit the expected behavior of each semi-blind receiver for the same parameters.

Therefore, through the insights acquired from the simulations in scenarios of perfect knowledge of the CSI, the semi-blind estimation of symbols and channels using the proposed receivers is set in the following section (§5.3). In addition, comparisons of BER and channel NMSE are done with state-of-the-art supervised receivers, reintroduced in Sec. 5.1.

The sequence of computational analyses suggested in this chapter, combined with the study of the properties of each transmission system and their receivers in Chapter 4, leads to a concise inference at the end of this chapter on the advantages of each estimation strategy.

5.1 Supervised estimation

Throughout this chapter, the semi-blind receivers proposed in Chapter 4 will be compared to two supervised channel estimators. The receivers are here named LS-SVD, introduced by Lioliou et al. [24], and Bilinear ALS (BALS), developed by Rong et al. [20].

Both receivers use the same relaying process, but they offer different proposals for channel estimation, as briefly shown in Table 5.1. This table also shows a comparison of these receivers with those proposed in this thesis. At first glance, it is possible to verify that the new receivers allow semi-blind estimation through the use of more complex tensor models. More details on these supervised receivers are presented in the following.

Receiver	Semi-blind	Protocol	Tensor model	Iterative	Direct link
LS-SVD [24]	No	§5.1.1	PARAFAC‡	No	No
BALS [20]	No	§5.1.2	PARAFAC	Yes	No
PT2-ALS	Yes	PT2-AF	PARATUCK2	Yes	No
SPP-ALS, CPP-ALS	Yes	PT2-AF	PARATUCK2	Yes	Yes
NPALS, DALS	Yes	NP-AF	Nested PARAFAC	Yes	No
DKRF	Yes	NP-AF	Nested PARAFAC	No	No
CNPALS, CALS-X	Yes	NP-AF	Nested PARAFAC	Yes	Yes
CKRF-X	Yes	NP-AF	Nested PARAFAC	No	Yes

‡: Single unfolding of a PARAFAC model

Table 5.1: Tensor-based receivers for two-hop one-way AF relaying systems

5.1.1 BALS channel estimator

The transmission scheme (protocol) used by both supervised channel estimators is similar, which corresponds of sending to the relay orthogonal training sequences known at the destination. As in the PT2-AF and NP-AF transmission schemes, the relay applies a time-dependent set of gains before forwarding the signals to the end node.

In the BALS channel estimator, the noiseless signals received via the SRD link during the n^{th} time-frame are given by $\mathbf{X}_{..n} = \mathbf{H}^{(RD)} D_n(\mathbf{G})\mathbf{H}^{(SR)}\bar{\mathbf{S}} \in \mathbb{C}^{M_D \times L}$, where the pilot symbol matrix $\bar{\mathbf{S}} \in \mathbb{C}^{M_S \times L}$ is chosen as a Discrete Fourier transform (DFT) matrix, L being the length of the training sequence, with $L \geqslant M_S$. Similarly to PT2-AF, $\mathbf{G} \in \mathbb{C}^{N \times M_R}$ is the relay gain matrix.

The filtered signals $\bar{\mathbf{X}}_{..n} \triangleq \mathbf{X}_{..n}\bar{\mathbf{S}}^H = \mathbf{H}^{(RD)} D_n(\mathbf{G})\mathbf{H}^{(SR)}$ satisfy a PARAFAC model whose matrix factors $\mathbf{H}^{(SR)}$ and $\mathbf{H}^{(RD)}$ can be estimated using an ALS algorithm based on the following equations

$$\widehat{\mathbf{H}}_i^{(SR)} = \left[\mathbf{G} \diamond \widehat{\mathbf{H}}_{i-1}^{(RD)}\right]^{\dagger} \bar{\mathbf{Y}}_{M_D N \times M_S}, \tag{5.1}$$

$$\left(\widehat{\mathbf{H}}_i^{(RD)}\right)^T = \left[(\widehat{\mathbf{H}}_i^{(SR)})^T \diamond \mathbf{G}\right]^{\dagger} \bar{\mathbf{Y}}_{N M_S \times M_D}, \tag{5.2}$$

where $(\bar{\mathcal{Y}}, \mathcal{Y}) \Leftrightarrow (\bar{\mathcal{X}}, \mathcal{X})$ is the correspondence between noisy and noise-free data.

Using lemma 1, Chapter 3, sufficient conditions to pseudoinvert the terms in (5.1) and (5.2) are

$$k_{\mathbf{G}} + k_{\mathbf{H}^{(RD)}} \geqslant M_R + 1,$$
$$k_{\left(\mathbf{H}^{(SR)}\right)^T} + k_{\mathbf{G}} \geqslant M_R + 1.$$

There are many possible ways to satisfy both conditions. Admitting for example that $\mathbf{G}$ is full column-rank (i.e. $k_{\mathbf{G}} = M_R$) and both channels are full rank (i.e. $k_{\mathbf{H}^{(SR)}}, k_{\mathbf{H}^{(RD)}} \geqslant 1$), then both channels can be estimated using the BALS estimator.

5.1.2 LS-SVD channel estimator

In the LS-SVD channel estimator, the same PARAFAC model as in [20] is exploited, but the mode-3 unfolding is taken into account

$$\bar{\mathbf{X}}_{M_D M_S \times N} = \left(\left(\mathbf{H}^{(SR)}\right)^T \diamond \mathbf{H}^{(RD)}\right) \mathbf{G}^T. \tag{5.3}$$

Assuming that $\mathbf{G}$ is full column rank which implies $N \geqslant M_R$, we have

$$\bar{\mathbf{Y}}_{M_D M_S \times N} (\mathbf{G}^T)^{\dagger} \approx \left(\left(\mathbf{H}^{(SR)}\right)^T \diamond \mathbf{H}^{(RD)}\right), \tag{5.4}$$

and the channels can be estimated using the LSKRF process described in Remark 2, Chapter 4. Although implicitly a PARAFAC model is exploited by LS-SVD, the original work [24] does not concern a tensor analysis or else discuss the solution of the estimator in the light of the uniqueness properties of the PARAFAC decomposition.

For the simulations involving either LS-SVD or BALS channel estimators, the BER results are obtained with a ZF receiver that estimates N_S vectors of M_S symbols during N_T time-blocks. The transmission of a symbol vector $\mathbf{s}_{n_S} \in \mathbb{C}^{M_S \times 1}$ is repeated during N_T time-frames, using N_T different AF gains, so that the received signal vector at the input of the ZF receiver is given by

$$\mathbf{y}_{n_S}^{(SRD)} = \begin{bmatrix} \mathbf{H}^{(RD)} D_1(\mathbf{G}) \mathbf{H}^{(SR)} \\ \vdots \\ \mathbf{H}^{(RD)} D_{N_T}(\mathbf{G}) \mathbf{H}^{(SR)} \end{bmatrix} \mathbf{s}_{n_S} + \mathbf{v}_{n_S}^{(SRD)}$$
$$= \mathbf{Z}_{M_D N_T \times M_S} \mathbf{s}_{n_S} + \mathbf{v}_{n_S}^{(SRD)}. \tag{5.5}$$

The output of the ZF receiver is then given by

$$\hat{\mathbf{s}}_{n_S} = \left(\hat{\mathbf{Z}}_{M_D N_T \times M_S}\right)^{\dagger} \mathbf{y}_{n_S}^{(SRD)},$$

where $\hat{\mathbf{Z}}_{M_D N_T \times M_S}$ is calculated using the estimate of $\mathbf{H}^{(SR)}$ and $\mathbf{H}^{(RD)}$. This ZF receiver exploits time redundancy due to the N_T time-frames generated by the relay. This is particularly useful when the number of receive antennas is smaller than the number of transmit antennas, since the necessary condition to pseudoinvert $\hat{\mathbf{Z}}_{M_D N_T \times M_S}$ is that $M_D N_T \geqslant M_S$.

Note that N_T and N_S do not need to be equal, as these design parameters are associated with two independent procedures when using the ZF receiver – N_T is the number of relay repetitions and N_S is the number of data-streams. Thus, in an ideal case, one may expected to maximize N_S and to minimize N_T, so that the transmission rate

$$r_s = \frac{N_S M_S}{L(1+N) + N_S(1+N_T)} \tag{5.6}$$

be maximized. Eq. (5.6) accounts for the overall transmission rate, taking into account the $N_S M_S$ information symbols sent, the $L(1+N)$ symbol periods expended for the channel estimation step and finally the $N_S(1+N_T)$ symbol periods dedicated to symbol estimation using the aforementioned ZF equalizer. Many are the possible combinations of such time variables (L, N, N_S,N_T), but once the transmission is limited by the inherent coherence time of the communication channels, a balance that set both transmission rate and BER at acceptable standards may be extremely difficult to achieve in fast fading scenarios.

Interestingly, these supervised strategies – channel estimation step followed by symbol estimation – have somewhat inverted procedures w.r.t. to the DALS and DKRF receivers introduced in Sec. 4.7.2, where symbol estimation (i.e. ALS-X or KRF-X) precedes the joint channel estimation step (i.e. ALS-Z or KRF-Z).

5.2 Analysis of the transmission schemes

The first set of simulations in this chapter involves the performance of the PT2-AF and NP-AF protocols when the receiver has perfect knowledge of the CSI. This hypothesis is used in most of the works on cooperative communications, especially those devoted to system optimization [14, 90]. The data received at the destination will be treated by simple ZF equalizers which estimates the symbols using

$$\mathbf{s}_n = \left(\mathbf{C} \diamond \bar{\mathbf{Z}}_k\right)^{\dagger} \bar{\mathbf{y}}_n, \tag{5.7}$$

with $\bar{\mathbf{Z}}_k$ being given accordingly to the k^{th} Monte Carlo realization of $\mathbf{H}^{(SD)}$, $\mathbf{H}^{(RD)}$ and $\mathbf{H}^{(SR)}$ (cf. Eq. (4.59)). In this section, the number of Monte Carlo realizations is $K = 10000$, and the number of data-streams for each realization is $N = 20$, so that a total of $NKM_S =$

$20000M_S$ symbols are used for each BER calculation. It may be noteworthy that the choice of N may be negligible, since it does not cause redundancy for detection of the symbols, but simply ensures that a greater number of symbols experience each set of randomly drawn channels.

The space-time diversities generated by the source and relay processing, as well as the use of multiple antennas at the destination, affect directly the symbol estimation with the ZF receiver, and they shall affect the proposed semi-blind receivers as well. It is likely that two different receivers, using the same transmission scheme, have close performances in terms of symbol estimation, since they exploit the same input signals. Therefore, it is also fair to expect that receivers of the same transmission scheme present divergences mainly in terms of computational cost and convergence speed. In this section the influence of the systems parameters is evaluated on the symbol estimation, while Sec. 5.3 will also cover the channel estimation performance.

In this chapter, the code matrix $\mathbf{C}$ is chosen as a truncated discrete Fourier transform (DFT) matrix with $c_{p,m_S} = exp\left(\frac{2j\pi(p-1)(m_S-1)}{M_S}\right)$ and $P \geqslant M_S$. Following the motivation of [61], this choice ensures that $\mathbf{C}$ has full column rank, which is a necessary condition for maximizing the diversity gain and also a partial condition introduced by Theorems 8 and 12 for symbol identifiability in Chapter 4. For the PT2-AF protocol the relay gain $\mathbf{G}$ is chosen as a Vandermonde (VD) matrix with random generators (see Eq. (4.96), in Chapter 4). This design avoids permutation ambiguities in the estimation of $\mathbf{H}^{(SR)}$ and $\mathbf{H}^{(RD)}$, and it is a good choice from the identifiability point of view. For NP-AF the relay gain matrix is a truncated DFT with unit energy entries. Sec 5.2.3 will discuss the impact of these choices on the outcome of the ZF receiver.

A PSK modulation with uniform distribution of symbols is used to generate the matrix $\mathbf{S} = \sqrt{E_S}\mathbf{S}_o$ at each run, where $\mathbf{S}_o$ is a matrix composed of unit energy symbols, and E_S is the symbol energy. In this section, $\mathbf{S}_o$ is a truncated DFT matrix, which is an optimal choice for the bit error minimization using the classic ZF equalizer [20, 91].

Channel matrices $\mathbf{H}^{(RD)}$, $\mathbf{H}^{(SR)}$ and $\mathbf{H}^{(SD)}$ have i.i.d. entries drawn from complex Gaussian distributions with zero mean and variances $1/M_R$, $1/M_S$, and $\frac{10^{-\alpha/10}}{M_S}$, respectively, where α is a tuning parameter allowing to set the energy of the SD link relatively to that of the SRD link (see below). The entries of the noise tensors $\mathcal{V}^{(R)}$ and $\mathcal{V}^{(D)}$ have the same zero-mean Gaussian distribution, but with unit variances. In the simulations, the average Signal-to-Noise Ratio (SNR) of the SRD and SD links are proportional to E_S, since the noise-free signals are proportional to E_S – the relay only scales the signals.

Handling the average energy of the direct link, specifically its proportion in relation to the average energy of the relay link, is important for two main reasons. The first one is to validate the utilization of relays stations to mitigate large propagation losses between the source and destination. The second reason is to establish the ideal conditions of use for the hybrid receivers, i.e. those that combine the signals of both links to improve the overall symbol and channel estimation.

For PT2-AF, from the above assumptions we deduce $E\left\{\mathbf{H}^{(SR)}\left(\mathbf{H}^{(SR)}\right)^H\right\} = E\left\{D_n(\mathbf{G})D_n^H(\mathbf{G})\right\} = \mathbf{I}_{M_R}$, $E\left\{\mathbf{H}^{(RD)}\left(\mathbf{H}^{(RD)}\right)^H\right\} = \mathbf{I}_{M_D}$, and $E\left\{\mathbf{H}^{(SD)}\left(\mathbf{H}^{(SD)}\right)^H\right\} = 10^{-\alpha/10}\mathbf{I}_{M_D}$. Thus, the ratio between the energies of the SRD link at the n^{th} time-block (deduced from (4.29)) and the direct link is given by

$$\begin{aligned}\frac{tr\left[\mathbf{R}^{(SRD)}\right]}{tr\left[\mathbf{R}^{(SD)}\right]} &= \frac{E\left\{||\mathbf{Z}_n||_F^2\right\}}{E\left\{||\mathbf{H}^{(SD)}||_F^2\right\}} \\ &= \frac{tr\left[E\left\{\mathbf{H}^{(RD)}\left(\mathbf{H}^{(RD)}\right)^H\right\}\right]}{tr\left[E\left\{\mathbf{H}^{(SD)}\left(\mathbf{H}^{(SD)}\right)^H\right\}\right]} = 10^{\alpha/10},\end{aligned} \tag{5.8}$$

where $\mathbf{R}^{(SRD)}$ is the autocovariance matrix of the effective channel, and $\mathbf{R}^{(SD)}$ is the analogous of the direct link channel.

From (5.8), we deduce that α in dB represents the difference between the energies of the SRD and SD channels in the PT2-AF protocol, i.e.

$$\alpha_{(dB)} = 10\log\left(tr\left[\mathbf{R}^{(SRD)}\right]\right) - 10\log\left(tr\left[\mathbf{R}^{(SD)}\right]\right). \tag{5.9}$$

For NP-AF, the relation between the energies of the relay and direct links can be calculated in a similar fashion. Since $\mathbf{G}$ is a DFT matrix, the average energy of the effective channel, taking into account all J time-frames, is equal to J times the average energy of the channel during a single frame. In other words, $\mathbf{G}$ is a deterministic matrix that introduces uniform energy distribution across all time frames, i.e. $\|\mathbf{G}_{1\cdot}\|_2^2 = \|\mathbf{G}_{2\cdot}\|_2^2 = \cdots = \|\mathbf{G}_{J\cdot}\|_2^2$, and therefore from (4.44)

$$\begin{aligned} tr\left[\mathbf{R}^{(SRD)}\right] = E\left\{\|\mathbf{Z}_{M_DJ\times M_S}\|_F^2\right\} &= JE\left\{\|\mathbf{H}^{(RD)}D_j(\mathbf{G})\mathbf{H}^{(SR)}\|_F^2\right\} \\ &= Jtr\left[E\left\{\mathbf{H}^{(RD)}\left(\mathbf{H}^{(RD)}\right)^H\right\}\right] \\ &= JM_D. \end{aligned} \tag{5.10}$$

According to the system settings defined above, the average energy of the effective channel of the relay link in the NP-AF scheme is J times greater than its correspondent in the PT2-AF. Therefore, the ratio between the average energies of the relay channel and direct channel in the NP-AF protocol is given by

$$\begin{aligned}\frac{tr\left[\mathbf{R}^{(SRD)}\right]}{tr\left[\mathbf{R}^{(SD)}\right]} &= \frac{E\left\{||\mathbf{Z}_{M_DJ\times M_S}||_F^2\right\}}{E\left\{||\mathbf{H}^{(SD)}||_F^2\right\}} \\ &= J10^{\alpha/10}.\end{aligned} \tag{5.11}$$

Although the AF gains provided by the PT2-AF and NP-AF relays are characterized respectively by NM_R and JM_R coefficients, in practice such relays amplify the signals continuously for PN and PNJ symbol periods. With all $\mathbf{G}$ entries with unit power for both transmission schemes, it is ensured that the total energy of the AF coefficients, whether under PT2-AF or NP-AF operation, is equal to M_R per symbol period.

For NP-AF, α given in dB can be written from (5.11) as

$$\alpha_{(dB)} = 10\log\left(tr\left[\mathbf{R}^{(SRD)}\right]\right) - 10\log\left(tr\left[\mathbf{R}^{(SD)}\right]\right) - 10\log\left(J\right). \tag{5.12}$$

Although the effective channel in NP-AF presents a positive energy offset (in dB scale) w.r.t. the PT2-AF channel, its additive noise at destination is also J times greater than the one in the PT2-AF, and therefore one does cannot simply infer that the SNR levels of the two transmission systems will vary based only on J. In fact, changing J, N or P does not affect *a priori* the average SNR of any link at destination, since both energies of the noise-free signals and of the addictive noises are proportional to these parameters.

The relation between P, N and J in terms of complexity, transmission rate and eventually estimation of symbols and channels are evaluated in this following subsections.

Remark 8. *In the rest of this chapter, the parameters used for the simulations may vary between a figure and another to better portrait a receiver's trait or behavior, especially in cases where the BER proved too low for a fair comparison involving high symbol energy values. In all cases, the parameters used for each comparison are stated in their own simulation figures, with the fixed parameters displayed on the top.*

5.2.1 Transmission rate

In this thesis, the term transmission rate corresponds directly to the number of transmitted symbols per unit of time, whether any of these symbols is properly decoded or not at the receiver. Hence, the maximum transmission rate is evidently linked to the transmission protocol rather than to a specific receiver.

In the discussions in Sections 4.5.1, 4.6.4 and 4.7.5, it was highlighted the possible existence of column scaling ambiguities on the matrix factors of each tensor model. Although they may have little or no impact on the channel matrices (see Appendix B), such ambiguities need to be removed from the solution of the symbol matrix. As proposed in Theorems 6, 10 , 14, Chapter 4, the knowledge of $\mathbf{C}$ and of a row of $\mathbf{S}$ is proposed for such task.

Therefore, in the case of using semi-blind receivers for joint symbol and channel estimation, the first data-stream of M_S symbols is known at the destination, and thus it is the remaining $N-1$ data-streams that carry the symbols that convey information. The overall total number of information symbols sent by the source is then $(N-1)M_S$.

What distinguishes the transmission rates of these different proposed schemes using the KRST coding at source is the time required for all signals to reach the destination antennas.

Neglecting the propagation delays instrinsic to wireless transmissions, the full transmission of the block of signals via direct link needs PN symbols periods, and therefore its rate is

$$r_{SD} = \frac{(N-1)M_S}{PN}. \tag{5.13}$$

For the PT2-AF protocol, its two-hop transmission means that two intervals of PN symbol periods are expected for a complete transmission, and therefore

$$r_{PT2-AF} = \frac{(N-1)M_S}{2PN}. \tag{5.14}$$

The overall transmission interval of the NP-AF scheme is slightly modified in relation to the PT2-AF, for the block of signals received from the source is spread by another KRST coding at the relay before its forwarding. Thus, its first hop takes PN symbol periods, but its the second one takes PNJ, resulting in the rate

$$r_{NP-AF} = \frac{(N-1)M_S}{PN(J+1)}. \tag{5.15}$$

Since $J \geqslant 1$, it is clear that for the same values of P, N and M_S the transmission rate of PT2-AF is equal to or greater than the one of NP-AF. For $J = 1$, both transmission schemes have the same rates, which is half as fast as the transmission rate through the non-cooperative link.

Fig. 5.1 shows the transmission rates of the two proposed transmission schemes for different values of N. From (5.14) and (5.15), we can see that both rates are proportional to the number of antennas at the source M_S, to the term $(N-1)/N$ and to the inverse of the source code length P.

Although in all cases the transmission rate is benefited by the increase of the number of transmitted symbols, it is not always possible to freely choose N, partly due to a higher complexity burden on the receivers, particularly in the case of joint channel estimation, or partly by the coherence time of the channels, i.e. the duration over which the channels do not vary.

5.2.2 Impact of source code length (P)

The possibility of joint symbol and channel estimation with the proposed transmission schemes is in part a consequence of the KRST coding at the source. In this sense, the

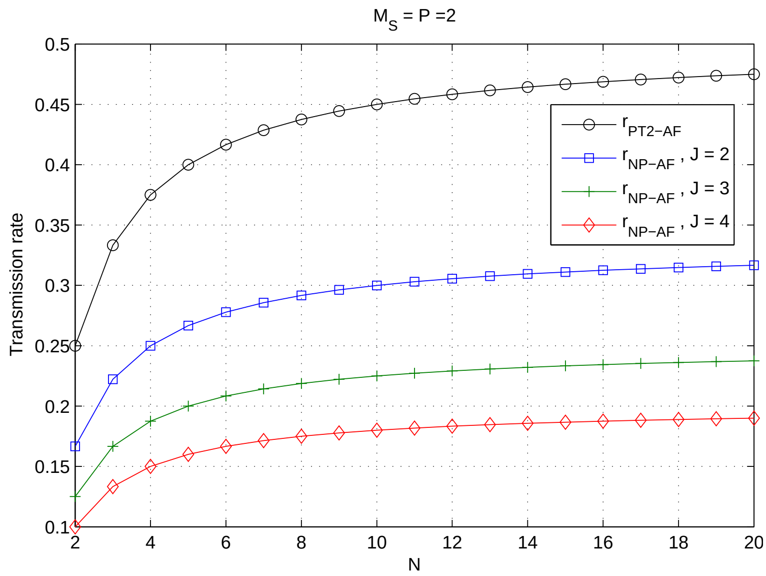

Figure 5.1: Transmission rate

choice of the code length P is one of the most important decisions when implementing the strategies of transmission and reception presented in this thesis.

Although increasing P reduces the transmission rates at the same ratio, as indicated by (5.14) and (5.15), a coding gain is expected, in some extent coming from the augmentation of the transmitted signal energy, i.e. given that $\mathbf{C}^T\mathbf{C}^* = P\mathbf{I}_{M_S}$, then from (4.1) or (4.2) one can deduce that the coded signals of the n^{th} data-stream have the total energy

$$\begin{aligned}\|\widetilde{S}_{\cdot\cdot n}\|_F^2 &= \|D_n(\mathbf{S})\mathbf{C}^T\|_F^2 \\ &= tr\left[D_n(\mathbf{S})\mathbf{C}^T\mathbf{C}^* D_n(\mathbf{S}^*)\right] \\ &= P \cdot tr\left[D_n(\mathbf{S})D_n(\mathbf{S}^*)\right] \\ &= E_S P M_S,\end{aligned} \tag{5.16}$$

and consequently the total transmitted energy is $\|\widetilde{S}\|_F^2 = E_S PNM_S$.

On the other hand, a visible diversity gain is not expected, since the maximum diversity gain should be proportional to $\min(P, M_S)$, as in the case of the blind CSI recovery of the direct link channel [61]. This conclusion can be extrapolated to the cooperative case, given that they employ the same source coding. As expected, P controls the trade-off between the diversity and transmission rate, but once $P \geqslant M_S$, the theoretical maximum diversity is no longer dependent of this parameter, i.e. in [61] $P = 1$ is said to maximize the transmission rate, while $P = M_S$ maximizes the diversity gain.

However, while increasing P beyond M_S may not increase the number of linearly independent columns of $\widetilde{\mathbf{S}}_{M_S \times PN}$, thus not contributing to a greater theoretical transmit diversity, it still provides signal redundancy without incurring in a reduction of the average SNR as shown by (5.16).

Fixing the same transmission rate for NP-AF and PT2-AF, Fig. 5.2 analyzes the impact of P in each protocol. We can see that the performances for both transmission scheme are clearly improved by increasing P. The almost parallel shifts of the BER curves for both transmission protocols indicate a coding gain obtained by NP-AF over PT2-AF – at BER$=10^{-3}$ the coding gain is around 4 dB between the two schemes, for the two transmission rates. Note that a greater P is used for PT2-AF to equal its transmission rates to those of NP-AF, and that doubling P cuts in half the rates of both protocols in exchange for their better BER performances.

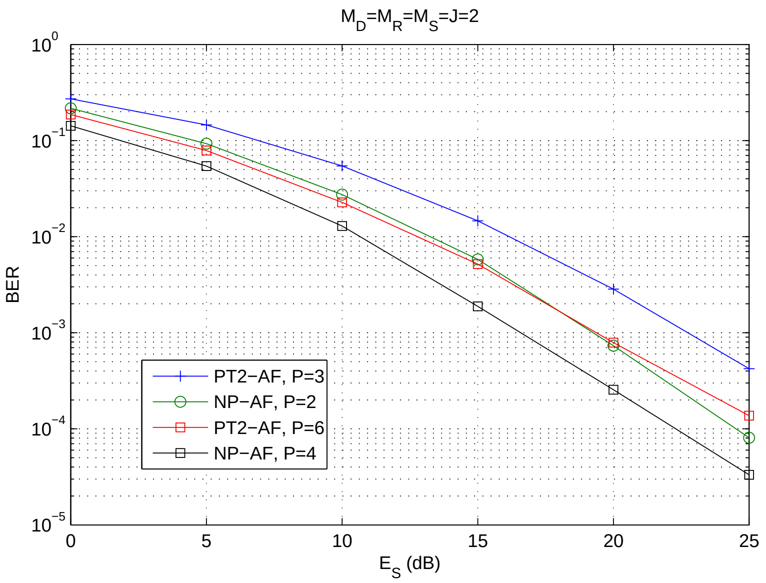

Figure 5.2: Impact of the code length P

Increasing P also has impact on the complexity of the estimation process. The greater the length of the source code, the larger the ensemble of data to be processed by the receiver. For a ZF equalizer the complexity in floating point operations, whether the data is received via direct link, PT2-AF or NP-AF is respectively $M_D P M_S^2$, $M_D P M_S^2$ or $M_D P J M_S^2$. These are the complexities to estimate a vector of M_S symbols transmitted by the source, using the LS minimization in (5.7). Note that a ZF equalizer using either signals from the SD link or from the PT2-AF scheme has the same computational cost per symbol vector, thanks to the absence of time-spreading by the relay – for the opposite reason, the cost is multiplied by J in the NP-AF scenario.

Therefore, the PT2-AF protocol offers not only faster transmission rates, but also lower computational complexity than NP-AF if such simple ZF receivers are taken into account. Since all proposed PT2-AF receivers are iterative, Sec. 5.3 will show that this conclusion is often not valid in a scenario of joint channel estimation.

5.2.3 Impact of relay code length (J)

As pointed in Secs.4.2 Chapter 4, the two proposed transmission systems mainly differ in how the signal processing is performed by the relay.

In general, the choice of the gain matrix $\mathbf{G}$ for both relaying schemes might take into account the available information on the system prior to the forwarding process. If the channel matrices were known, $\mathbf{G}$ could be optimized to maximize the capacity of the effective channel.

Here, firstly the performances of the PT2-AF and NP-AF systems are evaluated for two choices of $\mathbf{G}$. The first one is the truncated DFT matrix. The second option is a matrix with random complex Gaussian entries of zero mean and unit variance, i.e. $\mathbf{G} \sim \mathcal{CN}(0, 1)$. In any case, the relay gain matrix is known at the destination. The comparison is presented in Fig. 5.3, using different symbol modulations.

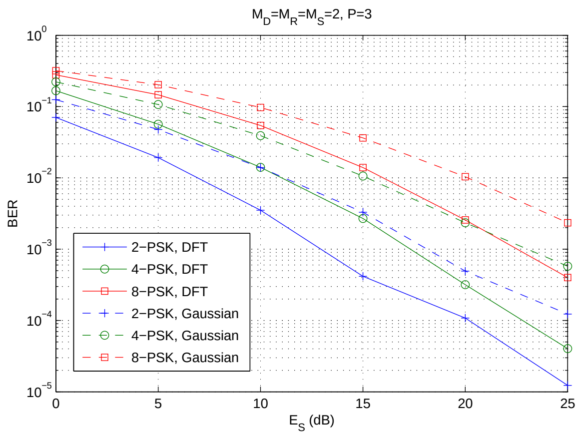

(a) PT2-AF

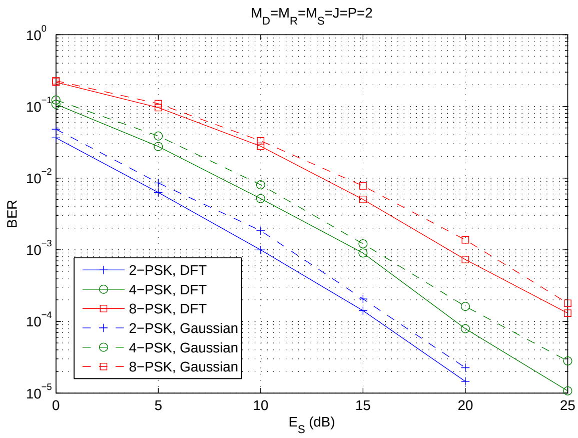

(b) NP-AF

Figure 5.3: Choice of relay gain matrix

For both transmission schemes, the choice of the DFT matrix proved the most appropriate for all levels of E_S. For NP-AF (see Fig. 5.3b), the DFT matrix showed coding gains of up to 2 dB over the Gaussian matrix.

For the PT2-AF scheme, the DFT matrix did not only provide coding gains greater than 5 dB, but also small diversity gains, illustrated by the slightly steeper slopes of the DFT curves at higher values of E_S. For instance, in Fig. 5.3a compare the “8-PSK, Gaussian” curve with the “8-PSK, DFT” and “4-PSK, Gaussian” curves. The slopes of the “Gaussian” curves are sensibly parallel for $E_S \geqslant 15$ dB, while “8-PSK, DFT” has a more pronounced decline with E_S, i.e. the “8-PSK, DFT” curve is clearly not parallel to the “4-PSK, Gaussian” curve.

Although the two choices of the relay gain matrix display entries with unit energy in average, the stochastic nature of the Gaussian matrix allows that, within each Monte Carlo run, it might exist an unbalance of the energies of the AF coefficients linked to each relay antenna, perhaps leading to an ill-conditioned effective channel matrix. In MIMO theory, the benefits of using multiple antennas is intrinsically linked to the eventual existence of a well-conditioned channel matrix. Even if $\mathbf{H}^{(RD)}$ and $\mathbf{H}^{(SR)}$ are i.i.d. matrices, $\mathbf{H}^{(RD)} D_n (\mathbf{G}) \mathbf{H}^{(SR)}$ may present a very high condition number (i.e. the ratio between the largest and smallest singular values) if the magnitudes of the diagonal elements of $D_n (\mathbf{G})$ are far apart.

This negative impact is reduced in the NP-AF system, perhaps attenuated by the KRST coding at the relay, where using more than one time-frame (i.e. $J > 1$) causes an averaging between the best and worst rows drawn for $\mathbf{G}$. In other words, one can say that with a random $\mathbf{G}$ the term $(\mathbf{G} \diamond \mathbf{H}^{(RD)})\mathbf{H}^{(SR)}$ in (4.62) is likely better conditioned than $\mathbf{H}^{(RD)} D_n (\mathbf{G}) \mathbf{H}^{(SR)}$ in (4.61).

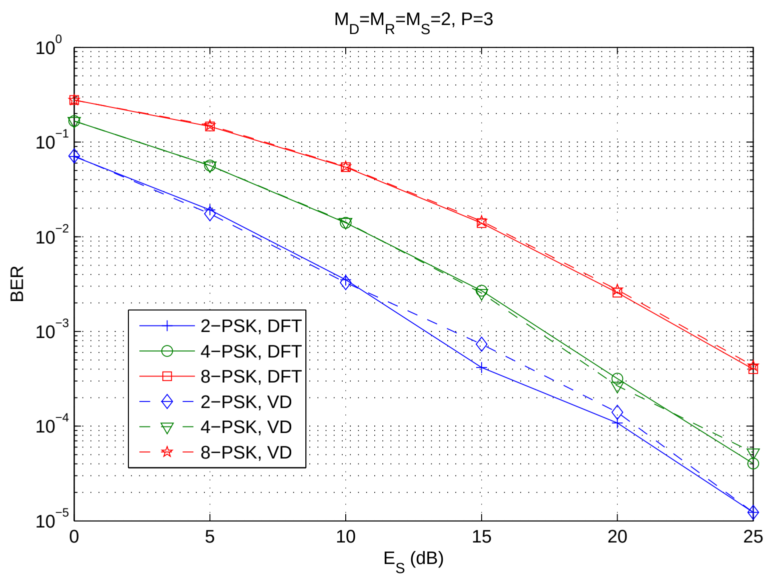

Figure 5.4: Vandermonde relay gain matrix

Figure 5.4 examines how PT2-AF performs with the VD relay gain matrix described in Remark 10, Chapter 4. Through this figure it is easy to note that this VD matrix gives the same diversity of the DFT matrix and a negligible coding gain. Since the DFT and Gaussian matrices achieved somewhat close performances for NP-AF in Fig. 5.3b, one could deduce that the VD matrix would present the same behavior for this protocol.

Now the performance of the NP-AF transmission system will be analyzed using different values of J. Once again, for a fair comparison, the transmission rates of PT2-AF and NP-AF are kept the same by setting P for PT2-AF to be equal to $(J+1)/2$ times the value of P for NP-AF. Figure 5.5 illustrates how the BER performance behaves as J is varied for NP-AF.

Looking at $\mathbf{Z}_{M_D J \times M_S}$ in (4.44), the effective channel in the NP-AF protocol whose esti-

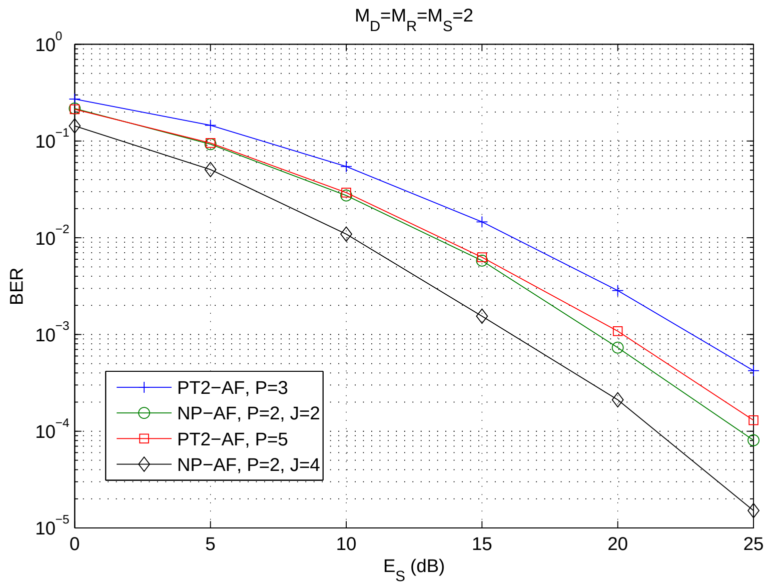

Figure 5.5: Impact of the code length J

mate is used to find $\hat{\mathbf{s}}_n$ via (5.7), its rank obeys $rank(\mathbf{Z}_{M_D J\times M_S}) \leqslant \min(M_D J, M_R, M_S) = \min(2J, 2)$. Since $J \geqslant 1$, then varying J would not change the possible maximum rank of $\mathbf{Z}_{M_D J\times M_S}$, although increasing J does provide more equations to estimate the symbols, which explains the gain in Fig. 5.5.

5.2.4 Impact of number of antennas (M_D,M_R,M_S)

The last set of simulations involving the ZF receivers with perfect CSI concerns the impact of the number of antennas. Once again, the same transmission rate for both transmission schemes are matched through the proper truncation of P.

For the direct link, the maximum diversity gain using a KRST coding is given by $M_D\min(P, M_S)$ [61]. Thus, one can expect that increasing the number of antennas at the destination will also provide a better BER using the relay-assisted link.

Fig. 5.6 shows the impact of the number M_D of antennas at the destination. The slopes of the BER curves indicate that the proposed transmission schemes satisfactorily benefit from an additional spatial diversity when more antennas are used at the destination node. In addition, for $M_D = 2$ the coding gain of the NP-AF scheme is around 4 dB over the PT2-AF scheme for a target BER of 10^{-3}, while this value drops to around 3 dB when M_D is increased to 4.

In Fig. 5.7, the impact of the number of both source (M_S) and relay (M_R) antennas is shown. For both transmission schemes, the slopes of the BER curves corroborate the increase of the spatial diversity gain when more antennas are used at the relay. While showing better performance for both $M_R = 2$ and $M_R = 4$, the NP-AF protocol has shown a

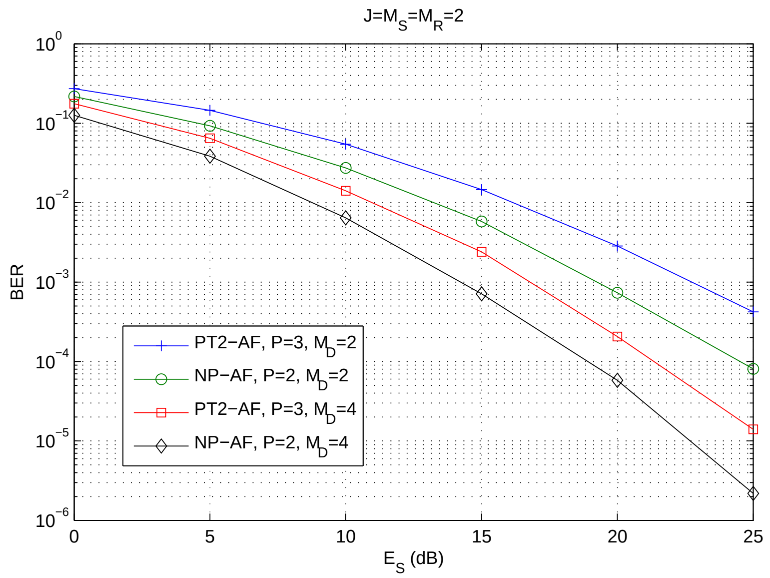

Figure 5.6: BER *versus* E_S. Impact of M_D

greater improvement when the number of antennas at the relay increases. Indeed, in the AF protocol, due to the absence of symbol recovery at the relay, then the maximum diversity order (i.e. maximum number of multipaths between source and destination) is proportional to M_R. For $M_R = 2$, its coding gain over PT2-AF is about 5 dB for high values of E_S, with this gain rising when $M_R = 4$.

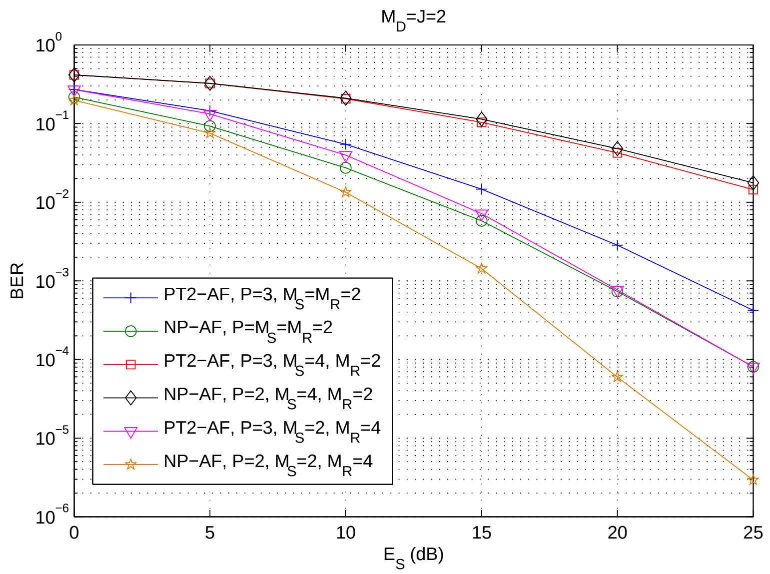

Figure 5.7: Impact of the number of source and relay antennas

For $M_S = 4$ there is an expected performance deterioration for the two transmission systems, since both PT2-AF and NP-AF exchange part of the transmit diversity for multiplexity gains, i.e. all M_S antennas transmit independent symbols. Therefore, with a greater number of symbols to be estimated with the same number of data signals arriving at the receiver, the BER got worse when passing from $M_S = 2$ to $M_S = 4$. For instance, for a BER of 10^{-2}, coding gains of 12 dB or more were achieved when choosing $M_S = 2$ over $M_S = 4$, with both protocols presenting negligible differences between them in this scenario.

From the simulations involving a ZF receiver in Sec. 5.2, the variation of the number of antennas at each node led to different diversity gains, while changing code lengths P and J brought only coding gain. The next section will evaluate the semi-blind receivers with regards to these conclusions.

5.3 Analysis of the semi-blind receivers

The rest of this chapter deals with the computational analysis of the proposed tensor-based semi-blind receivers. Since they concern symbol and channel estimation, we are interested in evaluating both BER performance and the channel NMSE. The channel NMSE of any channel $\mathbf{H}$ is given by

$$\text{NMSE} = \frac{1}{K}\left(\sum_{k=1}^{K} \frac{||\mathbf{H}_k - \widehat{\mathbf{H}}_k||_F^2}{||\mathbf{H}_k||_F^2}\right), \tag{5.17}$$

where K denotes once again the number of Monte Carlo runs, $\mathbf{H}_k$ is the channel generated at the k^{th} run, and $\widehat{\mathbf{H}}_k$ concerns its estimate after the whole estimation process. In Eq. (5.17) the channel $\mathbf{H}$ can either represent $\mathbf{H}^{(SR)}$ or $\mathbf{H}^{(RD)}$, or else one of the effective channels corresponding to one of the transmission protocol.

In the rest of the simulations of this chapter, the same system hypotheses presented in Sec. 5.2 are used, but this time $\mathbf{S}_o$ is indeed a random matrix of symbols taken from an 8-PSK alphabet. Furthermore, the first rows of $\mathbf{S}$ and $\mathbf{H}^{(RD)}$ are assumed known at the destination, in order to eliminate the scaling ambiguities on the solutions of the receivers, as proposed in sections 4.6.4 and 4.7.5, Chapter 4.

Due to the variety of proposed receivers and the number of system parameters, a large volume of comparisons can be done. To avoid redundancy of the results and conclusions, since many receivers exploit the same data models or have similar concepts, in most of the cases this section follows a gradual form of analysis: once established the advantages of a receiver (or class of receivers) over its direct competitor(s), the following analysis jumps to a new comparison, dropping the receivers that obtained the worst performances in the previous analysis. Thus, if receiver A has achieved better BER than receiver B, but worse channel NMSE, it may make sense to compare only A with an eventual receiver C in terms of BER (and to compare B and C mostly in channel estimation). Therefore, the advantages of each receiver in terms of BER, channel NMSE and computational cost can be deduced from the simulations without involving excessive number of receivers at each comparison.

At first, only the PT2-AF receivers are analyzed, highlighting the advantages of the semi-blind estimation over the supervised channel estimation methods detailed at the beginning of this chapter. The benefits of combining both relay and direct links, one of the novelties of this thesis, is also promptly stated in these first simulations.

Based on the benefits of employing a semi-blind estimation in a cooperative network, the simulations involving the NP-AF receivers firstly privilege the comparison with the PT2-AF receivers, mainly in terms of symbol and channel estimation. Afterwards, the comparisons are centered in the particularities of each NP-AF receiver.

5.3.1 Impact of the direct link on initialization

The use of the direct link in the cooperative relaying system is important for two purposes: to initialize the iterative receivers and/or to provide additional spatial diversity for the hybrid ones (e.g. CPP-ALS and CNPALS). The aim of here is to accentuate the benefits of exploiting the PARAFAC modeling of the SD link to initialize $\widehat{\mathbf{S}}_0$ in the iterative algorithms.

Figure 5.8 depicts the performance of the PT2-ALS and NPALS receivers in terms of the reconstruction errors in (4.81) and (4.110), respectively. Two levels of symbol energy (E_S = 10 dB and E_S = 25 dB) are considered and both receivers operate at the same transmission rate.The results clearly show that, for different signal energy values, the NPALS receiver provides better results in terms of convergence speed and reconstruction NMSE. More specifically, the NPALS receiver is around 20 times faster than the PARATUCK2-ALS receiver. In terms of computational cost, using the values in Table 4.4 and the approximate number of iterations of both receivers until their convergence, then NPALS is around 13 times less costly than PT2-ALS in this scenario.

Therefore, the conclusion that the PT2-AF receivers have smaller computational complexities than the NP-AF ones, which was valid for the ZF receiver with perfect CSI in Sec. 5.2.2, does not hold for the iterative semi-blind receivers, even though NPALS still processes a larger amount of data than PT2-ALS for iteration.

In Fig. 5.9, the SPP-ALS receiver is compared with the baseline PT2-ALS receiver which uses a random initialization and also to the NPALS receiver. The NMSE of the reconstruction error is plotted versus the number of ALS iterations required for convergence, for two different values of α. We can see that when α is increased (i.e. the energy of the SD link is decreased) both SPP-ALS and NPALS receivers converge more slowly. Indeed, due to the increase of α, the symbol estimates obtained via the SD link by the PARAFAC-SVD algorithm become less accurate, and then the initialization $\widehat{\mathbf{S}}_0$ for both NPALS and SPP-ALS becomes worse. When α passes from 20 dB to 0 dB, there is a sharp drop in the number of iterations for SPP-ALS to converge, while NPALS achieves comprehensibly a smaller benefit with a better initialization once its number of iterations is already small (less than 10 iterations). When

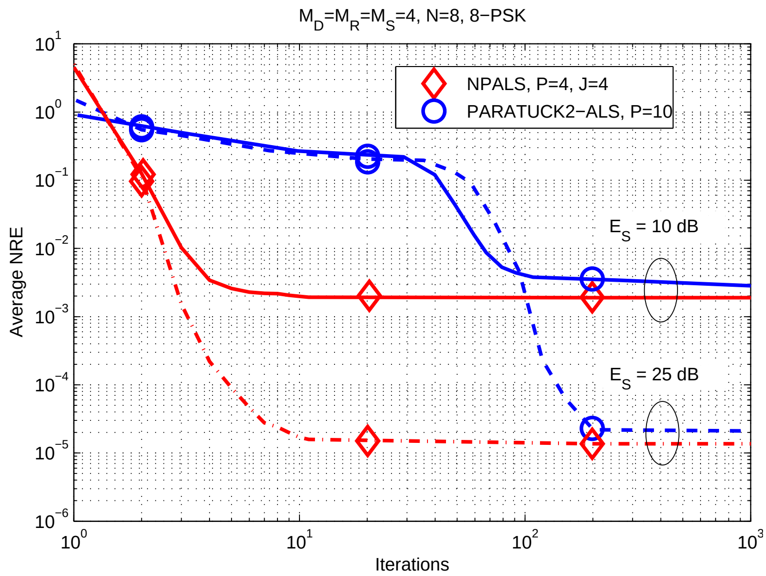

Figure 5.8: Convergence speed. Normalized reconstruction error (NRE) *versus* number of iterations

α is 0 dB, and then the direct link is as strong as the relay link, there is a certain parity in the number of iterations for convergence of SPP-ALS and of NPALS, and consequently they present very close computational costs.

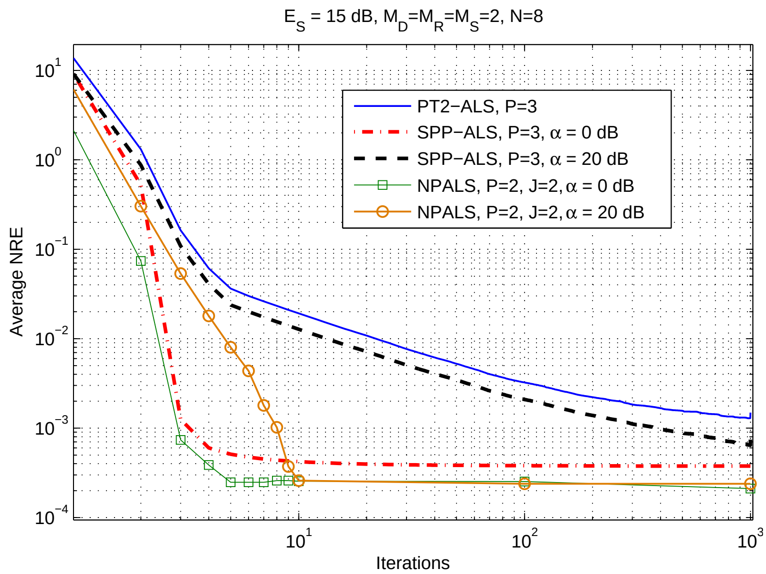

Figure 5.9: Impact of the initialization via direct link on convergence

5.3.2 PT2-AF receivers

In this section, the PT2-AF receivers are compared to the supervised channel estimators introduced at the beginning of this chapter. The three proposed PT2-AF iterative receivers are PT2-ALS, SPP-ALS and CPP-ALS. The last two use the direct link in their algorithms, and the benefits of a better initialization using this link in terms of convergence speed are discussed in Sec. 5.3.1. In this subsection, the comparison will be in terms of symbol and channel estimation.

5.3.2.1 Impact of P and M_D

In these first simulations, two system parameters (P and M_D) are analyzed, following the comparison already made to the ZF receiver with perfect CSI in Sec. 5.2. The intention here is to check, whether in the case of channel estimation, the semi-blind receivers present behaviors adequate to those predicted by the aforementioned supervised simulations.

Fig. 5.10 and 5.11 illustrate, respectively, the impact of the choice of P and M_D on the performance of the SPP-ALS and CPP-ALS receivers. Fig. 5.10 depicts the BER curves for two values of P. We can see that, by increasing P, the performance of both receivers is clearly improved at the cost of a reduction of the transmission rate. The almost parallel shifts of the BER curves for both receivers corroborate the coding gain obtained by increasing P, as demonstrated for the ZF receiver in Sec. 5.2.2.

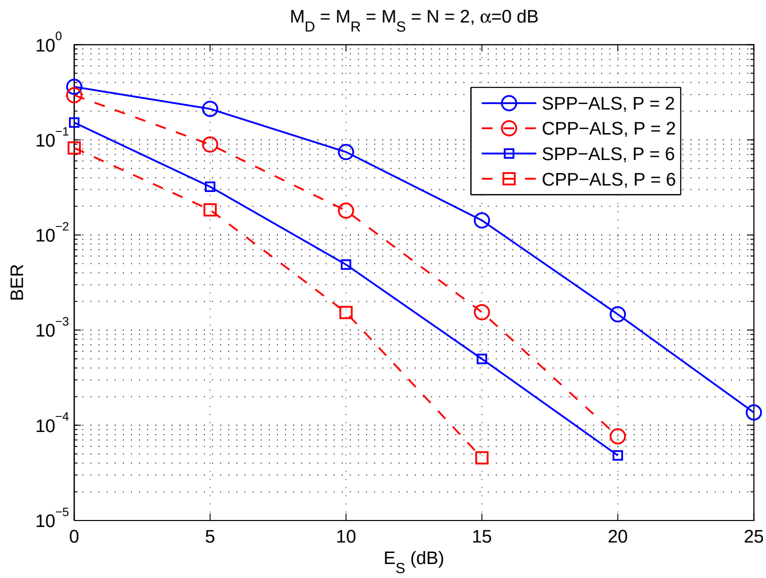

Figure 5.10: Impact of P on the PT2-AF receivers. BER *versus* E_S.

Fig. 5.11 shows the impact of the number M_D of antennas at the destination. The slopes of the BER curves indicate the benefit from an additional spatial diversity when more antennas are used at the destination node. The performance improvement of CPP-ALS over

SPP-ALS is due to an increase of space diversity with the CPP-ALS receiver, resulting from the combined use of the SD and SRD links for symbol estimation (cf. Eq. (4.83)). These results corroborate the more efficient use of cooperative diversity achieved by the CPP-ALS receiver.

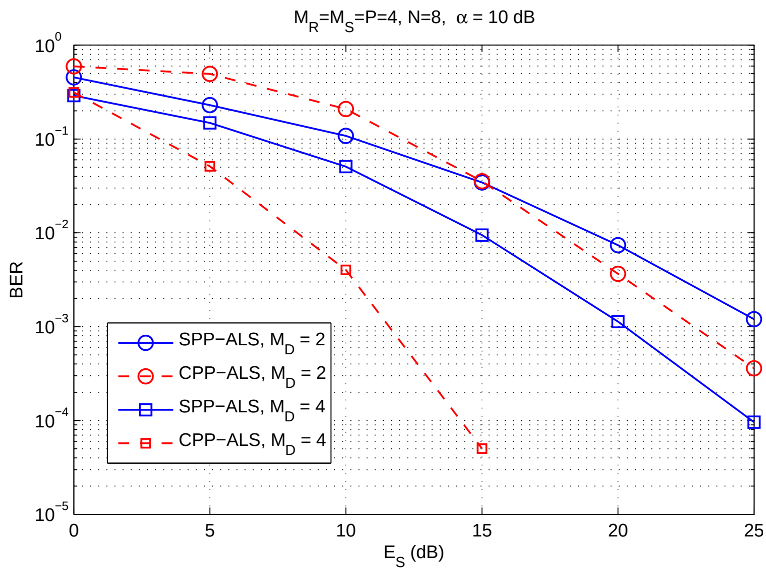

Figure 5.11: Impact of M_D on the PT2-AF receivers. BER *versus* E_S.

Remark 9. *Note that M_D inferior to M_S and M_R does not comply with all sufficient identifiability conditions of the PT2-AF receivers stated in Theorem 8, Chapter 4. However, the choice of parameters satisfy the necessary identifiability condition (4.86) in Theorem 4.6.3.*

Further parameter analyses involving the semi-blind receivers would bring redundant conclusions to those presented in Sec. 5.2. For this reason, the next simulations are concentrated mainly in the direct comparison between the different (classes of) receivers rather than their individual performance analyses.

5.3.2.2 PT2-AF receivers *vs.* supervised receivers

For the comparison with the supervised receivers, the channel NMSE and the BER are plotted in Figs. 5.12 and 5.13, respectively. The channel NMSE calculated by (5.17) will be given in terms of $\mathbf{H} \Leftrightarrow \mathbf{H}^{(RD)}\mathbf{H}^{(SR)}$ which is an effective channel matrix between source and destination.

In Fig. 5.12, we can see that the pilot-assisted receivers present the best channel estimation performance, with an indistinguishable difference between them. Such similarity between BALS and LS-SVD was expected, since they exploit the same data tensor in two different ways. The performance gain obtained with these receivers is due to the use of pilot symbols, which is not the case with the proposed receivers. In addition, the energy level of the direct link clearly impacts the channel estimation performance of the PT2-AF receivers. While the SPP-ALS receiver benefits from the SD link only to initialize the PT2-ALS algorithm (cf. Table 4.2, step 1), the CPP-ALS receiver also uses updated estimates $\hat{\mathbf{H}}^{(SD)}$ to (re-)estimate the symbols at each iteration (cf. Table 4.2, step 2.2). Therefore, reducing the energy of the direct link (i.e. increasing α) slightly degrades the performance of the SPP-ALS receiver, while the performance degradation is more sensitive with the CPP-ALS receiver.

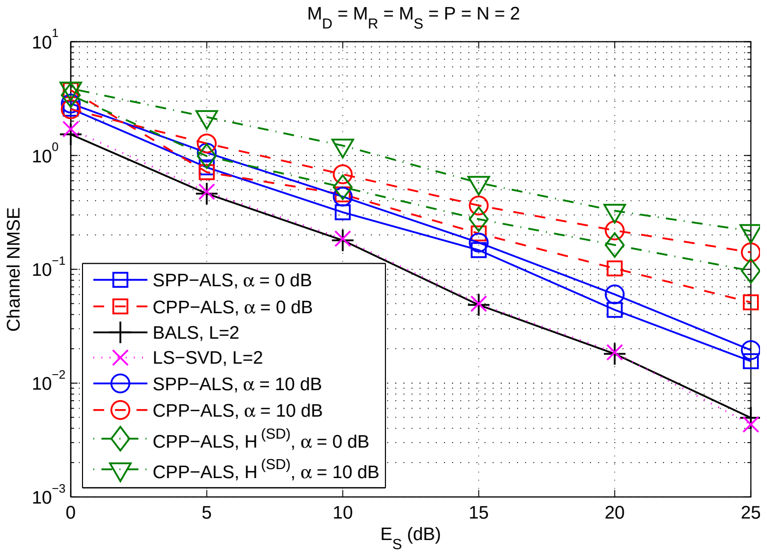

Figure 5.12: PT2-AF receivers *vs.* supervised receivers. Channel NMSE *versus* E_S.

The impact of α is also observed in the BER curves (Fig. 5.13). For the SPP-ALS receiver, the BER curves follow the tendency observed in the NMSE curves (Fig. 5.12). Concerning the CPP-ALS receiver, we can see it is more sensitive to the quality of the SD link. For $\alpha = 0$ dB, for instance, the estimate of $\mathbf{H}^{(SD)}$ is more accurate, and consequently the use of the SD link in the CPP-ALS algorithm benefits the overall receiver performance. On the other hand, when $\alpha = 10$ dB, a poorer quality of the SD link leads to worse estimates of $\mathbf{H}^{(SD)}$ and $\mathbf{S}$.

5.3.3 NP-AF receivers

In this section, the emphasis is given to the NP-AF receivers. More precisely, we focus on the comparison of the NP-AF receivers with the family of PT2-AF receivers and also among themselves.

Established that the PT2-AF receiver may have superior performance to the pilot-based receivers in terms of BER, this section is divided into the following comparisons:

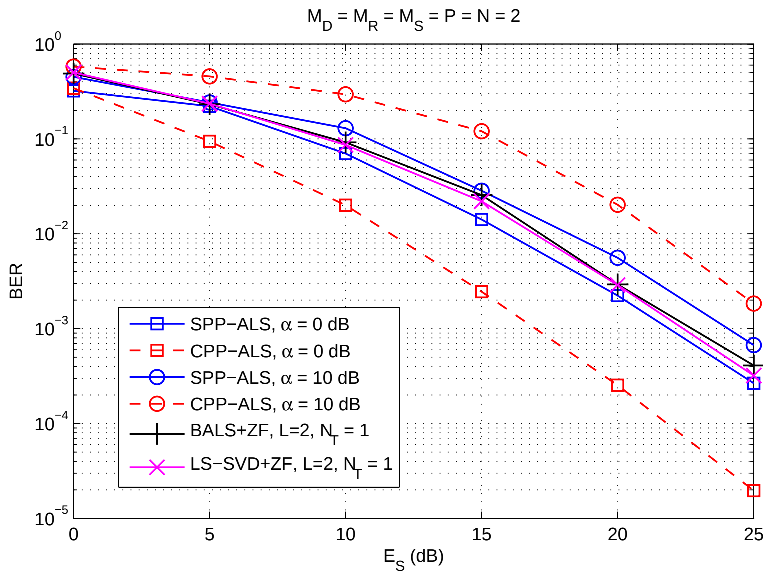

Figure 5.13: PT2-AF receivers *vs.* supervised receivers. BER *versus* E_S.

- NP-AF receivers *vs.* PT2-AF receivers;
- Single three-step ALS *versus* double two-step ALS;
- Iterative *versus* closed-form algorithms.

Thus, all classes of proposed semi-blind receivers in this thesis will be evaluated, and at the end a certain hierarchy of receivers in terms of performance and computational cost can be inferred.

5.3.3.1 NP-AF receivers *vs.* PT2-AF receivers

In the next few simulations, the NP-AF receivers are compared with the PT2-AF receivers. To ensure a fair comparison between them, once again the same transmission rate is used for both, which implies that the code length P of the PT2-AF receivers is set to be $(J+1)/2$ times greater than the source code length used for the NP-AF receivers.

In Fig. 5.14, the CPP-ALS and CNPALS receivers are added to demonstrate the impact that a strong direct link may have with such variants of PT2-ALS and NPALS.

The two figures (Figs. 5.14 and 5.15) depict the channel NMSE and BER as a function of E_S. In both figures, both NP-AF receivers NPALS and DALS achieve better performances than the competing PT2-ALS receiver. Theses gain come from the additional KRST coding operation applied at the relay, as shown with the ZF equalizer in Sec. 5.2. For a target BER of 10^{-2} and $J = 4$, the NPALS and DALS receivers provide a coding gain over the PT2-ALS receiver of around 7 dB – and a constant gain in E_S of the same 7 dB in channel NMSE. Increasing J, and thus automatically increasing P for PT2-ALS, the same coding gain remained for the same BER. In particular, for higher E_S levels (above 15 dB), the BER reduction of the proposed receivers is around two orders of magnitude. Such conclusions have also proved valid for the hybrid algorithms. With $\alpha = 0$ dB, CPNALS presented gains over CPP-ALS that are very close to those obtained by NPALS over PT2-ALS.

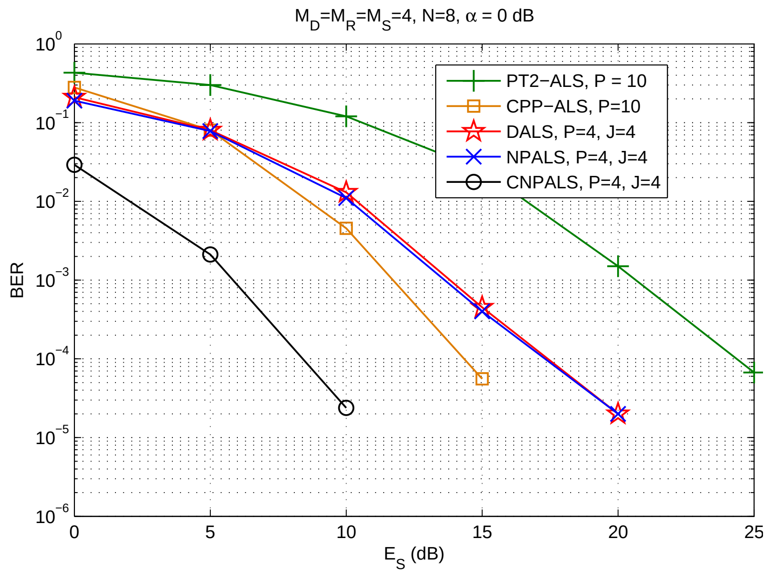

Figure 5.14: NP-AF receivers *versus* PT2-ALS receiver. BER *versus* E_S

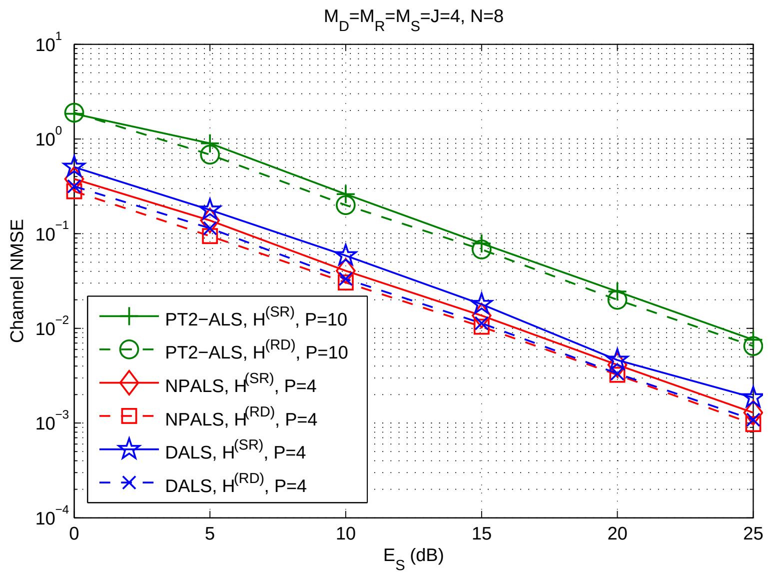

Figure 5.15: NP-AF receivers *versus* PT2-ALS receiver. Channel NMSE *versus* E_S

Furthermore, note that the difference, in terms of BER and channel NMSE, between NPALS and DALS receivers is very small. These results were certainly expected in the condition of proper convergence of the algorithms, since both exploit the same data tensor. In fact, the CALS-X variant (not depicted in the figure) has a very similar performance to

CNPALS, in the same way that DALS and NPALS presented close behaviors in Fig. 5.14.

Now a performance analysis is done in terms of the number N data-streams. Fig. 5.16 shows the channel NMSE obtained with the PT2-ALS and NPALS receivers for $N \in \{2, 8\}$. From this figure, we can conclude that increasing N provides a better channel estimation, since the estimation of the channels $\mathbf{H}^{(RD)}$ and $\mathbf{H}^{(SR)}$ using (4.71) and (4.73), and therefore of the effective channel $\mathbf{H}^{(RD)}\mathbf{H}^{(SR)}$, depends on N. However, such an improvement of channel estimation is at the cost of a higher computational complexity, as shown in Table 4.4.

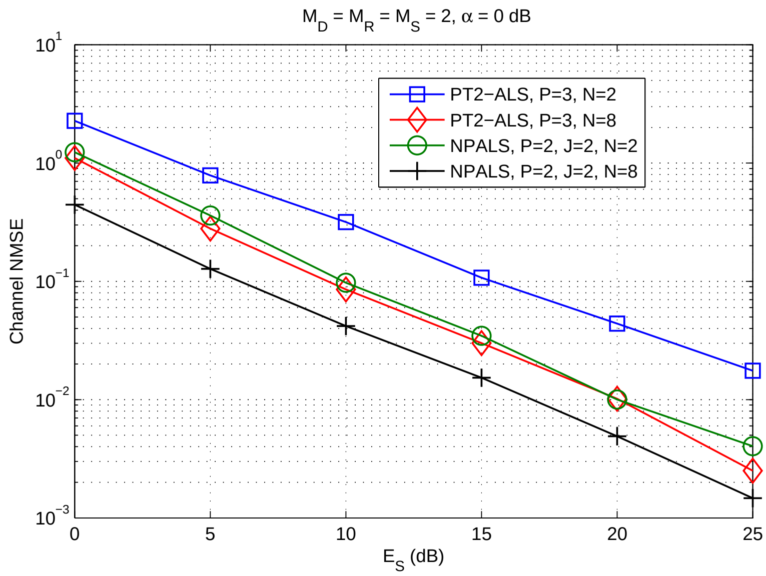

Figure 5.16: Impact of N on the PT2-ALS and NPALS receivers. Channel NMSE *versus* E_S.

At this point, through the simulations involving the semi-blind receivers (Figs. 5.14-5.16), a conclusion is that the NP-AF receivers achieve better estimation of symbols (and channels) than their direct PT2-AF correspondents for the same transmission rate. Furthermore, particularly for the NP-AF receivers, which present more distinct variations, the choice of one among them should be mainly based on the computational complexity, since the differences in their symbol and channel estimation are negligible.

5.3.3.2 Single three-step ALS *versus* double two-step ALS

The most remarkable trait of the nested PARAFAC decomposition is the possibility of writing a fourth-order tensor through two concatenated – "nested" – third-order tensors which follow PARAFAC models. Through this property, the receivers that can be employed for the NP-AF transmission scheme fall in two cases: the single three-step ALS-based receiver, e.g. NPALS, evaluated in Figs. 5.15-5.16; and also the double-step receivers, e.g. DALS and DKRF,

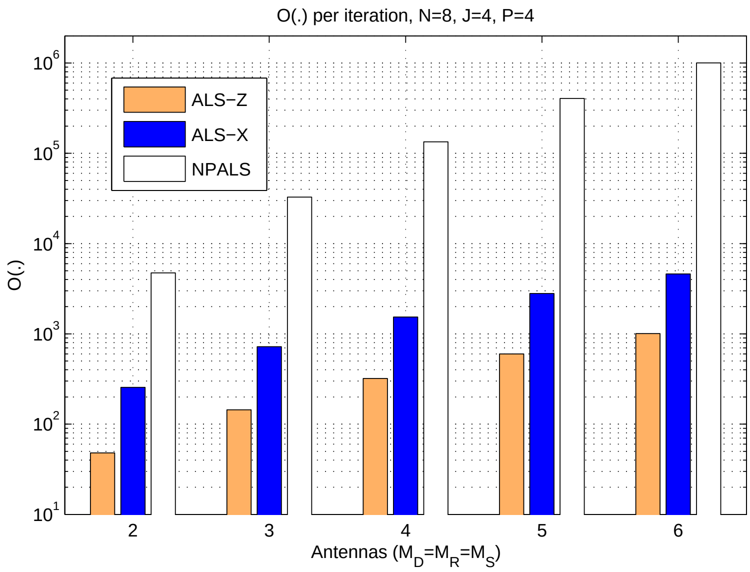

Figure 5.17: NP-AF iterative receivers. Computational cost *versus* antennas

introduced in Sec. 4.7.2.

In terms of the symbol and channel estimation, Figs. 5.15 and 5.14 showed that the ALS-based receivers NPALS and DALS have very similar solutions, and thus breaking down the estimation process in two procedures does not bring relevant gains in BER and channel NMSE. Thus, this section focuses on the possible computational gains when opting for one of them.

Fig. 5.17 compares the computational complexity of each proposed receiver (per iteration) by varying the size (number of antennas) of the cooperative network. Setting $M_D = M_R = M_S = M \geqslant 2$, which partially satisfies the identifiability and the uniqueness conditions of all proposed receivers, the number of antennas goes from 2 to 6. The higher computational cost for the NPALS algorithm is primarily a result of the big $M_D JPN \times M_R M_S$ matrix used to estimate $\mathbf{h}^{(SR)}$ (see Alg. 2 and Table 4.4), which for $M = 4$ corresponds to $\approx 97.71\%$ of the overall cost per iteration. In addition, the ALS-X algorithm is expectedly heavier than ALS-Z (see Table 4.5), since in general there are more elements in $\mathcal{Y}^{(SRD)}$ than in $\hat{\mathcal{Z}}$. The number of iterations of the first and second phases of these algorithms are crucial to verify whether NPALS or DALS is faster.

By choosing the stop criterion threshold $\delta = 10^{-6}$, Table 5.2 gives the average number ($Iter$) of iterations, the total computational cost (O(.)) and the NMSE of the reconstruction error of $\mathcal{Y}^{(SRD)}$ for each algorithm. These results were obtained for $(P, J) = \{(8, 4); (4, 8)\}$ and $E_S = 40$ dB.

Note that the NPALS algorithm is definitely much more numerically costly than the DALS receiver for nearly the same NMSE performance. Therefore, although NPALS was

Table 5.2: NP-AF iterative receivers (E_S@40 dB)

$\delta = 10^{-6}$						
	$J = 4$ and $P = 8$			$J = 8$ and $P = 4$		
Receiver	*Iter*	O(.) ($\times 10^4$)	NMSE ($\times 10^{-6}$)	*Iter*	O(.) ($\times 10^4$)	NMSE ($\times 10^{-6}$)
NPALS	7	187.8	5.72	9	241.5	7.41
DALS	—	4.1	6.24	—	3.6	7.78
ALS-X	12	3.7	—	10	2.6	—
ALS-Z	7	0.4	—	9	1.0	—

used for BER comparisons involving the NP-AF receivers in the previous simulations, it does not present the best solution for blind estimation in a cooperative communication system in terms of complexity. Unless a way to reduce its computational cost per iteration is proposed, which intuitively means reducing the cost of estimating $\mathbf{h}^{(SR)}$, there is no expected advantage in the estimation of the triplet ($\mathbf{S}$,$\mathbf{H}^{(RD)}$,$\mathbf{H}^{(SR)}$) using a single ALS procedure.

5.3.3.3 Iterative *versus* closed-form algorithms

Previous comparisons make clear that the NPALS and DALS receivers, by exploiting the same data tensor, have the same performance of BER and channel NMSE. However, Table 5.2 shows a considerable computational gain when choosing the two-step receiver DALS over the single-step NPALS.

In Sec. 4.7.2.2, Chapter 4, the DKRF receiver was proposed in order to offer a low-complexity alternative to the iterative receivers, especially with the advantage of avoiding some common convergence issues linked to ALS-based algorithms applied to tensor models.

In this subsection, the first conclusion to be drawn from the comparison between DKRF and DALS is whether they have the same performance for semi-blind estimation. Varying only E_S and M_S, we can see in Fig. 5.18 that both receivers had the same BER and channel NMSE performances, as expected.

The similar performance of these two receivers is even more obvious than that one between NPALS and DALS, since both DKRF and DALS exploit exactly the same $\mathcal{X}^{(SRD)}$ and $\mathcal{Z}$ input tensors, but using different unfoldings. Consequently, it is possible to expect beforehand that they will present closer computational costs, since DALS can have a low number of iterations to converge (e.g. Table 5.2), and the costs per iteration (cf. Table 4.5) of the two receivers are also closer.

For $E_S = 10$ dB, the complexity ratios between DALS and DKRF are calculated accord-

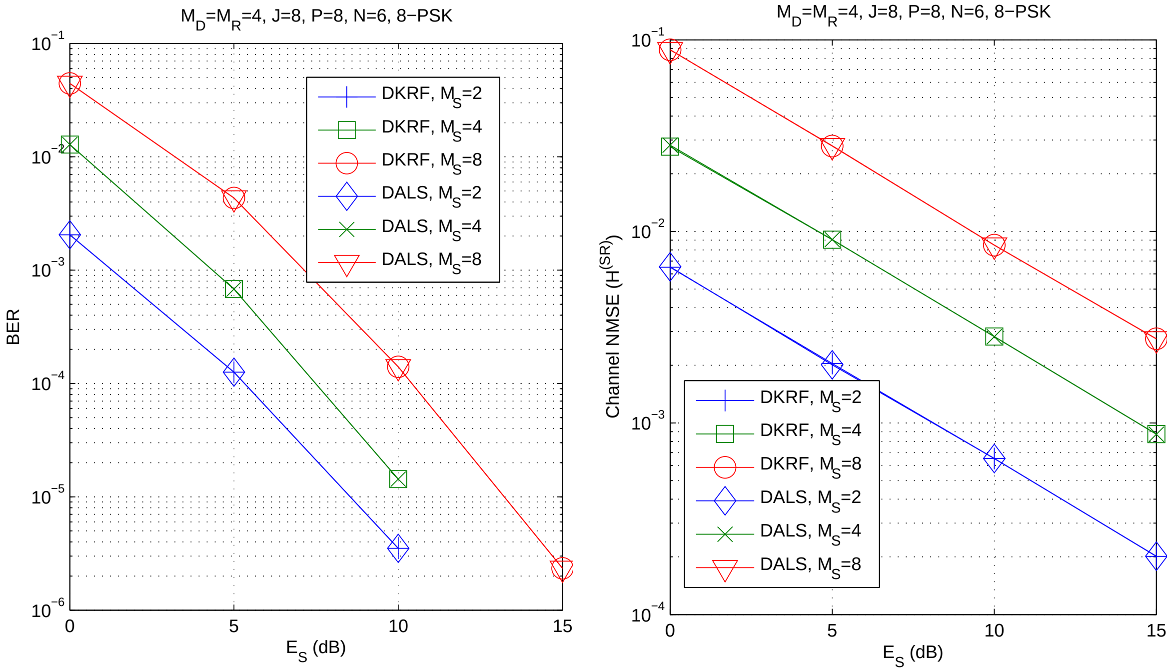

(a) BER *versus* E_S (b) Channel NMSE ($\mathbf{H}^{(SR)}$) *versus* E_S

Figure 5.18: Comparison between DALS and DRKF receivers. Joint symbol and channel estimation

ingly to

$$O_1 = \frac{O_B}{O_A}, \quad O_2 = \frac{O_D}{O_C}, \quad O_3 = \frac{O_B + O_D}{O_A + O_C}, \tag{5.18}$$

which denotes how many times the DALS are heavier than DKRF for symbol, channel and joint estimation, respectively. O_A, O_B, O_C and O_D are defined in Table 4.5. Varying M_S or M_R, such ratios are shown at Fig. 5.19.

The first and foremost conclusion from this figure is that, for either symbol and channel estimation, the DKRF receiver is the less demanding choice, since both O_1 and O_2 are greater than one. In addition, for joint symbol and channel estimation the DKRF receiver presents better overall behavior as M_S or M_R increase, as indicated by the growth of O_3. For the stage of symbol estimation, O_1 presented a apparently linear gain in computational complexity when increasing M_S, since from Table 4.5 it is clear that O_1 is linear with $l_1 M_S$ and the variation of the number of iterations l_1 was small.

Although O_2 has a decreasing slope in Fig. 5.19a, thanks to the presence of M_S in O_C and its absence in O_D, the complexity of the symbol estimation is still dominant on the overall cost of the receivers, i.e. $O_A \gg O_C$ and $O_B \gg O_D$, justifying the growth of O_3 along O_1. For instance, in Fig. 5.19a for $M_S = 8$ we have $O_A = 16384$, while O_C is only equal to 512.

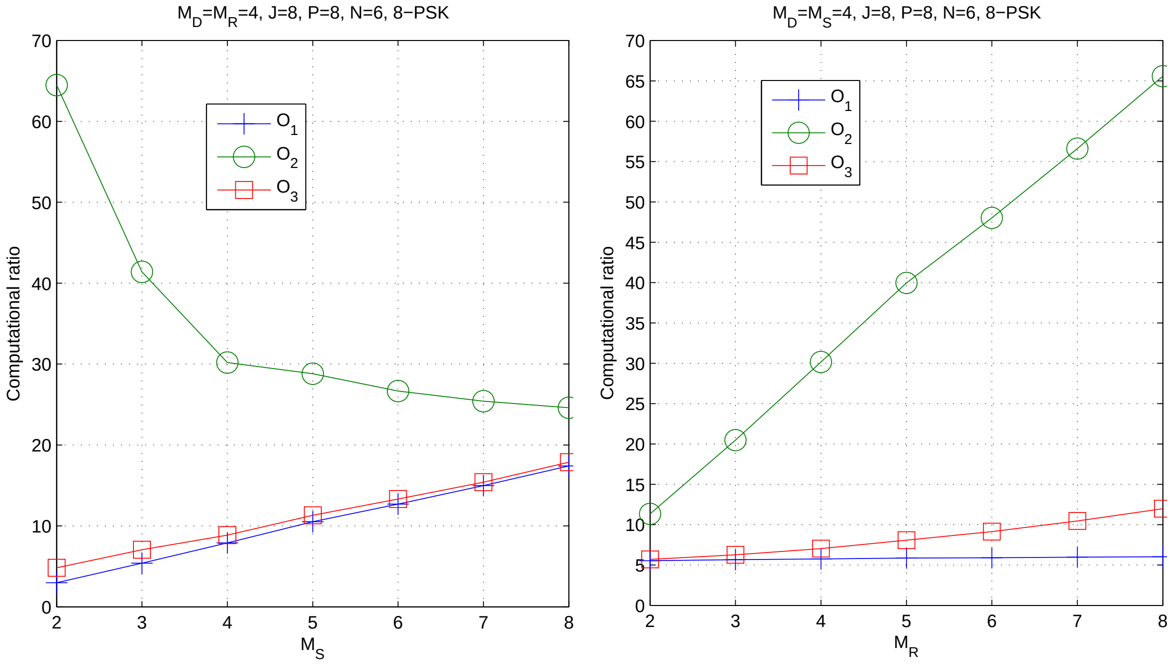

(a) Comp. ratio *vs* M_S

(b) Comp. ratio *vs* M_R

Figure 5.19: Complexity comparison between DALS and DKRF receiver

Varying M_R in Fig. 5.19b only benefited DKRF over DALS, mostly because of the computational gain in the step of channel estimation (O_2). Since both O_A and O_B are independent of M_R, the ratio for symbol estimation (O_1) has no visible variation.

5.4 Summary of the chapter

In this chapter, the behavior of the tensor-based transmission systems and their semi-blind receivers proposed in Chapter 4 are analyzed through Monte Carlo experiments.

For both PT2-AF and NP-AF systems, it was demonstrated through the aid of a ZF equalizer that, within a scenario of perfect knowledge of the CSI, it is possible to obtain a spatial diversity through increasing the number of antennas at the destination and at the relay. Furthermore, coding gains can be achieved through the increase of the code lengths at the source or relay – with the latter being possible only in the NP-AF protocol.

The first receivers evaluated were those dedicated to the PT2-AF protocol – i.e. PT2-ALS, SPP-ALS and CPP-ALS. The performance of the PT2-ALS receiver greatly depends on initialization. Due to the absence of *a priori* information on channels, a random initialization is used, which generally implies a slow convergence. A performance improvement can be obtained by initializing the PT2-ALS receiver with symbol initial values ($\hat{\mathbf{S}}_0$) provided by the PARAFAC-SVD algorithm associated with the direct link. That is the idea behind the SPP-ALS and CPP-ALS receivers.

Since each block of signals transmitted via the SD link is received right after the first hop of the protocol, and due to the fast computation of the PARAFAC-SVD method, this processing is likely finished before the end of the second hop, during which the relay forwards the amplified signals. Therefore, the use of the SD link does not increase the total estimation time, but on the contrary, the overall computational cost can be reduced using a better initialization. From another point of view, combining the two links for estimating the symbols is equivalent to doubling the number of receive antennas at the destination node, which implies an increase of space diversity and consequently a performance improvement. That is the idea exploited by some hybrid receivers (i.e. CPP-ALS, CNPALS, CALS-X and CKRF-X).

Concerning the NP-AF receivers, they have achieved better performance than the PT2-AF ones in most of the cases, either in terms of BER, channel NMSE and computational cost. In terms of BER and channel NMSE performances, differences among the NP-AF receivers are minimum, such that the proper choice for a receiver in this case should be based mainly on computational cost, with the usual best choice being DKRF, followed by DALS.

If the direct link is strong, the hybrid variants of the NP-AF receivers (i.e. CNPALS, CALS-X and CKRF-X) can be employed to provide better symbol estimation. They have shown coding gains over the CPP-ALS receiver, albeit simulations show that there is no diversity gain between these receivers, in the same way that the conventional NP-AF receivers (e.g. NPALS) also did not display gains of this nature over the PT2-ALS receiver.

When the comparison is made between the semi-blind receivers and two tensor-based pilot-based approaches, the proposed ones have presented better results in symbol estimation, corroborating the expected gain in the spectral efficiency. Given that this specific comparison takes into account the same transmission rates for both strategies, with the same number of information-bearer symbols sent in each simulation, the proposed receivers could exploit a greater level of time-diversity (introduced by the source and relay) to jointly estimate symbols and channels, since the supervised methods had to spare part of the total time only for the CSI recovery.

Taking into account the results of simulation of this chapter, and the properties of transmission systems and their receivers summarized in Tables 4.6 and 4.7, one can state the following observations:

- All semi-blind receivers can properly exploit the spatial diversities introduced by the presence of multiple antennas at the relay and destination;
- For the same transmission rate, the NP-AF receivers present a coding gain over the PT2-AF receivers, although the PT2-AF protocol is twice as fast as NP-AF;

- By satisfying their sufficient identifiability conditions (Table 4.6), all proposed receivers can present coding gains, but not diversity gains, when P or J is augmented;
- In a large relaying network (large M_R), the PT2-AF receivers can be used as long as M_D is increased. In this scenario, this compensation in the NP-AF protocol can be done through the increase of J, although invariably causing a reduction in the transmission rate;
- The existence of the direct link can either be used to boost the convergence speed of the iterative receivers or to enhance the joint estimation using the hybrid receivers. The latter purpose is recommended only when the direct link is strong enough (no less than 10 dB weaker than the relay-assisted link), since employing low-power signals coming from this link can even deteriorate the estimation using the proposed receivers;
- Among the NP-AF receivers, DKRF is recommended over DALS and NPALS, since it has in general the smallest computational cost with the same estimation performance. The utilization of these ALS-based receivers may be preferable if new sufficient identifiability conditions, using different hypotheses of the system parameters and more relaxed than those in Table 4.6, are stated.

Chapter 6

Conclusion

This thesis manuscript has proposed two new tensor-based AF relaying protocols for one-way two-hop MIMO relay systems exploiting spatial, time and code diversities. For each transmission scheme, several semi-blind receivers were proposed for the application of joint symbol and channel estimation, and eventually for joint channel estimation, i.e. estimation of the Source-Relay (SR) and Relay-Destination (RD) channels that compose the two-hop network.

The two transmission protocols arise from the use of a simplified KRST coding at the source node, combined with two different AF processing schemes at the relay node. In the PT2-AF protocol the third-order data tensor received at destination follows a PARATUCK2 model, whereas in the NP-AF protocol a fourth-order data tensor is modeled with a nested PARAFAC decomposition. The conceptual difference between PT2-AF and NP-AF is that, in the former, for each symbol data-stream there is associated a different set of AF gains, whereas the latter applies a new KRST coding over the signals, spreading the data-streams along a new time-domain.

The NP-AF transmission protocol has greater flexibility than PT2-AF, particularly due to the wider range of choices of semi-blind receivers. Among the factors that contribute to the benefit of NP-AF one can cite:

- the possibility of dealing either with the fourth-order nested PARAFAC decomposition of the data tensor or through one of its PARAFAC modeling;
- the variety of strategies for joint symbol and channel estimation, with special regard to the two-step receivers (DALS and DKRF), where the joint channel estimation step (i.e. ALS-Z and KRF-Z) is not mandatory for symbol estimation;

Indeed, these two factors above are intrinsically linked to each other and to the properties of nested PARAFAC. For this tensor decomposition, two new uniqueness theorems were proposed in Chapter 3.

Briefly, the main contributions of this thesis can be summarized (in order of presentation) by:

- Proposition of two theorems on the uniqueness properties of the nested PARAFAC decomposition;

- Development of two tensor-based transmission schemes for one-way two-hop AF relaying network using a KRST coding at the source;

- Design of 4 semi-blind receivers (PT2-ALS, NPALS, DALS and DKRF) dedicated to joint symbol and channel estimation using the relay-assisted link;

- Design of 5 variants (SPP-ALS, CPP-ALS, CNPALS, CALS-X and CKRF-X) dedicated to combine both direct and relay links for estimation improvement;

- Study of the properties of the proposed receivers, in terms of identifiability conditions, symbol and channel estimation performances, transmission rate and computational cost.

From the simulation results, we conclude that all proposed semi-blind receivers have presented better symbol estimation than two state-of-the-art pilot-based strategies, corroborating the already expected gain in spectral efficiency so often achieved from blind estimation.

In addition, the NP-AF receivers have presented better performance than the PT2-AF receivers in symbol and channel estimation and also in computational complexity. However, an advantage of the PT2-AF protocol is that it can display higher transmission rates than NP-AF, which is crucial for fast fading channels.

The conventional NP-AF receivers (i.e. NPALS, DALS and DKRF) are similar in terms of NMSE and BER performances, while the complexity analysis shows that DKRF and then DALS are the less computationally demanding receivers. It is worth mentioning that the choice between the single-stage NPALS algorithm and the two-stage DALS and DKRF algorithms also depends on the final goal of the receiver. If both symbol and channel estimations are needed, any of them can be used. On the other hand, if we are interested in symbol estimation only, we can limit ourselves to the first stage (i.e. ALS-X or KRF-X) of the two-step receivers, which allows to further simplify the receiver processing.

Moreover, the combination of the direct and relay-assisted links leads to the formulation of the so-called hybrid receivers. Using the PT2-AF relaying protocol, the combination of the PARAFAC and PARATUCK2 tensor models lead to the development of two variants named SPP-ALS and CPP-ALS. In the case of the NP-AF protocol, the combination of the PARAFAC and nested PARAFAC models allows the proposition of CNPALS, CALS-X and CKRF-X, which are variants respectively to the NPALS, DALS and DKRF receivers. All these hybrid receivers take advantage of the availability of a strong direct link in a two-hop relaying scenario, gathering additional spatial diversity (except SPP-ALS) to further improve symbol estimation.

Perspectives

Since this thesis covers the use of semi-blind receivers in multi-antenna relaying networks, a subject that had not been explored in the literature apart from the publications involving this work, one may extrapolate some techniques and concepts developed herein for more complex relaying systems. Below are some perspectives that seem possible after the contributions of this manuscript:

- *New blind-receivers*: The first and most tangible extension of this work is to develop new (semi-)blind receivers for the PT2-AF and NP-AF protocols. As stated in Chapter 4, particularly the NP-AF scheme allows a wide variety of receivers, including the combination of iterative and non-iterative algorithms described in Sec. 4.7.2, but not analyzed in this thesis. In addition, other estimators have already been successfully used for cooperative and/or tensor-based applications, as the Minimum Mean Square Error (MMSE)-based [92, 93] and Levenberg-Marquardt (LM) [57] algorithms.

- *System optimization*: Given that the priority of this work was to develop tensor-based semi-blind receivers for relaying networks, this thesis did not rigorously addressed optimization techniques or theoretical studies on the statistical performance of the proposed receivers. There is in the literature a large body of work on symbol error probability [94, 95] in conventional cooperative scenarios, while at the other hand the prediction of the estimation accuracy of tensor decompositions is less studied – mostly focusing only on the PARAFAC decomposition [96, 97]. Therefore, there is an abundant number of promising topics in the area of system optimization for tensor-based relaying networks.

- *New tensor models*: An interesting feature of the nested PARAFAC model is its nesting property. More precisely, when the entries of a 4^{th}-order tensor is arranged as 3^{rd}-order tensor, one of the matrix factors of its PARAFAC decomposition is an unfolding of another tensor. While this tensor also follows a PARAFAC model, one can think of extending this idea to embrace different decompositions. One of the possible applications of these new models would be the utilization of a wider range of ST coding strategies for blind estimation in cooperative systems, e.g. nesting an unfolding of the TST tensor coding [63] in a two-hop cooperative model.

- *Multihop*: Based on the idea of nesting two or more tensor models, a generalized nested PARAFAC decomposition for higher-order tensors is straightforwardly possible. This generalization would allow a tensor of order N to be described by a number of PARAFAC models of lower order, which treating individually may tend to reduce the overall complexity. A practical and innovative application would be the joint channel estimation in multihop scenarios. First simulations for a scenario with 3 hops were done for the semi-blind channel estimation, with satisfactory results.

- *Two-way*: In the literature, the PARAFAC decomposition is used for supervised channel estimation for both one-way and two-way relay networks. Although the latter protocol has better spectral efficiency than the former, communicating nodes in two-way systems suffer from undesirable self-interference. In [18, 19] this problem is addressed through the use of orthogonal pilot sequences. The orthogonality property, applied to the source coding proposed in this thesis, can also be used to design semi-blind receivers for two-way scenarios. Development in this subject is already in course.

- *Adaptive estimation*: the NP-AF protocol could achieve the best BER performance among the different forms of communication presented in this thesis, but at an expense of a lower transmission rate given the additional KRST coding at the relay. A greater delay to start the estimation at the destination node may be highly undesirable, especially with unpredictable occurrences such as the disappearance of a relaying node during the transmission. In these cases, the signal received at the destination node can be greatly distorted from its original model.

  An AF strategy where smaller signal blocks received by the relay are instantly amplified and sent to the destination, without need to store all the block of data prior to its forwarding process, could mitigate some issues described in the previous paragraph. In this case, the destination node should not need to receive all block of signals to start the symbol estimation process, and adaptive semi-blind receivers could be thought to perform a tracking process, where at each new instant another slice of the receiving tensor is added to improve the estimation. Adaptive algorithms for estimation of the PARAFAC decomposition have already been proposed in [98].

Chapter 7

Conclusion

Ce manuscrit de thèse a proposé deux nouveaux protocoles de transmission avec relaisbasés sur tenseurs pour systèmes MIMO à deux sauts en exploitant les diversités spatiales, temporelle et de code. Pour chaque système de transmission du type *amplifying-and-forwarding* (AF), plusieurs récepteurs semi-aveugles ont été proposées pour l'application de estimation conjointe de symboles et des canaux qui composent le réseau deux-hop.

Les deux protocoles de transmission proviennent de l'utilisation de codages KRST simplifiées au niveau du noeud de la source, combinés avec deux différents types de traitement de signaux au niveau du noeud du relais. Dans le protocol PT2-AF le tenseur de troisième ordre de données reçus au noeud de destination suit un modèle PARATUCK2, alors que dans le protocole NP-AF le tenseur de quatrième ordre est modélisée avec une decomposition PARAFAC imbriqué. La différence conceptuelle entre le PT2-AF et le NP-AF est que, dans le premier, pour chaque paquet de symboles est associé un ensemble différent de gains au relais, alors dans le NP-AF une nouvelle codage KRST est appliqué sur les signaux reçus au relais.

Le protocole de transmission NP-AF a une plus grande flexibilité que le PT2-AF, notamment en raison d'une plus grande variété de récepteurs semi-aveugles. Parmi les facteurs qui contribuent à l'avantage de NP-AF, on peut citer:

- la possibilité de traiter les données soit par une décomposition tensorielle du type PARAFAC imbriquée de quatrième ordre, soit par deux décompositions du type PARAFAC de troisième ordre.;

- la variété de stratégies pour l'estimation conjointe de symboles et de canaux, avec une attention particulière les récepteurs en deux étapes (DALS et DKRF), où l'étape d'estimation de canaux individuales (i.e. ALS-Z et KRF-Z) ne est pas obligatoire pour l'estimation de symboles;

En bref, les principales contributions de cette thèse peuvent être résumées (dans l'ordre de présentation) par:

- Proposition de deux théorèmes sur les propriétés d'unicité de la décomposition du type PARAFAC imbriquée;

- Le développement de deux systèmes de transmission basés sur tenseurs pour un reseau avec un relais du type AF à deux sauts, en utilisant une codage KRST à la source;
- Conception de quatre récepteurs semi-aveugles (PT2-ALS, NPALS, DALS et DKRF) dédiés à l'estimation conjointe de symboles et canaux canal en utilisant le lien avec relais;
- Conception de 5 variantes (SPP-ALS, CPP-ALS, CNPALS, CALS-X et CKRF-X) dédiés à combiner les liens directs et avec relais pour l'amélioration de l'estimation;
- L'étude des conditions d'identifiabilité des récepteurs proposées et de ses performances en termes d'estimation de symboles, de canaux et de coût de calcul.

A partir des résultats de simulation, nous concluons que tous les récepteurs semi-aveugles proposées ont présenté une meilleure estimation de symbole en comparaison avec deux récente stratégies d'estimation basées sur séquences de symboles pilots, corroborant le gain déjà attendue de l'efficacité spectrale provenant des estimations du type semi-aveugle.

En outre, les récepteurs pour le NP-AF ont présenté de meilleures performances que les recepteurs pour le PT2-AF en termes d'estimation de symboles et canaus, et aussi dans le coût de calcul. Cependant, un avantage de le protocol PT2-AF est qu'il peut afficher des taux de transmission plus élevés que le NP-AF, qui est crucial sous les canaux avec évanouissement rapide.

Les récepteurs de base pour le NP-AF (c'est-à-dire NPALS, DALS et DKRF) sont similaires en termes de performances de BER et NMSE de canaux, tandis que l'analyse de la complexité montre que le DKRF et puis le DALS sont les récepteurs moins coûteux. Il est intéressant de noter aussi que le choix entre l'algorithme NPALS et les lesquelles à deux étages (i.e. DALS et DKRF) dépend aussi de l'objectif final du récepteur. Si les estimations de symboles et de canaux sont nécessaires, quelqu'un d'eux peut être utilisé. D'autre part, si nous sommes que intéressés dans l'estimation de symbole, nous pouvons nous limiter à la première étape (i.e. la ALS-X ou KRF-X) des récepteurs en deux étapes, ce qui permet de simplifier davantage le traitement du récepteur.

De plus, la combinaison des liens directs et avec relais conduit à la formulation des récepteurs dits hybrides. En utilisant le protocole PT2-AF, la combinaison des modèles PARAFAC and PARATUCK2 conduit à l'élaboration de deux variantes nommées SPP-ALS et CPP-ALS. Dans le cas du protocole NP-AF, la combinaison du modèle PARAFAC avec le modèle PARAFAC imbriqués permet la proposition des récepteurs CNPALS, CALS-X et CKRF-X, qui sont des variantes respectivement aux NPALS, DALS DKRFs. Tous ces récepteurs hybrides profitent de la disponibilité d'un lien direct fort dans un scénario de relais à deux sauts, la collecte de la diversité spatiale supplémentaire (sauf SPP-ALS) d'améliorer encore estimation de symboles

.

Appendix A

Properties of matrix operations

In order to follow the development of this thesis, it is necessary the clear understanding of a few mathematical operators, such as the $vec(.)$ and $D_n(.)$ operators.

Definition 8. *The operator vec(.) vectorizes its matrix argument by stacking its columns, as for example*

$$\mathbf{A} = \begin{bmatrix} a_{1,1} & a_{1,2} \\ a_{2,1} & a_{2,2} \end{bmatrix} \Rightarrow vec\left(\mathbf{A}\right) = \begin{bmatrix} a_{1,1} \\ a_{2,1} \\ a_{1,2} \\ a_{2,2} \end{bmatrix}.$$

Definition 9. *The term $D_n(\mathbf{A})$ corresponds to the diagonal matrix with the n^{th} row of $\mathbf{A}$ forming its diagonal, as for example:*

$$\mathbf{A} = \begin{bmatrix} a_{1,1} & a_{1,2} \\ a_{2,1} & a_{2,2} \end{bmatrix} \Rightarrow D_1\left(\mathbf{A}\right) = \begin{bmatrix} a_{1,1} & 0 \\ 0 & a_{1,2} \end{bmatrix},$$

$$\Rightarrow D_2\left(\mathbf{A}\right) = \begin{bmatrix} a_{2,1} & 0 \\ 0 & a_{2,2} \end{bmatrix}.$$

Furthermore, two of the most important mathematical operations in multilinear algebra are the Kronecker and Khatri-Rao products. The Kronecker product between two matrices is a generalization of the outer product between two vectors, and it is commonly found in the matricization of tensors. On the other hand, the Khatri-Rao product, also known as column-wise Kronecker product, yields an elegant writing of the matrix unfoldings of the PARAFAC-family decompositions present in this thesis. The basic definitions and some properties of the Kronecker and Khatri-Rao products are given in the following.

Definition 10. *(Kronecker product) The operator $\otimes$ denotes the Kronecker product. For any matrices $\mathbf{A} \in \mathbb{C}^{I\times J}$ and $\mathbf{B} \in \mathbb{C}^{K\times L}$ we have*

$$\mathbf{A} \otimes \mathbf{B} = \begin{bmatrix} a_{1,1}\mathbf{B} & a_{1,2}\mathbf{B} & \cdots a_{1,J}\mathbf{B} \\ a_{2,1}\mathbf{B} & a_{2,2}\mathbf{B} & \cdots a_{2,J}\mathbf{B} \\ \vdots & \vdots & \vdots \\ a_{I,1}\mathbf{B} & a_{I,2}\mathbf{B} & \cdots a_{I,J}\mathbf{B} \end{bmatrix} \in \mathbb{C}^{KI\times LJ}. \tag{A.1}$$

Lemma 15. *Some properties of the Kronecker product are*

$$\mathbf{A} \otimes \mathbf{B} \neq \mathbf{B} \otimes \mathbf{A} \tag{A.2}$$

$$(\mathbf{A} \otimes \mathbf{B})^H = \left(\mathbf{A}^H \otimes \mathbf{B}^H\right) \tag{A.3}$$

$$(\mathbf{A} \otimes \mathbf{B})^\dagger = \left(\mathbf{A}^\dagger \otimes \mathbf{B}^\dagger\right) \tag{A.4}$$

$$(\mathbf{A} \otimes \mathbf{B}) \otimes \mathbf{C} = \mathbf{A} \otimes (\mathbf{B} \otimes \mathbf{C}) \tag{A.5}$$

$$\mathbf{AB} \otimes \mathbf{CD} = (\mathbf{A} \otimes \mathbf{C})(\mathbf{B} \otimes \mathbf{D}) \tag{A.6}$$

$$rank(\mathbf{A} \otimes \mathbf{B}) = rank(\mathbf{A})\, rank(\mathbf{B}) \tag{A.7}$$

$$\mathbf{A}_{.i} \otimes \mathbf{B}_{.j} = vec\left(\mathbf{B}_{.j}\mathbf{A}_{.i}^T\right) \tag{A.8}$$

$$vec\left(\mathbf{ABC}^T\right) = (\mathbf{C} \otimes \mathbf{A})\, vec(\mathbf{B}) \tag{A.9}$$

Definition 11. *(Khatri-Rao product) The operator $\diamond$ denotes the Khatri-Rao product. For $\mathbf{A} \in \mathbb{C}^{L\times M}$ and $\mathbf{B} \in \mathbb{C}^{N\times M}$ we have*

$$\begin{aligned} \mathbf{A} \diamond \mathbf{B} &= \begin{bmatrix} \mathbf{B}D_1(\mathbf{A}) \\ \vdots \\ \mathbf{B}D_L(\mathbf{A}) \end{bmatrix} \in \mathbb{C}^{NL\times M} \\ &= [\mathbf{A}_{\cdot 1} \otimes \mathbf{B}_{\cdot 1}, \; \cdots, \; \mathbf{A}_{\cdot M} \otimes \mathbf{B}_{\cdot M}]. \end{aligned} \tag{A.10}$$

Lemma 16. *Some properties of the Khatri-Rao product are*

$$\mathbf{A} \diamond \mathbf{B} \neq \mathbf{B} \diamond \mathbf{A} \tag{A.11}$$

$$\mathbf{AB} \diamond \mathbf{CD} = (\mathbf{A} \otimes \mathbf{C})(\mathbf{B} \diamond \mathbf{D}) \tag{A.12}$$

$$vec\left(\mathbf{A}D_n(\mathbf{B})\mathbf{C}^T\right) = (\mathbf{C} \diamond \mathbf{A})\, \mathbf{B}_{n\cdot}^T \tag{A.13}$$

Appendix B

Channel scaling ambiguities

The scaling ambiguities affecting the estimated parameters (i.e. the columns of $\mathbf{H}^{(RD)}$ and $(\mathbf{H}^{(SR)})^T$) are intrinsic to many blind/semi-blind algorithms, including the ones based on tensor decompositions. If one is interested in blind symbol recovery only, such a scaling ambiguity problem is not relevant, since the estimated symbol matrix only depends on the effective (compound) channel, and not on the individual channels. Consider for example the PT2-AF protocol. The effective channel at n^{th} data-stream from (4.29), considering the alternative solution $(\bar{\mathbf{H}}^{(RD)}, \bar{\mathbf{H}}^{(SR)})$, is given by

$$\begin{aligned}\mathbf{Z}_n &= \bar{\mathbf{H}}^{(RD)} D_n(\mathbf{G}) \bar{\mathbf{H}}^{(SR)} \\ &= \sum_{m_R=1}^{M_R} g_{n,m_R} \mathbf{H}^{(RD)}_{\cdot m_R} \mathbf{H}^{(SR)}_{m_R \cdot}.\end{aligned}$$

Given that the permutation ambiguity is completely avoided based on Theorem 10, Chapter 4, then all rank-one matrices $\mathbf{H}^{(RD)}_{\cdot m_R} \mathbf{H}^{(SR)}_{m_R \cdot} = \bar{\mathbf{H}}^{(RD)}_{\cdot m_R} \bar{\mathbf{H}}^{(SR)}_{m_R \cdot}$ $\forall\, m_R$ can be fully recovered. Based on the knowledge of these matrices, the gain g_{n,m_R} can be further calculated to optimize $\mathbf{Z}_n$ that gives the best performance in symbol estimation.

However, if there is interest in exploiting $\mathbf{H}^{RD}$ and $\mathbf{H}^{(SR)}$ without the scaling ambiguities, a simple solution can be used to fix it, which consists in sending a training sequence from the relay to destination and applying a simple LS algorithm to estimate the channel $\mathbf{H}^{(RD)}$ that can be used to calculate the scaling ambiguity matrix $\mathbf{\Delta}^{(RD)}$.

For example, suppose an orthogonal training sequence $\bar{\mathbf{R}} \in \mathbb{C}^{M_R \times L}$, where L is the number of training sequences of M_R pilot symbols transmitted by the relay to the destination. The noise-free signal arriving at destination is

$$\mathbf{X}^{(RD)} = \mathbf{H}^{(RD)} \bar{\mathbf{R}} \in \mathbb{C}^{M_D \times L}. \tag{B.1}$$

Therefore, if $\bar{\mathbf{R}}$ is full rank and $L \geqslant M_R$, then $\mathbf{H}^{(RD)}$ can be directly estimated through a simple Least Square (LS) estimator, i.e.

$$\hat{\mathbf{H}}^{(RD)} = \mathbf{Y}^{(RD)} (\bar{\mathbf{R}})^{\dagger}, \tag{B.2}$$

where $\mathbf{Y}^{(RD)}$ is the observed sample of $\mathbf{X}^{(RD)}$ with correspondent additive noise $\mathbf{V}^{(D)} \in \mathbb{C}^{M_D \times L} \sim \mathcal{CN}(0,1)$.

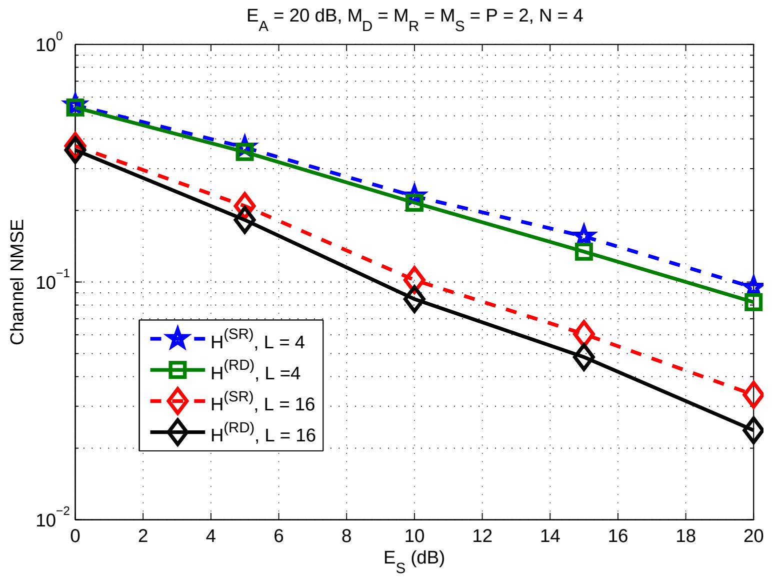

Figure B.1: LS procedure for scaling ambiguity removal. Channel NMSE *versus* E_S.

The strategy for estimating the channels is slightly modified from the Chapter 4, and it is summarized below:

1. Find $\widehat{\mathbf{H}}_0^{(RD)}$ using (B.2);
2. Perform the joint channel estimation process, using any of the proposed receivers, initializing with $\widehat{\mathbf{H}}_0^{(RD)}$ in the iterative algorithms;
3. Identify and eliminate the (estimated) scaling ambiguities of $\widehat{\mathbf{H}}^{(RD)}$ using knowledge of the estimate from step 1. Compensate this scaling ambiguity in the estimate of $\mathbf{H}^{(SR)}$.

This simple LS estimation step would allow to fix the scaling ambiguity affecting $\mathbf{H}^{(RD)}$ (and thus $\mathbf{H}^{(SR)}$). Additionally, the iterative receivers could be initialized with this estimate, which can help the algorithm to converge faster. However, this benefit comes with an extra usage of bandwidth due to the transmission of pilots from the relay to the destination.

In order to show that the use of the solution described above is feasible, we show in Fig. B.1 the NMSE of the individual channel matrices after eliminating the scaling ambiguities affecting their estimation. The parameters L and E_A denote the length of the pilot sequences sent by the relays and the average energy of the pilot symbols, respectively.

Bibliography

[1] D. Tse and P. Viswanath, *Fundamentals of Wireless Communication.* Boston, MA, USA: Cambridge University Press, 2005. (Cited on page 1.)

[2] A. Goldsmith, *Wireless Communications.* New York, NY, USA: Cambridge University Press, 2005. (Cited on pages 1 and 7.)

[3] A. Sendonaris, E. Erkip, and B. Aazhang, "User cooperation diversity - part I: system description," *IEEE Transactions on Communications*, vol. 51, no. 11, pp. 1927–1938, Nov. 2003. (Cited on page 2.)

[4] ——, "User cooperation diversity - part II: implementation aspects and performance analysis," *IEEE Transactions on Communications*, vol. 51, no. 11, pp. 1939–1948, Nov. 2003. (Cited on pages 2, 8, 9 and 11.)

[5] R. Pabst, B. Walke, D. Schultz, P. Herhold, H. Yanikomeroglu, S. Mukherjee, H. Viswanathan, M. Lott, W. Zirwas, M. Dohler, H. Aghvami, D. Falconer, and G. Fettweis, "Relay-based deployment concepts for wireless and mobile broadband radio," *IEEE Communications Magazine*, vol. 42, no. 9, pp. 80–89, Sep. 2004. (Cited on pages 2 and 8.)

[6] P. Kumar and S. Prakriy, *Bidirectional Cooperative Relaying.* InTech, Apr. 2010. (Cited on pages 2 and 8.)

[7] L. Cao, J. Zhang, and N. Kanno, "Multi-user cooperative communications with relay-coding for uplink IMT-advanced 4G systems," in *Proceedings in IEEE GLOBECOM*, Honolulu, HI, Dec. 2009, pp. 1–6. (Cited on pages 2 and 8.)

[8] P. Gupta and P. Kumar, "The capacity of wireless networks," *IEEE Transactions on Information Theory*, vol. 46, no. 2, pp. 388–404, Mar 2000. (Cited on pages 2 and 9.)

[9] K. Liu, A. Sadek, W. Su, and A. Kwasinski, *Cooperative communications and networking.* Boston, MA, USA: Cambridge University Press, 2008. (Cited on pages 2, 8 and 9.)

[10] M. Dohler and Y. Li, *Cooperative communications: hardware, channel and PHY.* John Wiley & Sons, 2010. (Cited on pages 2 and 9.)

[11] J. Laneman, G. W. Wornell, and D. Tse, "An efficient protocol for realizing cooperative diversity in wireless networks," in *IEEE International Symposium on Information Theory*, 2001, pp. 294–. (Cited on pages 2, 3, 9 and 12.)

[12] T. Cover and A. Gamal, "Capacity theorems for the relay channel," *IEEE Transactions on Information Theory*, vol. 25, no. 5, pp. 572–584, 1979. (Cited on pages 2, 9 and 11.)

[13] J. Laneman, D. Tse, and G. W. Wornell, "Cooperative diversity in wireless networks: Efficient protocols and outage behavior," *IEEE Transactions on Information Theory*, vol. 50, no. 12, pp. 3062–3080, Dec 2004. (Cited on pages 2, 8 and 9.)

[14] M. Biguesh and A. Gershman, "Training-based MIMO channel estimation: a study of estimator tradeoffs and optimal training signals," *IEEE Transactions on Signal Processing*, vol. 54, no. 3, pp. 884–893, 2006. (Cited on pages 4, 13 and 84.)

[15] M. Shariat, M. Biguesh, and S. Gazor, "Relay design for SNR maximization in MIMO communication systems," in *5th International Symposium on Telecommunications (IST)*, Tehran, Iran, 2010, pp. 313–317. (Cited on pages 4 and 13.)

[16] Y. Rong, X. Tang, and Y. Hua, "A unified framework for optimizing linear nonregenerative multicarrier MIMO relay communication systems," *IEEE Transactions on Signal Processing*, vol. 57, no. 12, pp. 4837–4851, Dec. 2009. (Cited on pages 4 and 13.)

[17] Y. Rong, "Optimal joint source and relay beamforming for MIMO relays with direct link," *IEEE Communications Letters*, vol. 14, no. 5, pp. 390–392, May 2010. (Cited on pages 4 and 13.)

[18] F. Roemer and M. Haardt, "Tensor-based channel estimation (TENCE) for two-way relaying with multiple antennas and spatial reuse," in *IEEE International Conference on Acoustics, Speech and Signal Processing (ICASSP)*, Taipei, Taiwan, Apr. 2009, pp. 3641–3644. (Cited on pages 4, 5, 14, 15, 16, 51 and 114.)

[19] ——, "Tensor-based channel estimation and iterative refinements for two-way relaying with multiple antennas and spatial reuse," *IEEE Transactions on Signal Processing*, vol. 58, no. 11, pp. 5720–5735, Nov. 2010. (Cited on pages 4, 14, 16 and 114.)

[20] Y. Rong, M. Khandaker, and Y. Xiang, "Channel estimation of dual-hop MIMO relay system via parallel factor analysis," *IEEE Transactions on Wireless Communications*, vol. 11, no. 6, pp. 2224 –2233, Jun. 2012. (Cited on pages 4, 5, 14, 15, 16, 46, 62, 81, 82, 83 and 85.)

[21] C. A. R. Fernandes, A. L. F. de Almeida, and D. B. da Costa, "Unified tensor modeling for blind receivers in multiuser uplink cooperative systems," *IEEE Signal Processing Letters*, vol. 19, no. 5, pp. 247 –250, May 2012. (Cited on pages 4, 5, 14, 15 and 16.)

[22] A. L. F. de Almeida, C. A. R. Fernandes, and D. B. da Costa, "Multiuser detection for uplink ds-cdma amplify-and-forward relaying systems," *IEEE Signal Processing Letters*, vol. 20, no. 7, pp. 697–700, July 2013. (Cited on pages 4, 5, 14, 15 and 16.)

[23] I. V. Cavalcante, A. L. F. de Almeida, and M. Haardt, "Tensor-based approach to channel estimation in amplify-and-forward MIMO relaying systems," in *Proceedings in IEEE Sensor Array and Multichannel Signal Processing Woskshop (SAM2014)*, La Coruña , Spain, 2014, pp. 1–4. (Cited on pages 4, 14 and 16.)

[24] P. Lioliou and M. Viberg, "Least-squares based channel estimation for MIMO relays," in *International ITG Workshop on Smart Antennas, 2008. WSA 2008*, Feb 2008, pp. 90–95. (Cited on pages 4, 5, 14, 15, 16, 46, 51, 81, 82 and 83.)

[25] P. Lioliou, M. Viberg, and M. Coldrey, "Performance analysis of relay channel estimation," in *IEEE Conference on Signals, Systems and Computers (ASILOMAR)*, Gothenburg, Sweden, 2009, pp. 1533–1537. (Cited on pages 4 and 14.)

[26] ——, "Efficient channel estimation techniques for amplify and forward relaying systems," *IEEE Transactions on Wireless Communications*, vol. 60, no. 11, pp. 3150–3155, Oct. 2012. (Cited on pages 4, 14 and 62.)

[27] C. E. Shannon, "A mathematical theory of communication," *Bell System Technical Journal*, vol. 27, no. 3, pp. 379–423, July 1948. (Cited on page 7.)

[28] L. Zheng and D. Tse, "Diversity and multiplexing: a fundamental tradeoff in multiple-antenna channels," *IEEE Transactions on Information Theory*, vol. 49, no. 5, pp. 1073–1096, May 2003. (Cited on page 8.)

[29] G. J. Foschini and M. J. Gans, "On limits of wireless communications in a fading environment when using multiple antennas," *Wireless Personal Communications*, vol. 6, pp. 311–335, 1998. (Cited on pages 8 and 9.)

[30] E. Telatar, "Capacity of Multi antenna Gaussian Channels," *European Transactions on Telecommunications*, vol. 10, no. 6, 1999. (Cited on pages 8 and 9.)

[31] J. Guey, M. Fitz, M. Bell, and W. Kuo, "Signal design for transmitter diversity wireless communication systems over rayleigh fading channels," in *IEEE 46th Vehicular Technology Conference*, vol. 1, Apr 1996, pp. 136–140 vol.1. (Cited on page 8.)

[32] G. J. Foschini, "Layered space-time architecture for wireless communication in a fading environment when using multi-element antennas," *Bell Labs Technical Journal*, vol. 1, no. 2, pp. 41–59, 1996. (Cited on pages 8 and 9.)

[33] V. Tarokh, N. Seshadri, and A. Calderbank, "Space-time codes for high data rate wireless communication: performance criterion and code construction," *IEEE Transactions on Information Theory*, vol. 44, no. 2, pp. 744–765, Mar 1998. (Cited on pages 8 and 9.)

[34] V. Tarokh, A. Naguib, N. Seshadri, and A. Calderbank, "Space-time codes for high data rate wireless communication: performance criteria in the presence of channel estimation errors, mobility, and multiple paths," *IEEE Transactions on Communications*, vol. 47, no. 2, pp. 199–207, Feb 1999. (Cited on pages 8 and 9.)

[35] S. Alamouti, "A simple transmit diversity technique for wireless communications," *IEEE Journal on Selected Areas in Communications*, vol. 16, no. 8, pp. 1451–1458, Oct 1998. (Cited on pages 8 and 9.)

[36] V. Tarokh, H. Jafarkhani, and A. Calderbank, "Space-time block coding for wireless communications: performance results," *IEEE Journal on Selected Areas in Communications*, vol. 17, no. 3, pp. 451–460, Mar 1999. (Cited on pages 8 and 9.)

[37] ——, "Space-time block codes from orthogonal designs," *IEEE Transactions on Information Theory*, vol. 45, no. 5, pp. 1456–1467, Jul 1999. (Cited on pages 8 and 9.)

[38] A. Nosratinia, T. E. Hunter, and A. Hedayat, "Cooperative communication in wireless networks," *IEEE Communications Magazine*, vol. 42, no. 10, pp. 74–80, Oct. 2004. (Cited on page 8.)

[39] T. Unger and A. Klein, "Duplex schemes in multiple antenna two-hop relaying," *ELSEVIER Journal on Advances in Signal Processing*, vol. 2008, no. 92, pp. 1–18, Jan. 2008. (Cited on page 8.)

[40] S. Cui, A. Goldsmith, and A. Bahai, "Energy-efficiency of MIMO and cooperative MIMO techniques in sensor networks," *IEEE Journal on Selected Areas in Communications*, vol. 22, no. 6, pp. 1089–1098, Aug 2004. (Cited on page 9.)

[41] A. Sendonaris, E. Erkip, and B. Aazhang, "Increasing uplink capacity via user cooperation diversity," in *IEEE International Symposium on Information Theory*, Aug 1998, pp. 156–. (Cited on page 9.)

[42] T. Elkourdi and O. Simeone, "Femtocell as a relay: An outage analysis," *IEEE Transactions on Wireless Communications*, vol. 10, no. 12, pp. 4204–4213, December 2011. (Cited on page 9.)

[43] Y. Chen, C. Li, and W. Chiang, "A femtocell-assisted data forwarding protocol in relay enhanced LTE networks," in *40th International Conference on Parallel Processing Workshops (ICPPW)*, Sept 2011, pp. 127–136. (Cited on page 9.)

[44] M. Tehrani, M. Uysal, and H. Yanikomeroglu, "Device-to-device communication in 5G cellular networks: challenges, solutions, and future directions," *IEEE Communications Magazine*, vol. 52, no. 5, pp. 86–92, May 2014. (Cited on page 9.)

[45] A. Akhlaq, A. Sulyman, H. Hassanein, A. Alsanie, and S. Alshebeili, "Performance analysis of relay-multiplexing scheme in cellular systems employing massive multiple-input multiple-output antennas," *IET Communications*, vol. 8, no. 10, pp. 1788–1799, July 2014. (Cited on page 9.)

[46] E. C. van der Meulen, "Transmission of information in a T-terminal discrete memoryless channel," Ph.D. dissertation, University of California, 1968. (Cited on page 9.)

[47] ——, "Three-terminal communication channels," *Advances in Applied Probability*, vol. 3, pp. 120–154, 1971. (Cited on page 9.)

[48] T. Oechtering and H. Boche, "Relay selection in bidirectional relay communication," in *IEEE 8th Workshop on Signal Processing Advances in Wireless Communications*, June 2007, pp. 1–5. (Cited on page 9.)

[49] H. Eghbali, S. Muhaidat, S. Hejazi, and Y. Ding, "Relay selection strategies for single-carrier frequency-domain equalization multi-relay cooperative networks," *IEEE Transactions on Wireless Communications*, vol. 12, no. 5, pp. 2034–2045, May 2013. (Cited on page 9.)

[50] C. Xing, S. Ma, M. Xia, and Y. Wu, "Cooperative beamforming for dual-hop amplify-and-forward multi-antenna relaying cellular networks," *ELSEVIER Signal Processing*, vol. 92, no. 11, pp. 2689 – 2699, 2012. (Cited on page 9.)

[51] X. He and A. Yener, "Cooperation with an untrusted relay: A secrecy perspective," *IEEE Transactions on Information Theory*, vol. 56, no. 8, pp. 3807–3827, Aug 2010. (Cited on page 9.)

[52] C. E. Shannon, "Two-way Communication Channels," in *4th Berkeley Symposium on Mathematical Statistics and Probability*, vol. 1. University of California Press, 1961, pp. 611–644. (Cited on page 10.)

[53] S. J. Kim, N. Devroye, and V. Tarokh, "Bi-directional half-duplex relaying protocols," *Journal of Communications and Networks*, vol. 11, no. 5, pp. 433–444, Oct 2009. (Cited on page 10.)

[54] N. D. Sidiropoulos, G. B. Giannakis, and R. Bro, "Blind PARAFAC receivers for DS-CDMA systems," *IEEE Transactions on Signal Processing*, vol. 48, no. 3, pp. 810–823, Mar. 2000. (Cited on pages 13 and 27.)

[55] A. L. F. de Almeida, G. Favier, and J. C. M. Mota, "A constrained factor decomposition with application to MIMO antenna systems," *IEEE Transactions in Signal Processing*, vol. 56, pp. 2429–2442, Jun. 2008. (Cited on page 13.)

[56] ——, "Space-time spreading-multiplexing for MIMO wireless communications systems using the PARATUCK-2 tensor model," *ELSEVIER Signal Processing*, vol. 89, no. 11, pp. 2103–2116, Nov. 2009. (Cited on pages 13 and 31.)

[57] A. L. F. de Almeida, G. Favier, and L. R. Ximenes, "Space-time-frequency (STF) MIMO communication systems with blind receiver based on a generalized PARATUCK2 model," *IEEE Transactions on Signal Processing*, vol. PP, no. 99, p. 1, 2013. (Cited on pages 13 and 113.)

[58] R. A. Harshman, "Foundations of the PARAFAC procedure: Models and conditions for an "explanatory" multimodal factor analysis," *UCLA Working Papers in Phonetics*, vol. 16, pp. 1–84, Dec. 1970. (Cited on pages 13, 21 and 26.)

[59] J. D. Carroll and J. J. Chang, "Analysis of individual differences in multidimensional scaling via an N-way generalization of "Eckart-Young" decomposition," *Psychometrika*, vol. 35, no. 3, pp. 283–319, Sep. 1970. (Cited on pages 13, 21 and 26.)

[60] R. Bro, "Multi-Way analysis in the food industry," Ph.D. dissertation, Royal Veterinary and Agricultural University, Denmark, 1998. (Cited on page 13.)

[61] N. D. Sidiropoulos and R. S. Budampati, "Khatri-Rao space-time codes," *IEEE Transactions on Signal Processing*, vol. 50, no. 10, pp. 2396–2407, Oct. 2002. (Cited on pages 13, 17, 40, 42, 85, 89 and 93.)

[62] R. A. Harshman and M. E. Lundy, "Uniqueness proof for a family of models sharing features of Tucker's three-mode factor analysis and PARAFAC/CANDECOMP," in *Psychometrika*, vol. 61, 1996, pp. 133–154. (Cited on pages 13, 21, 29 and 31.)

[63] G. Favier, M. N. da Costa, A. L. F. de Almeida, and J. M. T. Romano, "Tensor space-time (TST) coding for MIMO wireless communication systems." *ELSEVIER Signal Processing*, no. 4, pp. 1079–1092, 2012. (Cited on pages 13, 29, 31 and 113.)

[64] A. L. F. de Almeida and G. Favier, "Double Khatri-Rao space-time-frequency coding using semi-blind PARAFAC based receiver," *IEEE Signal Processing Letters*, vol. 20, no. 5, pp. 471–474, 2013. (Cited on pages 14, 21 and 33.)

[65] G. Favier and A. de Almeida, "Tensor space-time-frequency coding with semi-blind receivers for MIMO wireless communication systems," *IEEE Transactions on Signal Processing*, vol. 62, no. 22, pp. 5987–6002, Nov 2014. (Cited on page 14.)

[66] A. L. F. de Almeida, G. Favier, and J. C. M. Mota, "PARAFAC-based unified tensor modeling for wireless communication systems with application to blind multiuser equalization," *ELSEVIER Signal Processing*, vol. 87, no. 2, pp. 337–351, 2007. (Cited on page 14.)

[67] J. B. Kruskal, "Three-way arrays: Rank and uniqueness of trilinear decompositions, with application to arithmetic complexity and statistics," *Linear Algebra Applications*, vol. 18, pp. 95–138, 1977. (Cited on pages 14, 21, 23 and 28.)

[68] L. R. Ximenes, G. Favier, A. L. F. de Almeida, and Y. C. B. Silva, "PARAFAC-PARATUCK semi-blind receivers for two-hop cooperative MIMO relay systems," *IEEE Transactions on Signal Processing*, vol. 62, no. 14, pp. 3604–3615, July 2014. (Cited on page 16.)

[69] L. R. Ximenes, G. Favier, and A. L. F. de Almeida, "Semi-blind receivers for non-regenerative cooperative MIMO communications based on nested PARAFAC modeling," *Submitted to IEEE Transactions on Signal Processing*, 2014. (Cited on pages 16, 33 and 68.)

[70] R. Bro, A. Smilde, and P. Geladi, *Multi-way analysis - applications in the chemical sciences*. England: Wiley, 2004. (Cited on pages 21 and 31.)

[71] N. Sidiropoulos, R. Bro, and G. Giannakis, "Parallel factor analysis in sensor array processing," *IEEE Transactions on Signal Processing*, vol. 48, no. 8, pp. 2377–2388, 2000. (Cited on page 22.)

[72] N. Sidiropoulos and R. Bro, "On the uniqueness of multilinear decomposition of N-way arrays," *Journal of Chemometrics*, vol. 14, pp. 229–239, 2000. (Cited on pages 22 and 26.)

[73] F. L. Hitchcock, "The expression of a tensor or a polydiac as a sum of products," *Journal of Mathematics and Physics*, vol. 6, pp. 164–189, 1927. (Cited on pages 23 and 26.)

[74] L. Tucker, "Some mathematical notes of three-mode factor analysis," *Psychometrika*, vol. 31, no. 3, pp. 279–311, 1966. (Cited on page 25.)

[75] A. Kapteyn, H. Neudecker, and T. Wansbeek, "An approach to n-mode components analysis," *Psychometrika*, vol. 51, pp. 269–275, 1986. (Cited on page 25.)

[76] L. de Lathauwer, B. de Moor, and J. Vandewalle, "A multilinear singular value decomposition," *SIAM Journal on Matrix Analysis and Applications*, vol. 21, pp. 1253–1278, 2000. (Cited on page 25.)

[77] J. B. Kruskal, "Rank, decomposition, and uniqueness for 3-way and n-way arrays," *Multiway Data Analysis*, pp. 7–18, 1989. (Cited on page 26.)

[78] J. JáJá, "Optimal evaluation of pairs of bilinear forms," *SIAM Journal on Computing*, vol. 8, no. 3, pp. 443–462, 1979. (Cited on page 26.)

[79] P. Comon, J. M. F. Ten Berge, L. de Lathauwer, and J. Castaing, "Generic and typical ranks of multi-way arrays," *Linear Algebra and its Applications*, vol. 430, no. 1112, pp. 2997 – 3007, 2009. (Cited on page 26.)

[80] H. A. L. Kiers, "Towards a standardized notation and terminology in multiway analysis," *Journal of Chemometrics*, vol. 14, no. 3, pp. 105–122, 2000. (Cited on page 26.)

[81] A. L. F. de Almeida, X. Luciani, and P. Comon, "Fourth-order CONFAC decomposition approach for blind identification of underdetermined mixtures," in *Proceedings of the 20th European Signal Processing Conference (EUSIPCO)*, Aug 2012, pp. 290–294. (Cited on page 27.)

[82] J. M. F. Ten Berge and N. D. Sidiropoulos, "On uniqueness in CANDECOMP/PARAFAC," *Psychometrika*, vol. 67, no. 3, pp. 399–409, 2002. (Cited on page 28.)

[83] A. Stegeman and N. D. Sidiropoulos, "On Kruskal's uniqueness condition for the CANDECOMP/PARAFAC decomposition," *Linear Algebra and its Applications*, vol. 420, no. 2-3, pp. 540 – 552, 2007. (Cited on page 28.)

[84] T. G. Kolda and B. W. Bader, "Tensor decompositions and applications," *SIAM Review*, vol. 51, no. 3, pp. 455–500, Sep. 2009. (Cited on page 31.)

[85] L. R. Ximenes, G. Favier, and A. L. F. Almeida, "Closed-form semi-blind receiver for two-hop MIMO relay systems using a double Khatri-Rao space-time coding," *To be submitted*, 2014. (Cited on pages 33 and 68.)

[86] A. Y. Kibangou and G. Favier, "Noniterative solution for PARAFAC with a Toeplitz factor," in *7th European Signal Processing Conference (EUSIPCO-2009)*, Glasgow, Scotland, Aug 2009. (Cited on page 51.)

[87] C. V. Loan and N. Pitsianis, "Approximation with kronecker products," in *Linear Algebra for Large Scale and Real Time Applications.* Kluwer Publications, 1993, pp. 293–314. (Cited on page 51.)

[88] G. H. Golub and C. Reinsch, "Singular Value Decomposition and least square solutions," *Numerische Mathematik*, vol. 14, pp. 403–420, 1970. (Cited on page 76.)

[89] G. H. Golub and C. F. Van Loan, *Matrix Computations.* Baltimore, MD, USA: Johns Hopkins University Press, 1996. (Cited on page 76.)

[90] A. Toding, M. R. A. Khandaker, and Y. Rong, "Joint source and relay optimization for parallel mimo relay networks," *ELSEVIER Jouyrnal on Advances in Signal Processing*, vol. 2012, p. 174, 2012. (Cited on page 84.)

[91] T. Kong and Y. Hua, "Optimal channel estimation and training design for MIMO relays," in *IEEE Conference on Signals, Systems and Computers (ASILOMAR)*, Pacific Grove, CA, USA, Nov. 2010, pp. 663–667. (Cited on page 85.)

[92] P. Lioliou, M. Viberg, and M. Matthaiou, "Bayesian approach to channel estimation for AF MIMO relaying systems," *IEEE Journal on Selected Areas in Communications*, vol. 30, no. 8, pp. 1440–1451, 2012. (Cited on page 113.)

[93] F. Gao, R. Zhang, and Y.-C. Liang, "Optimal channel estimation and training design for two-way relay networks," *IEEE Transactions on Communications*, vol. 57, no. 10, pp. 3024–3033, October 2009. (Cited on page 113.)

[94] Y. Ding, J.-K. Zhang, and K. M. Wong, "The amplify-and-forward half-duplex cooperative system: Pairwise error probability and precoder design," *IEEE Transactions on Signal Processing*, vol. 55, no. 2, pp. 605–617, Feb 2007. (Cited on page 113.)

[95] J.-B. Kim and D. Kim, "Performance of dual-hop amplify-and-forward beamforming and its equivalent systems in rayleigh fading channels," *IEEE Transactions on Communications*, vol. 58, no. 3, pp. 729–732, March 2010. (Cited on page 113.)

[96] X. Liu and N. Sidiropoulos, "Cramer-Rao lower bounds for low-rank decomposition of multidimensional arrays," *IEEE Transactions on Signal Processing*, vol. 49, no. 9, pp. 2074–2086, Sep 2001. (Cited on page 113.)

[97] P. Tichavsky, A. Phan, and Z. Koldovsky, "Cramer-Rao-induced bounds for CANDECOMP/PARAFAC tensor decomposition," *IEEE Transactions on Signal Processing*, vol. 61, no. 8, pp. 1986–1997, April 2013. (Cited on page 113.)

[98] D. Nion and N. Sidiropoulos, "Adaptive algorithms to track the parafac decomposition of a third-order tensor," *IEEE Transactions on Signal Processing*, vol. 57, no. 6, pp. 2299–2310, June 2009. (Cited on page 114.)

Index